NAVAL SHIP RESEARCH AND DEVELOPMENT CENTER
Bethesda, Md. 20084

FINITE ELEMENT FRACTURE MECHANICS ANALYSIS OF TWO-DIMENSIONAL AND AXISYMMETRIC ELASTIC AND ELASTIC-PLASTIC CRACKED STRUCTURES

by
Peter D. Hilton, L. Nash Gifford, Jr., and
Oles Lomacky

APPROVED FOR PUBLIC RELEASE: DISTRIBUTION UNLIMITED

STRUCTURES DEPARTMENT
RESEARCH AND DEVELOPMENT REPORT

November 1974

Report 4493

Report 4493

FINITE ELEMENT FRACTURE MECHANICS ANALYSIS OF TWO-DIMENSIONAL AND AXISYMMETRIC ELASTIC AND ELASTIC-PLASTIC CRACKED STRUCTURES

The Naval Ship Research and Development Center is a U. S. Navy center for laboratory effort directed at achieving improved sea and air vehicles. It was formed in March 1967 by merging the David Taylor Model Basin at Carderock, Maryland with the Marine Engineering Laboratory at Annapolis, Maryland.

Naval Ship Research and Development Center
Bethesda, Md. 20084

MAJOR NSRDC ORGANIZATIONAL COMPONENTS

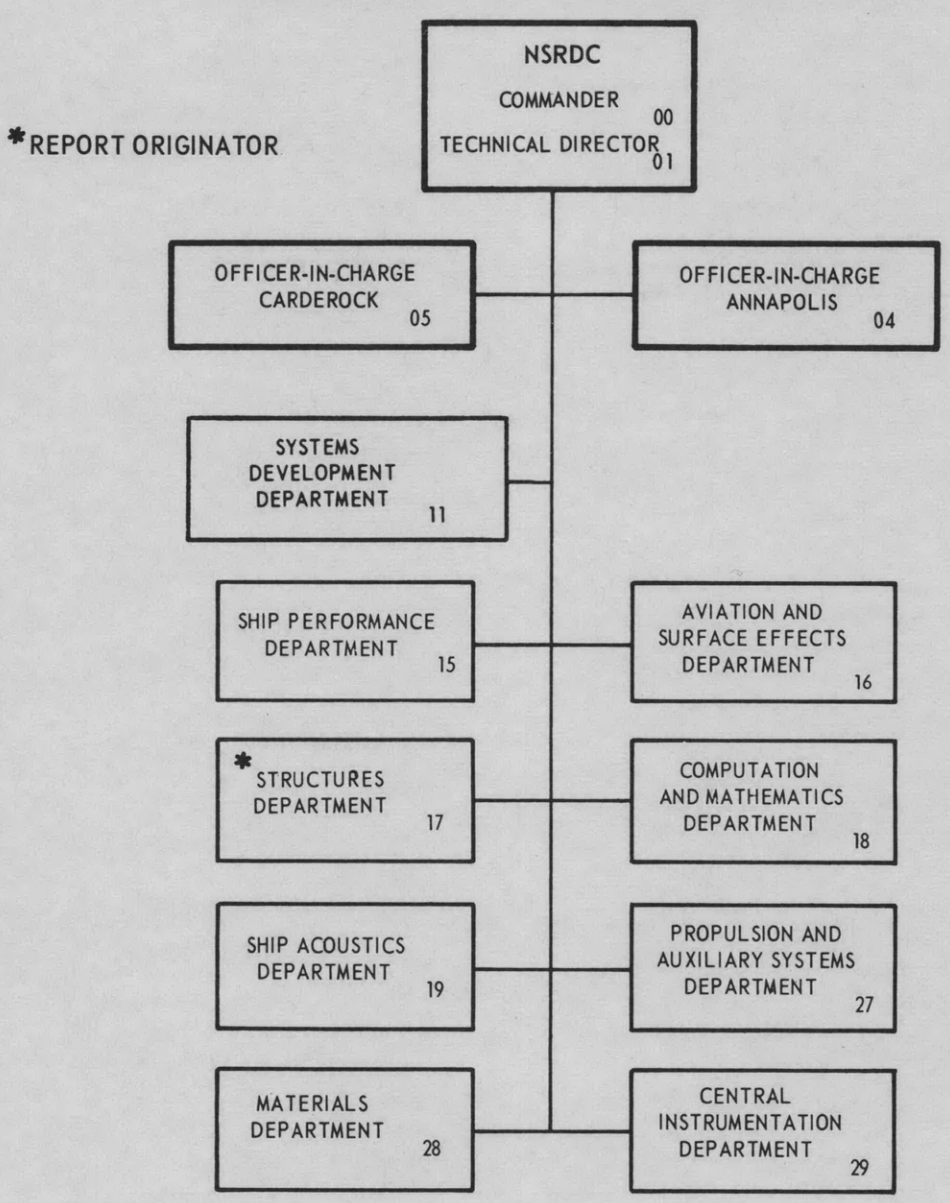

NDW-NSRDC 3960/43b (Rev. 3-7
GPO 928-10

UNCLASSIFIED

SECURITY CLASSIFICATION OF THIS PAGE *(When Data Entered)*

REPORT DOCUMENTATION PAGE		READ INSTRUCTIONS BEFORE COMPLETING FORM
1. REPORT NUMBER 4493	2. GOVT ACCESSION NO.	3. RECIPIENT'S CATALOG NUMBER
4. TITLE *(and Subtitle)* FINITE ELEMENT FRACTURE MECHANICS ANALYSIS OF TWO-DIMENSIONAL AND AXISYMMETRIC ELASTIC AND ELASTIC-PLASTIC CRACKED STRUCTURES		5. TYPE OF REPORT & PERIOD COVERED 6. PERFORMING ORG. REPORT NUMBER
7. AUTHOR(s) Peter D. Hilton, L. Nash Gifford, Jr., and Oles Lomacky		8. CONTRACT OR GRANT NUMBER(s)
9. PERFORMING ORGANIZATION NAME AND ADDRESS Naval Ship Research and Development Center Bethesda, Maryland 20084		10. PROGRAM ELEMENT, PROJECT, TASK AREA & WORK UNIT NUMBERS NAVSHIPS Subprojects SF 43.422.210; Tasks 15055, 15062 Work Units 1-1727-297, 1-1727-392
11. CONTROLLING OFFICE NAME AND ADDRESS Naval Ship Systems Command Washington, D.C. 20360		12. REPORT DATE November 1974 13. NUMBER OF PAGES 119
14. MONITORING AGENCY NAME & ADDRESS(*if different from Controlling Office*)		15. SECURITY CLASS. *(of this report)* UNCLASSIFIED 15a. DECLASSIFICATION/DOWNGRADING SCHEDULE

16. DISTRIBUTION STATEMENT *(of this Report)*

APPROVED FOR PUBLIC RELEASE: DISTRIBUTION UNLIMITED

17. DISTRIBUTION STATEMENT *(of the abstract entered in Block 20, if different from Report)*

18. SUPPLEMENTARY NOTES

19. KEY WORDS *(Continue on reverse side if necessary and identify by block number)*

Fracture mechanics
Stress intensity factors
Plastic intensity factors
J-integral
Finite element methods
Singular elements
Numerical methods

20. ABSTRACT *(Continue on reverse side if necessary and identify by block number)*

Improved methods for calculating fracture mechanics parameters at critical fatigue and fracture prone areas of complex structural details are summarized. This work is a part of a broader effort aimed at the development of analytical methods for fatigue and fracture analysis of submarine hulls.

(Continued on reverse side)

DD FORM 1 JAN 73 1473 EDITION OF 1 NOV 65 IS OBSOLETE
S/N 0102-014-6601 |

UNCLASSIFIED

SECURITY CLASSIFICATION OF THIS PAGE *(When Data Entered)*

(Block 20 continued)

An approach based on the combination of high order isoparametric finite elements with a singular crack tip element is described and applied to the prediction of elastic stress intensity factors for Mode I or combined Modes I and II crack behavior. It is shown that this approach offers high accuracy and computational convenience. The technique is applicable to any two-dimensional (plane stress/strain) or three-dimensional axisymmetric problem.

A singular, plastic, crack tip element featuring the Hutchinson-Rice singularity is then combined with a lower order finite element for the study of elastic-plastic fracture problems in the strain-hardening range. The parameters of interest are the plastic stress and strain intensity factors, plastic zone sizes, crack opening displacements, and J-integral values.

Examples of the application of these methods to two-dimensional and axisymmetric problems are presented along with recommendations for future studies and applications.

TABLE OF CONTENTS

LIST OF FIGURES

LIST OF TABLES

NOTATION

A	Area
a	Crack length or half crack length
a_{1i}, a_{2i}, a_{3i}, a_{4i}	Coefficients defined by Equation (5)
B	Constant defined in Equations (43) and (44), strain-displacement transformation matrix
B_1, B_2	Constants defined by Equation (7)
c	Subscript denoting critical value
COD	Crack opening displacement
D	Strain-stress transformation matrix
E	Young's modulus
e_e	Effective strain
e_{ij}	Components of strain deviator tensor
G	Shear modulus, Griffith energy release rate
h	Basic dimension of a finite element
J	Energy integral evaluated about a contour
K_I	Elastic Mode I stress intensity factor
K_{II}	Elastic Mode II stress intensity factor
K_p	Plastic stress intensity factor
k_1	Normalized Mode I stress intensity factor
k_2	Normalized Mode II stress intensity factor
k_ϵ	Plastic strain intensity factor
K_{ij}	Term ij of master structural stiffness matrix
k_{ij}	Term ij of element stiffness matrix
N_i	Displacement functions for a finite element
n	Strain hardening exponent, normal vector
n, s	Coordinates along crack face as depicted in Figure 3
ND	Subscript indicating nondimensionalized quantity
N1	Number of nodes about singular element
PE	Potential energy

r, θ	Polar coordinates centered at crack tip
$\bar{R}$	Distance from axis of symmetry to crack tip
R_i	Concentrated force corresponding to degree of freedom i
r_0	Radius of singular crack tip element
SE	Strain energy
SED	Strain energy density
SSY	Subscript implying small scale yielding range
S_{ij}	Components of stress deviator tensor
T_x, T_y	Surface tractions in x and y coordinate directions
u_{0x}, u_{0y}	Displacements of crack tip in x and y coordinate directions
u_r, u_θ	Displacement components referred to polar coordinates r, θ
u_x, u_y	Displacement components in x and y coordinate directions
w	Width of body into which crack penetrates
x, y, z	Cartesian coordinates
α	Crack angle
Γ	Closed contour about a crack tip or within a body
δ_{ij}	Kroneker delta
ϵ	Nondimensionalized strain
$\epsilon_r, \epsilon_\theta, \epsilon_{r\theta}$	Strain components referred to polar coordinates r, θ
$\epsilon_x, \epsilon_y, \epsilon_z, \gamma_{xy}$	Strain components referred to x, y, z coordinates
κ	Constant defined by Equation (2)
ν	Poisson's ratio
σ	Nondimensionalized stress
σ_e	Effective (von Mises) stress
σ_n, τ_{ns}	Surface tractions along a crack as depicted in Figure 3
$\sigma_r, \sigma_\theta, \sigma_{r\theta}$	Stress components referred to polar coordinates r, θ
$\sigma_x, \sigma_y, \sigma_z, \tau_{xy}$	Stress components referred to x, y, z coordinates
σ_y	Yield stress

σ_∞	Remote applied stress, reference stress
ϕ	Airy stress function

ABSTRACT

Improved methods for calculating fracture mechanics parameters at critical fatigue and fracture prone areas of complex structural details are summarized. This work is a part of a broader effort airmed at the development of analytical methods for fatigue and fracture analysis of submarine hulls.

An approach based on the combination of high order isoparametric finite elements with a singular crack tip element is described and applied to the prediction of elastic stress intensity factor for Mode I or combined Modes I and II crack behavior. It is shown that this approach offers high accuracy and computational convenience. The technique is applicable to any two-dimensional (plane stress/strain) or three-dimensional axisymmetric problem.

A singular, plastic, crack tip element featuring the Hutchinson-Rice singularity is then combined with a lower order finite element for the study of elastic-plastic fracture problems in the strain-hardening range. The parameters of interest are the plastic stress and strain intensity factors, plastic zone sizes, crack opening displacements, and J-integral values.

Examples of the application of these methods to two-dimensional and axisymmetric problems are presented along with recommendations for future studies and applications.

ADMINISTRATIVE INFORMATION

This work was supported by the Naval Ship Systems Command (0342) under Project SF 43.422.210, Tasks 15055 and 15062, Work Unit 1-1727-392.

The senior author is an assistant professor in the Department of Mechanical Engineering and Mechanics, Lehigh University. This report was written in the course of his consulting work for NSRDC under Contract N00167-74-M-1124.

INTRODUCTION

BACKGROUND

Many materials commonly used in naval structures contain (or are prone to develop) cracks or flaws. In particular, cracks in new, higher strength structural steels and other metals of interest for construction of advanced surface ships and submarines are of critical concern since such structures are subject to high tensile residual stresses resulting from fabrication (welding, rolling, etc.), to a harsh chemical environment, and to high cyclic loads. Such

conditions can lead to the formation of cracks which may propagate through the structure, ultimately resulting in structural failure at stress levels considered moderate in relation to the theoretical strength of the material. It is perhaps ironic that this problem has become even more acute with the development of new materials; an increase in material strength is generally not accompanied by a comparable increase in resistance to the initiation and growth of cracks caused by fatigue or stress corrosion.

In the design of high performance structures, therefore, one must be concerned not only with keeping stresses at acceptable levels but must also give consideration to the effects of notches and cracks on the ability of the structure to continue in its load-carrying function. The goal of fracture mechanics is to provide the structural designer with rational methods for assessing the load-carrying capacity of structures that contain cracks. The underlying rationale is that the same key parameters (or functions) which characterize crack tip deformation of a small specimen also govern the behavior of full-scale structural members containing cracks. The implementation of fracture mechanics principles requires the development of analytical procedures for the determination of crack tip parameters which can be used to correlate the behavior of laboratory specimens with that of full-scale structural details.

So long as conditions in the structural member are essentially elastic (except for a small region surrounding the crack tip), the elastic stress intensity factor K_I appears to be the most useful parameter for correlating behavior in the laboratory specimen and the full-scale structure. Provided that the loading geometry of the specimen or structural member is sufficiently simple, elastic stress intensity factors may be estimated from known closed-form solutions available in a number of excellent sources.[1,2]

However, for complex hull details containing cracks, numerical solutions based on finite element procedures may have to be used. Toward this end, as reported by Oglesby and Lomacky,[3] NSRDC has augmented its standard (constant strain) finite element computer code[4] with a singular core element to carry out stress intensity factor calculations. However,

---

[1]Sih, G.C., "Handbook of Stress Intensity Factors," Institute of Fracture and Solid Mechanics, Lehigh University (1973). A complete listing of references is given on page 107.

[2]Tada, Hiroshi, "The Stress Analysis of Cracks Handbook," Del Research Corporation (1973).

[3]Oglesby, J.J. and O. Lomacky, "An Evaluation of Finite Element Methods for the Computation of Elastic Stress Intensity Factors," NSRDC Report 3751 (Dec 1971).

[4]Gifford, L.N., "Finite Element Analysis for Arbitrary Axisymmetric Structures," NSRDC Report 2641 (Mar 1968).

there are distinct computational advantages, particularly for extensive parametric studies, to be gained by employing a combination of a singular core tip element and higher order isoparametric finite elements, as will be discussed in the main body of this report.

When a significant* degree of plasticity, referred to as the large-scale yielding range, takes place either in the small laboratory specimen or in the full-scale structural member, the usefulness of the elastic stress intensity factor as a correlating parameter becomes questionable. For this reason, the concepts of elastic-plastic fracture mechanics are receiving increased attention. Here, the motivation is to enable material characterization data to be obtained on small specimens and to ultimately provide the structural designer with the means for predicting structural performance where the strict limitations of linear fracture mechanics have been removed. In terms of submarine hull applications where the emphasis is on preventing the growth of small flaws in tough materials, the conditions of large-scale yielding can be expected to be quite typical. Some of the correlating parameters that have been suggested for this case in recent years include the J-integral, crack opening displacement, and plastic stress and strain intensity factors. However, in the context of material nonlinearity, the application of these concepts to complex structural details is possible only through the utilization of numerical techniques such as the finite element method. As in the case of elastic analysis, the most promising approach appears to be the exploitation of specialized crack tip elements.

SCOPE

The present report begins with a discussion of the elastic singular solution for plane stress, plane strain, and axisymmetric cracked bodies for which both Mode I and Mode II crack tip behavior is encountered. A method is then described whereby the singular solution may be embedded into a standard finite element computer program by using a special crack tip element. In this manner, stress intensity factors K_I and K_{II} may be directly calculated for arbitrary geometries and loading conditions, including crack face loading. Sample calculations are then presented to demonstrate the practicality of the method; these include the combination of the singular crack tip element with three different "standard" finite elements. Wherever possible, the results obtained by the proposed finite element procedures are compared to solutions obtained by different means and by other investigators.

---

*Here, the term significant denotes primarily the large size of the plastic zone of the crack tip with respect to any of the principal dimensions of the cracked body, i.e., crack depth, plate thickness, etc. Through-thickness yielding is not essential in order for this condition to be reached. For example, very small flaws in tough materials loaded to nominally elastic conditions may approach large-scale yielding conditions.

The procedure is then extended into the elastic-plastic realm for Mode I crack problems associated with planar or axisymmetric bodies subject to monotonic loading. The result of such calculations is the previously mentioned plastic intensity factor. The relationship between this factor and the J-integral is discussed, and some light is thereby shed on the limits of applicability of elastic fracture mechanics. Again, numerical examples are presented to demonstrate the method.

The report concludes with an overall discussion of the significance of this work and how it may best be utilized in the future. Recommendations are made for paths of future research, particularly with regard to fracture mechanics analyses for pressure vessels under internal or external pressure.

ELASTIC SINGULAR SOLUTIONS BY THE FINITE ELEMENT METHOD

BACKGROUND

The asymptotic behavior of the linear elasticity solution is known (1) for crack problems based on the two-dimensional formulations of plane stress and plane strain and (2) for axisymmetric bodies having external circumferential or internal penny-shaped cracks. In order to exhibit the general character of these near-tip solutions, it is convenient to introduce local polar coordinates at the crack tip with $\theta = \pm \pi$ on the crack faces as shown in Figure 1.

The singular solution for stresses in the vicinity of the crack tip may be written[5] in terms of the primed coordinate system (x′, y′) of Figure 1:

$$\sigma_{x'} = \frac{K_I}{\sqrt{2\pi r}} \cos\frac{\theta}{2}\left(1 - \sin\frac{\theta}{2}\sin\frac{3\theta}{2}\right) - \frac{K_{II}}{\sqrt{2\pi r}} \sin\frac{\theta}{2}\left(2 + \cos\frac{\theta}{2}\cos\frac{3\theta}{2}\right)$$

$$\sigma_{y'} = \frac{K_I}{\sqrt{2\pi r}} \cos\frac{\theta}{2}\left(1 + \sin\frac{\theta}{2}\sin\frac{3\theta}{2}\right) + \frac{K_{II}}{\sqrt{2\pi r}} \sin\frac{\theta}{2}\cos\frac{\theta}{2}\cos\frac{3\theta}{2}$$

$$\sigma_z = \begin{cases} \nu(\sigma_{x'} + \sigma_{y'}) & \text{for plane strain and axisymmetric cases*} \\ 0 & \text{for plane stress} \end{cases} \qquad (1)$$

$$\tau_{x'y'} = \frac{K_I}{\sqrt{2\pi r}} \sin\frac{\theta}{2}\cos\frac{\theta}{2}\cos\frac{3\theta}{2} + \frac{K_{II}}{\sqrt{2\pi r}} \cos\frac{\theta}{2}\left(1 - \sin\frac{\theta}{2}\sin\frac{3\theta}{2}\right)$$

[5] Sih, G.C. and P.C. Paris, "Sympoisum of Fracture Toughness Testing and Its Applications," Am. Soc. Mech. Eng. STP-381 (1965).

*Here σ_z is the out of plane stress for plane strain problems and the circumferential stress in axisymmetric problems.

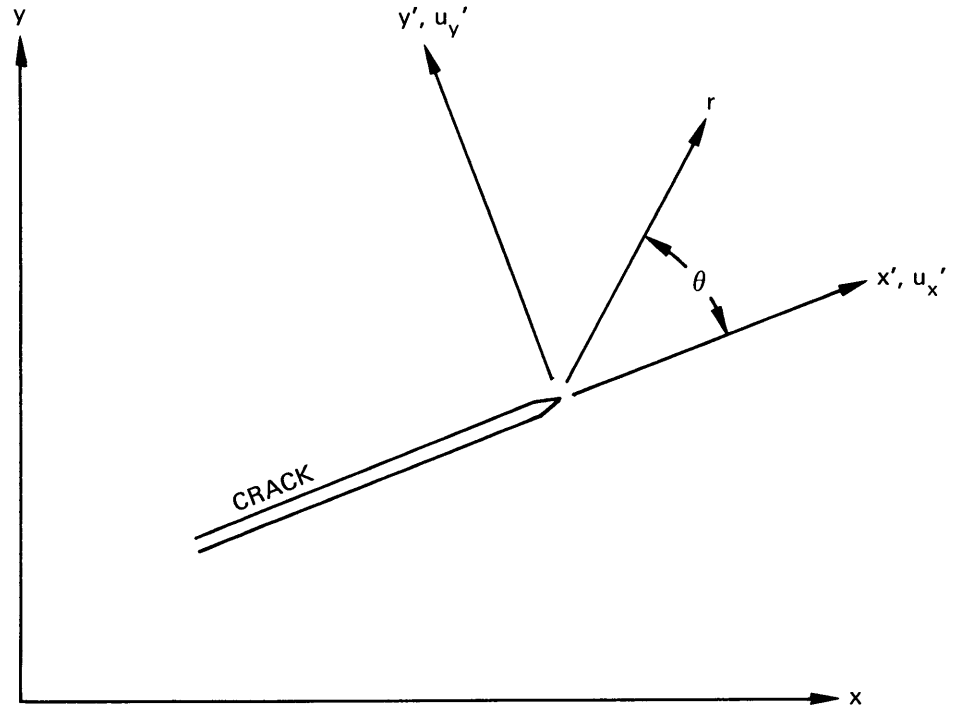

Figure 1 – Polar Coordinate System at Crack Tip

where ν is Poisson's ratio. The shearing components of stress $\tau_{x'z}$ and $\tau_{y'z}$ are nonsingular and, in fact, are zero in plane and axisymmetric problems. Note that the stresses exhibit a singularity of $1/\sqrt{r}$ and thus become infinite at the tip of the crack.*

It is not apparent at first that the singular stress solution, Equation (1), is identical for plane strain and axisymmetric cases. To demonstrate that the singular portion of the axisymmetric solution for crack problems satisfies the plane strain condition, $\sigma_z = \nu\,(\sigma_{x'} + \sigma_{y'})$, note that the circumferential strain component $\epsilon_z = U_x/x$ is nonsingular in any axisymmetric structure since the crack tip cannot coincide with the axis of symmetry (always taken in this report as x = 0). The general three-dimensional stress-strain relations are

$$\sigma_{ij} = \frac{E}{1+\nu}\left[\epsilon_{ij} + \frac{\nu}{1-2\nu}\,\epsilon_{pp}\,\delta_{ij}\right]$$

where E is Young's modulus and δ_{ij} is the Kroneker delta. Neglecting the nonsingular circumferential strain component ϵ_z, the stress-strain relations for the axisymmetric case reduce to

$$\sigma_{x'} = \frac{E}{(1+\nu)(1-2\nu)}\,[\epsilon_{x'}(1-\nu) + \nu\,\epsilon_{y'}]$$

$$\sigma_{y'} = \frac{E}{(1+\nu)(1-2\nu)}\,[\epsilon_{y'}(1-\nu) + \nu\,\epsilon_{x'}]$$

$$\sigma_z = \frac{\nu E}{(1+\nu)(1-2\nu)}\,[\epsilon_{x'} + \epsilon_{y'}]$$

$$\tau_{x'y'} = \frac{E}{2(1+\nu)}\,\gamma_{x'y'}$$

in the immediate vicinity of the crack tip. Adding the first two of these equations yields the result

$$\sigma_{x'} + \sigma_{y'} = \frac{E}{(1+\nu)(1-2\nu)}\,[\epsilon_{x'} + \epsilon_{y'}]$$

---

*This is consistent with the fracture mechanics assumption that the crack tip is infinitely sharp.

By comparing this result with the equation for σ_z, one obtains

$$\sigma_z = \nu (\sigma_{x'} + \sigma_{y'})$$

which is identical to the result for plane strain.

The components of displacement relative to the crack tip are also given in asymptotic form by the near-field elastic solution. These are:

$$u_{x'} = \frac{K_I}{4G}\sqrt{\frac{r}{2\pi}}\left[(2\kappa-1)\cos\frac{\theta}{2} - \cos\frac{3\theta}{2}\right] + \frac{K_{II}}{4G}\sqrt{\frac{r}{2\pi}}\left[(2\kappa+3)\sin\frac{\theta}{2} + \sin\frac{3\theta}{2}\right]$$

$$u_{y'} = \frac{K_I}{4G}\sqrt{\frac{r}{2\pi}}\left[(2\kappa+1)\sin\frac{\theta}{2} - \sin\frac{3\theta}{2}\right] - \frac{K_{II}}{4G}\sqrt{\frac{r}{2\pi}}\left[(2\kappa-3)\cos\frac{\theta}{2} + \cos\frac{3\theta}{2}\right] \quad (2)$$

where $G = \dfrac{E}{2(1+\nu)}$ is the shear modulus and

$$\kappa = \begin{cases} 3 - 4\nu & \text{for plane strain and axisymmetric bodies} \\ \dfrac{3-\nu}{1+\nu} & \text{for plane stress} \end{cases}$$

The stress intensity factors K_I and K_{II}, which relate the near-tip behavior to the global geometry and boundary conditions of the particular problem under consideration, are *not* determined from the preceding asymptotic analysis. The coefficient K_I is the amplitude of the portion of the stress field associated with the opening mode (Mode I) of crack extension whereas K_{II} is the amplitude associated with the in-plane sliding mode of crack deformation (Mode II).

Although the asymptotic solution clearly breaks down at the crack tip where it predicts infinite stresses and strains, it can nevertheless be employed to characterize the crack tip behavior under conditions of small-scale yielding. In other words, if the region in which the assumptions of linear elasticity are violated is sufficiently small, then the elastic singular solution, Equations (1) and (2), accurately describe the state of stress and strain in a domain surrounding the crack tip. Under these conditions, once the stress intensity factors K_I and K_{II} are determined, they can be employed to predict unstable crack propagation as well as to characterize slow crack growth for bodies subjected to cyclic loading.

Since elastic fracture mechanics is based on the stress intensity factors as parameters for correlating fracture results, it is important to develop a numerical procedure which is capable of determining accurate values of K_I and K_{II} for a wide range of structural geometries and loading conditions. The finite element method is one approach which has received considerable attention because of its ability to treat very general geometries and boundary conditions in a standard manner. There are, however, some difficulties in applying the finite element method to crack problems because of the inherent crack tip singularity. Standard finite elements are not capable of representing this singularity; consequently, the usual finite element programs give inaccurate results in the vicinity of the crack tip. What is needed, then, is a combination of the asymptotic solution to describe the near-tip behavior and the finite element solution to describe the behavior away from the crack tip. Several such specialized finite element procedures for crack problems have been developed.[6-11] The finite element approach implemented at NSRDC will be discussed here.

EMBEDDED SINGULARITY FINITE ELEMENT PROCEDURE

The purpose of carrying out a numerical calculation for crack problems is to determine the stress and strain fields in the body containing the crack and, more particularly, to obtain values for the stress intensity factors K_I and K_{II}. The near-tip solution is given by Equations (1) and (2) except for these parameters, which govern its amplitude. The usual finite element approximation can be employed to describe the stress and strain fields accurately everywhere in the body except in the immediate vicinity of the crack tip. Thus in developing a numerical

---

[6]Wilson, W.K., "On Combined Mode Fracture Mechanics," Ph.D. Dissertation, University of Pittsburgh (1969).

[7]Hilton, P.D. and J.W. Hutchinson, "Plastic Intensity Factors for Cracked Plates," Eng. Fract. Mech., Vol. 3 (1971).

[8]Byskov, E., "The Calculation of Stress Intensity Factors Using the Finite Element Method with Cracked Elements," J. Fract. Mech., Vol. 6, No. 2 (1970).

[9]Tracey, D.M., "Finite Elements for Determination of Crack Tip Elastic Stress Intensity Factors," Eng. Fract. Mech., Vol. 3 (1971).

[10]Hilton, P.D. and G.C. Sih, "Application of the Finite Element Method to the Calculation of Stress Intensity Factors," in "Mechanics of Fracture," Vol. 1, Noordhoff, Leydon, Netherlands (1973).

[11]Wilson, W.K., "Finite Element Methods for Elastic Bodies Containing Cracks," in "Mechanics of Fracture," Vol. 1, Noordhoff, Leydon, Netherlands (1973).

procedure for solving crack problems, it is logical to use the asymptotic solution to approximate the solution in the neighborhood of the crack tip and to employ finite elements outside this region, i.e., to embed the known crack tip singularity into the finite element procedure.

This is accomplished by introducing a special circular element[6-11] centered at the crack tip with radius r_0.* Within this element, the singular solution, Equations (1) and (2), is assumed to govern. From Equation (2), the displacement field on the boundary of this element is then given in the local x′-y′ coordinate system of Figure 1 by:

$$
\begin{aligned}
u_{x'} &= u_{0x'} + k_1 \left\{ \frac{(1+\nu)}{2} \sqrt{\frac{r_0}{2\pi}} \left[(2\kappa - 1) \cos \frac{\theta}{2} - \cos \frac{3\theta}{2} \right] \right\} \\
&\quad + k_2 \left\{ \frac{(1+\nu)}{2} \sqrt{\frac{r_0}{2\pi}} \left[(2\kappa + 3) \sin \frac{\theta}{2} + \sin \frac{3\theta}{2} \right] \right\} \\
u_{y'} &= u_{0y'} + k_1 \left\{ \frac{(1+\nu)}{2} \sqrt{\frac{r_0}{2\pi}} \left[(2\kappa + 1) \sin \frac{\theta}{2} - \sin \frac{3\theta}{2} \right] \right\} \\
&\quad - k_2 \left\{ \frac{(1+\nu)}{2} \sqrt{\frac{r_0}{2\pi}} \left[(2\kappa - 3) \cos \frac{\theta}{2} + \cos \frac{3\theta}{2} \right] \right\}
\end{aligned}
\tag{3}
$$

where k_1 and k_2 are normalized stress intensity factors defined by $k_1 = \frac{K_I}{E}$ and $k_2 = \frac{K_{II}}{E}$ and where $u_{0x'}$ and $u_{0y'}$ are displacements of the crack tip in the x′ and y′ directions, respectively. κ is defined in Equation (2). The unknown parameters k_1, k_2, $u_{0x'}$, and $u_{0y'}$ are to be determined through the finite element solution.

The circular singular element, hereinafter referred to as the "core element," is connected to standard finite elements along its boundary by imposing the displacement constraints contained in Equation (3) at all nodal points along the mutual interface; see Figure 2. Thus the core element has a variable number of nodal points (say, N1) along its perimeter, depending on the number and type of standard elements joined to it. It should be noted that if elements with straight edges are employed, there will be geometric incompatibility between the core and the standard finite elements. This has been found to be of negligible effect if a

---

*In cases of Mode I behavior only, the special element becomes a half-disk as described earlier[3] and in other sections of this report.

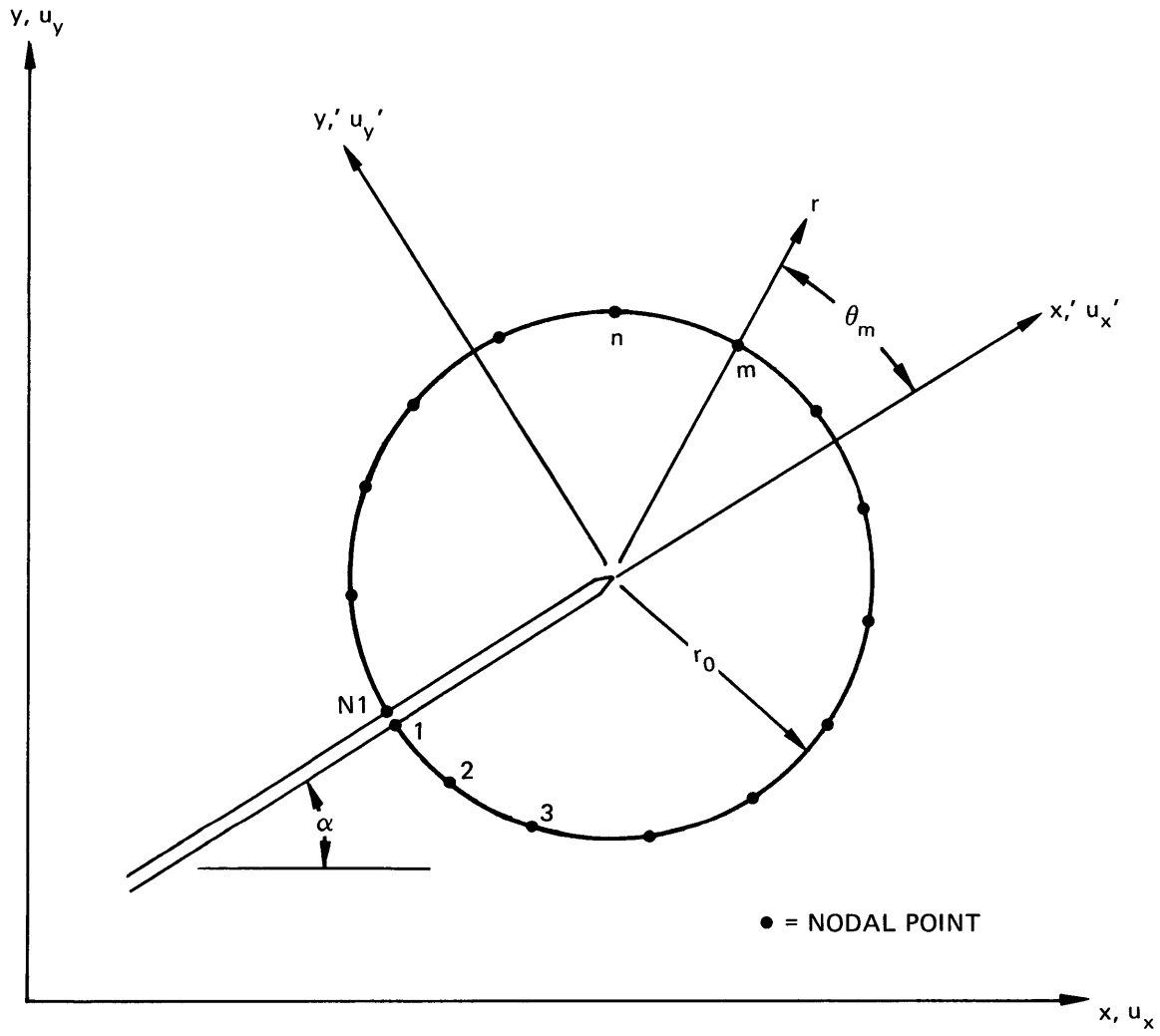

Figure 2 – Singular "Core Element" and Nodal Points Joining Standard Finite Elements

sufficient number of straight-edged elements are joined to the core; the difficulty may be eliminated entirely by the use of higher order isoparametric elements[12] with curved edges. It must also be noted that continuity of displacement between the core element and the standard elements is enforced only at the nodal points. The procedure is nonetheless convergent since—in the limit of decreasing standard element size—continuity of displacements will be restored.[12] This point is discussed in more detail elsewhere,[3,10,11]; it was found that the induced errors are negligible provided (1) a sufficient number of elements surround the core element and (2) that the radius of the core element is sufficiently small.

With these details aside, it is now desirable to transform to the global x-y coordinate system* associated with the particular problem to be considered; the stiffness equations governing the whole structure are generally written in this system. The global nodal displacements along the boundary of the core element are given by

$$\begin{aligned} u_x &= u_{x'} \cos\alpha - u_{y'} \sin\alpha \\ u_y &= u_{x'} \sin\alpha + u_{y'} \cos\alpha \end{aligned} \tag{4}$$

where α is defined in Figure 2. If the nodes about the core element are numbered in a counterclockwise manner from 1 to N1, then the 2(N1) global displacements u_i can be expressed as ($u_i = u_{x_{\frac{i+1}{2}}}$, i odd, $u_i = u_{y_{\frac{i}{2}}}$, i even):

$$\begin{aligned} u_i &= a_{1i}\, k_1 + a_{2i}\, k_2 + a_{3i}\, u_{0x'} + a_{4i}\, u_{0y'} \\ i &= 1, 2, \cdots 2(N1) \end{aligned} \tag{5}$$

where

$$a_{1i} = \begin{cases} \bar{u}_{x1}\left(\theta_{\frac{i+1}{2}}\right) \cos\alpha - \bar{u}_{x2}\left(\theta_{\frac{i+1}{2}}\right) \sin\alpha & \text{i odd} \\ \bar{u}_{x1}\left(\theta_{\frac{i}{2}}\right) \sin\alpha + \bar{u}_{y1}\left(\theta_{\frac{i}{2}}\right) \cos\alpha & \text{i even} \end{cases}$$

---

[12] Zienkiewicz, O.C., "The Finite Element Method in Engineering Science," McGraw-Hill Book Company, London (1971).

*For the axisymmetric case, the y axis always corresponds with the axis of symmetry.

$$a_{2i} = \begin{cases} \bar{u}_{y1}\left(\frac{\theta_{i+1}}{2}\right)\cos\alpha + \bar{u}_{y2}\left(\frac{\theta_{i+1}}{2}\right)\sin\alpha & \text{i odd} \\ \bar{u}_{y1}\left(\frac{\theta_{i}}{2}\right)\sin\alpha - \bar{u}_{y2}\left(\frac{\theta_{i}}{2}\right)\cos\alpha & \text{i even} \end{cases}$$

$$a_{3i} = \begin{cases} \cos\alpha & \text{i odd} \\ \sin\alpha & \text{i even} \end{cases}$$

$$a_{4i} = \begin{cases} -\sin\alpha & \text{i odd} \\ \cos\alpha & \text{i even} \end{cases}$$

In the above, the functions $\bar{u}_{x1}$, $\bar{u}_{y1}$, $\bar{u}_{x2}$, and $\bar{u}_{y2}$ are dependent on the angle θ to node (i+1)/2 or (i/2) which immediately follows the function, and are given by

$$\bar{u}_{x1} = \frac{1+\nu}{2}\sqrt{\frac{r_0}{2\pi}}\left[(2\kappa-1)\cos\frac{\theta}{2} - \cos\frac{3\theta}{2}\right]$$

$$\bar{u}_{y1} = \frac{1+\nu}{2}\sqrt{\frac{r_0}{2\pi}}\left[(2\kappa+3)\sin\frac{\theta}{2} + \sin\frac{3\theta}{2}\right]$$

$$\bar{u}_{x2} = \frac{1+\nu}{2}\sqrt{\frac{r_0}{2\pi}}\left[(2\kappa+1)\sin\frac{\theta}{2} - \sin\frac{3\theta}{2}\right]$$

$$\bar{u}_{y2} = \frac{(1+\nu)}{2}\sqrt{\frac{r_0}{2\pi}}\left[(2\kappa-3)\cos\frac{\theta}{2} + \cos\frac{3\theta}{2}\right]$$

The governing equations for the embedded singularity finite element procedure can be obtained from the variational principle of minimum potential energy[13] in much the same manner as they are determined in standard finite element analysis. The potential energy is expressed as the sum of the strain energies of the elements minus the work done by the

---

[13]Hoff, N.J., "The Analysis of Structures," John Wiley and Sons (1956).

applied forces. (For simplicity, only boundary tractions are considered in this discussion, but body forces can be treated as well.) The potential energy is thus

$$PE = SE_{CORE} + \Sigma\ SE_{EL} - \int_s \Sigma\ T_j\ u_j\ ds \qquad j = x, y \tag{6}$$

Here SE_{CORE} represents the strain energy of the singular element, $\Sigma\ SE_{EL}$ represents the strain energy of all the standard finite elements, and the integral term represents the work done by applied forces resulting from boundary tractions.

The traction integral can be expressed in terms of the displacement components of the nodes on the exterior boundary of the body by standard finite element techniques in the form

$$\int_s \Sigma\ T_j\ u_j\ ds = \Sigma\ R_i\ u_i \qquad \begin{matrix} j = x, y \\ i = 1,2,3\ \cdots \end{matrix}$$

where the R_i terms are the "consistent" concentrated forces acting on external nodes which result from surface tractions.* Similarly, the strain energy of each standard finite element can be expressed in terms of the displacements of its nodes in the form

$$SE_{EL} = 1/2\ \Sigma\ \Sigma\ k_{ij}\ u_i\ u_j$$

where the k_{ij} are terms of the element stiffness matrix [k] found in the usual manner. Thus the real concern here is with the strain energy of the core element, SE_{CORE}, as singled out in Equation (6). The strain energy of the core element is to be determined in terms of k_1, u_{0x}, k_2, and u_{0y}, from the asymptotic solution, Equation (1). The strain energy density (SED) per unit volume is defined as**

$$SED = 1/2 \sum_{i=1}^{2} \sum_{j=1}^{2} \sigma_{ij}\ \epsilon_{ij}$$

Substitution into Equation (1) gives

---

*"Consistent" nodal loads will be discussed in the next section, with particular reference to the special case which arises when tractions are applied to portions of the crack face adjacent to and including the singular core element.

**Again, circumferential strains are of second order in the vicinity of the crack tip; they are therefore ignored in the axisymmetric case.

$$SED = \frac{(1+\nu)\, E\, k_1^2}{8\pi r} \left[(3 + 2\cos\theta - \cos^2\theta) - 4\nu\,(1 + \cos\theta)\right]$$

$$+ \frac{(1+\nu)\, E\, k_2^2}{8\pi r} \left[(3 - 2\cos\theta + 3\cos^2\theta) - 4\nu\,(1 - \cos\theta)\right]$$

for plane strain and axisymmetric cases and

$$SED = \frac{E\, k_1^2}{8\pi r} \left[(3 + 2\cos\theta - \cos^2\theta) - 2\nu\,(1 + \cos\theta)\right]$$

$$+ \frac{E\, k_2^2}{8\pi r} \left[(3 - 2\cos\theta + \cos^2\theta) + \nu\,(2 - 7\cos\theta - 9\cos^3\theta)\right]$$

for plane stress problems.

The strain energy per unit thickness of the singular core element for plane problems is obtained by integrating the strain energy density function over the area of the element, i.e.,

$$SE_{CORE} = \int_{r=0}^{r_0} \int_{\theta=-\pi}^{\pi} (SED)\; r\,dr\,d\theta$$

The result may be expressed rather simply as

$$SE_{CORE} = B_1\, k_1^2 + B_2\, k_2^2 \tag{7a}$$

where

$$B_1 = \begin{cases} \dfrac{(1+\nu)}{2}\, E\, r_0 \left(\dfrac{5}{4} - 2\nu\right) & \text{(plane strain)} \\ \dfrac{E\, r_0}{2} \left(\dfrac{5}{4} - \nu\right) & \text{(plane stress)} \end{cases}$$

$$B_2 = \begin{cases} \dfrac{(1+\nu)}{2} \; E \; r_0 \left(\dfrac{9}{4} - 2\nu\right) & \text{(plane strain)} \\ \dfrac{E \; r_0}{2} \left(\dfrac{7}{4} + \nu\right) & \text{(plane stress)} \end{cases}$$

For the axisymmetric case, the strain energy of the core element is the integral of the strain energy density function over the volume of the now toroidal core element. If $\bar{R}$ is the distance from the y axis to the crack tip, then

$$SE_{CORE} = 2\pi \int_{\theta=-\pi}^{\pi} \int_{r=0}^{r_0} (SED)\,(\bar{R} + r)\, r dr d\theta$$

Again, the result may be put in the simple form of Equation (7a) with

$$\begin{aligned} B_1 &= \pi \, \bar{R} \, (1+\nu) \, E \, r_0 \left(\frac{5}{4} - 2\nu\right) \\ B_2 &= \pi \, \bar{R} \, (1+\nu) \, E \, r_0 \left(\frac{9}{4} - 2\nu\right) \end{aligned} \tag{7b}$$

It should be noted that for simplicity, higher order terms in r_0 are assumed to be negligible and have been omitted in the equations for B_1 and B_2.

With the contributions to the potential energy functional for the plane stress, plane strain, and axisymmetric cases determined in a similar manner, the potential energy of a cracked body in any one of these formulations may now be written in the form

$$PE = B_1 \, k_1^2 + B_2 \, k_2^2 + \frac{1}{2} \sum_{EL} \left(\sum_i \sum_j k_{ij} \, u_i \, u_j \right) - \Sigma \, R_i \, u_i \tag{8}$$

Note that the nodal displacement components for nodes on the boundary of the singular element are prescribed by Equation (5), which involves the unknown crack tip displacements $u_{0x'}$ and $u_{0y'}$ as well as the stress intensity parameters k_1 and k_2.

Minimization of the potential energy functional, Equation (8), with respect to the unknown parameters k_1, $u_{0x'}$, k_2, $u_{0y'}$, and u_i (the subscript on u_i varies only over the nodes not on the core element) leads to the following set of linear algebraic equations:

$$\frac{\partial(PE)}{\partial k_1} = 2 B_1 k_1 + \sum_{EL} \left(\sum_i \sum_j k_{ij} u_i \frac{\partial u_j}{\partial k_1} \right) = 0 \tag{9a}$$

$$\frac{\partial(PE)}{\partial u_{0x'}} = \sum_{EL} \left(\sum_i \sum_j k_{ij} u_i \frac{\partial u_j}{\partial u_{0x'}} \right) = 0 \tag{9b}$$

$$\frac{\partial(PE)}{\partial k_2} = 2 B_2 k_2 + \sum_{EL} \left(\sum_i \sum_j k_{ij} u_i \frac{\partial u_j}{\partial k_2} \right) = 0 \tag{9c}$$

$$\frac{\partial(PE)}{\partial u_{0y'}} = \sum_{EL} \left(\sum_i \sum_j k_{ij} u_i \frac{\partial u_j}{\partial u_{0y'}} \right) = 0 \tag{9d}$$

$$\frac{\partial(PE)}{\partial u_L} = \sum_{EL} \left(\sum_i k_{iL} u_i \right) - R_L = 0 \tag{9e}$$

where L varies over nodal degrees of freedom not associated with the core element.

Now from Equation (5), which constrains the displacements of nodes on the core element,

$$\frac{\partial u_j}{\partial k_1} = \begin{cases} a_{1j} & j \leq 2(N1) \\ 0 & j > 2(N1) \end{cases}$$

$$\frac{\partial u_j}{\partial u_{0x'}} = \begin{cases} a_{3j} & j \leq 2(N1) \\ 0 & j > 2(N1) \end{cases}$$

$$\frac{\partial u_j}{\partial k_2} = \begin{cases} a_{2j} & j \leq 2(N1) \\ 0 & j > 2(N1) \end{cases}$$

$$\frac{\partial u_j}{\partial u_{0y'}} = \begin{cases} a_{4j} & j \leq 2(N1) \\ 0 & j > 2(N1) \end{cases}$$

Thus Equations (9a)–(9d) may be rewritten in the form

$$\left.\begin{aligned}\frac{\partial(PE)}{\partial k_1} &= \left[2B_1 + \sum_{EL}\left(\sum_{i=1}^{2(N1)}\sum_{j=1}^{2(N1)} k_{ij}\, a_{1i}\, a_{1j}\right)\right] k_1 \\ &+ \sum_{EL}\left(\sum_{i=1}^{2(N1)}\sum_{j=1}^{2(N1)} k_{ij}\, a_{3i}\, a_{1j}\right) u_{0x'} + \sum_{EL}\left(\sum_{i=1}^{2(N1)}\sum_{j=1}^{2(N1)} k_{ij}\, a_{2i}\, a_{1j}\right) k_2 \\ &+ \sum_{EL}\left(\sum_{i=1}^{2(N1)}\sum_{j=1}^{2(N1)} k_{ij}\, a_{4i}\, a_{1j}\right) u_{0y'} + \sum_{EL}\sum_{i=2(N1)+1}^{N}\left(\sum_{j=1}^{2(N1)} k_{ij}\, a_{1j}\right) u_i = 0\end{aligned}\right\} \quad (10a)$$

$$\left.\begin{aligned}\frac{\partial(PE)}{\partial u_{0x'}} &= \sum_{EL}\left(\sum_{i=1}^{2(N1)}\sum_{j=1}^{2(N1)} k_{ij}\, a_{1i}\, a_{3j}\right) k_1 + \sum_{EL}\left(\sum_{i=1}^{2(N1)}\sum_{j=1}^{2(N1)} k_{ij}\, a_{3i}\, a_{3j}\right) u_{0x'} \\ &+ \sum_{EL}\left(\sum_{i=1}^{2(N1)}\sum_{j=1}^{2(N1)} k_{ij}\, a_{2i}\, a_{3j}\right) k_2 + \sum_{EL}\left(\sum_{i=1}^{2(N1)}\sum_{j=1}^{2(N1)} k_{ij}\, a_{4i}\, a_{3j}\right) u_{0y'} \\ &+ \sum_{EL}\sum_{i=2(N1)+1}^{N}\left(\sum_{j=1}^{2(N1)} k_{ij}\, a_{3j}\right) u_i = 0\end{aligned}\right\} \quad (10b)$$

$$\left.\begin{aligned}\frac{\partial(PE)}{\partial k_2} &= \sum_{EL}\left(\sum_{i=1}^{2(N1)}\sum_{j=1}^{2(N1)} k_{ij}\, a_{1j}\, a_{2j}\right) k_1 + \sum_{EL}\left(\sum_{i=1}^{2(N1)}\sum_{j=1}^{2(N1)} k_{ij}\, a_{3i}\, a_{2j}\right) u_{0x'} \\ &+ \left[2B_2 + \sum_{EL}\left(\sum_{i=1}^{2(N1)}\sum_{j=1}^{2(N1)} k_{ij}\, a_{2i}\, a_{2j}\right)\right] k_2 + \sum_{EL}\left(\sum_{i=1}^{2(N1)}\sum_{j=1}^{2(N1)} k_{ij}\, a_{4i}\, a_{2j}\right) u_{0y'} \\ &+ \sum_{EL}\sum_{i=2(N1)+1}^{N}\left(\sum_{j=1}^{2(N1)} k_{ij}\, a_{2j}\right) u_i = 0\end{aligned}\right\} \quad (10c)$$

$$\left.\begin{aligned}\frac{\partial(PE)}{\partial u_{0y'}} &= \sum_{EL}\left(\sum_{i=1}^{2(N1)}\sum_{j=1}^{2(N1)} k_{ij}\, a_{1i}\, a_{4j}\right) k_1 + \sum_{EL}\left(\sum_{i=1}^{2(N1)}\sum_{j=1}^{2(N1)} k_{ij}\, a_{3i}\, a_{4j}\right) u_{0x'} \\ &+ \sum_{EL}\left(\sum_{i=1}^{2(N1)}\sum_{j=1}^{2(N1)} k_{ij}\, a_{2i}\, a_{4j}\right) k_2 + \sum_{EL}\left(\sum_{i=1}^{2(N1)}\sum_{j=1}^{2(N1)} k_{ij}\, a_{4i}\, a_{4j}\right) u_{0y'} \\ &+ \sum_{EL}\sum_{i=2(N1)+1}^{N}\left(\sum_{j=1}^{2(N1)} k_{ij}\, a_{4j}\right) u_i = 0\end{aligned}\right\} \quad (10d)$$

In the standard finite element manner, the remaining part of the governing simultaneous equations may be expressed

$$\frac{\partial(PE)}{\partial u_L} = \sum_{E\,L} \sum_{i=2(N\,1)+1}^{N} k_{iL}\, u_i - R_L = 0 \qquad (10e)$$

where L varies over the nodal displacements not on the boundary of the core element and N is equal to twice the number of nodes in the problem idealization.

The set of modified governing equations, Equations (10), can be expressed in the usual finite element matrix form

$$\sum_j K_{ij}\, u_j - R_i = 0 \qquad (11)$$

For simplicity of presentation, the development here implies that $u_1 = k_1$, $u_2 = u_{0x'}$, $u_3 = k_2$, $u_4 = u_{0y'}$, and $R_i = 0^*$ (i = 1,2,3,4). Thus the first four rows of the master stiffness matrix are special whereas the remainder may be developed by standard finite element procedures. It should be pointed out that this simplification is not essential in embedding a singular element (or elements) into a standard finite element mesh; however, it does aid in simplifying the programming and in minimizing additional input data. It should also be noted that the procedures described here in no way affect the positive-definiteness, symmetry, or bandedness of of the master stiffness matrix. Most importantly, however, it is reemphasized that the solution of Equation (11) yields explicit values for the normalized stress intensity factors k_1 and k_2 as well as the crack tip displacements and all nodal displacements throughout the finite element idealization. (Displacements of nodes on the core element are recovered through Equation (5).) Thus strains and stresses may be calculated in all the standard finite elements and, if desired, even in the singular element through the use of Equations (1).

---

*This is not so if surface tractions are prescribed on the crack surfaces adjacent to and including the singular element, as discussed in the next section.

CONSISTENT APPROACH TO CRACK FACE LOADING

As mentioned earlier, the finite element displacement method employed here is derived from the variational principle of minimum potential energy.[13] The displacement field within each element may be expressed in terms of the displacements at the nodes of the element in the form

$$u_x = \Sigma N_i u_{x_i}$$
$$u_y = \Sigma N_i u_{y_i} \qquad (12)$$

where u_{x_i} and u_{y_i} are the x and y displacements at node i. The N_i are known interpolating polynomials frequently referred to as "shape functions." In the absence of body forces, the potential energy for a given finite element subjected to surface tractions may be expressed as

$$PE = SE_{EL} - \int_A \Sigma T_j u_j \, dA \quad (j = x, y)$$

where the strain energy of the element is calculated in terms of the nodal displacement componets in the usual finite element manner and where A denotes the surface area over which tractions are prescribed.

The work done by the surface tractions can be calculated in a manner consistent with the element displacement assumption, Equation (12), by expressing the displacement components along the element surfaces with prescribed tractions in terms of the nodal displacements u_i on the surface, i.e.,

---

[13]Hoff, N.J., "The Analysis of Structures," John Wiley and Sons, New York (1956).

$$u_x/_{SURF} = \Sigma\ N_i/_{SURF}\ u_{x_i}$$

$$u_y/_{SURF} = \Sigma\ N_i/_{SURF}\ u_{y_i}$$

Then the integral $\int_A \Sigma\ T_j\ u_j\ dA$ can be integrated and expressed explicitly in terms of the unknown nodal displacement components in the form

$$\int_A \Sigma\ T_j\ u_j\ dA = \Sigma\ R_i\ u_i$$

Here $u_{2i-1} = u_{x_i}$, $u_{2i} = u_{y_i}$, and the R_i terms are "consistent" concentrated nodal forces equivalent to the distributed tractions. Then for an element, the potential energy as calculated by the finite element procedure becomes

$$PE = \frac{1}{2}\ \Sigma\ \Sigma\ k_{ij}\ u_i\ u_j - \Sigma\ R_i\ u_i$$

Minimization with respect to the unknown nodal displacements gives the usual set of governing equations

$$\sum_j k_{ij}\ u_j - R_i = 0$$

which are assembled in the standard manner into the master stiffness matrix and master load matrix.

Such a procedure is adequate to describe crack face loading for all elements lying on the crack face except for the two elements which join the singular core element and the core element itself. In this region, nonhomogeneous "load" terms arise for the specialized equations corresponding to k_1, u_{0x}, k_2, and u_{0y}, as well as for the equations corresponding to the u_i along the crack face.

In this section, special consideration is given to the procedure for calculating crack face loading terms associated with the embedded singular core element. For convenience, the integral $\int_A \Sigma\ T_j\ u_j\ dA$ is rewritten in terms of a local coordinate system (n,s):

$$\int_A \Sigma\, T_j\, u_j\, dA = \int_s (\sigma_n\, u_n + \tau_{ns}\, u_s)\, dA \tag{13}$$

In the above, n is the unit outward normal to the crack face and s is a unit tangent vector to the crack face measured in a counterclockwise sense about the crack face as shown in Figure 3. The integration is taken in a counterclockwise sense along the crack edges.

Figure 4 shows a typical nodal point layout in the vicinity of the singular crack tip element. Nodes i and j are the extreme nodes of the element on the lower crack surface; nodes k and ℓ are the extreme nodes of the element on the upper crack surface, with nodes j and k lying on the perimeter of the core element.* Special treatment of loading, therefore, must be given to the portion of the crack subject to tractions along the surface i – j – 0 – k – ℓ.

Over this surface, the work integral is divided into four segments, i.e.,

$$\begin{aligned} w = &\int_i^j [\sigma_n\, u_n + \tau_{ns}\, u_s]\, dA + \int_j^0 [\sigma_n\, u_n + \tau_{ns}\, u_s]\, dA \\ &+ \int_0^k [\sigma_n\, u_n + \tau_{ns}\, u_s]\, dA + \int_k^\ell [\sigma_n\, u_n + \tau_{ns}\, u_s]\, dA \end{aligned} \tag{14}$$

The quantities u_n and u_s over each of the integrals may be obtained by evaluating Equations (3) at $\theta = \pm \pi$ or by evaluating Equations (12) at the crack surface as follows:

$$\text{integral 1:} \begin{cases} u_n = -\sin\alpha\, \Sigma\, N_i/_{SURF}\, u_{x_i} + \cos\alpha\, \Sigma\, N_i/_{SURF}\, u_{y_i} = \Sigma\, N_i/_{SURF}\, u_{n_i} \\ u_s = \cos\alpha\, \Sigma\, N_i/_{SURF}\, u_{x_i} + \sin\alpha\, \Sigma\, N_i/_{SURF}\, u_{y_i} = \Sigma\, N_i/_{SURF}\, u_{s_i} \end{cases} \tag{15a}$$

$$\text{integral 2:} \begin{cases} u_n = u_y,\ (r, -\pi) = u_{0y},\ - k_1\, (1+\nu)\, \sqrt{\dfrac{r}{2\pi}}\, (\kappa + 1) \\ u_s = u_x,\ (r, -\pi) = u_{0x},\ - k_2\, (1+\nu)\, \sqrt{\dfrac{r}{2\pi}}\, (\kappa + 1) \end{cases} \tag{15b}$$

*Depending on the standard element used, nodal points may be intermediate to nodes i and j or k and ℓ. These are not shown for simplicity, but account of their possible presence is taken in this development, thus forcing the presentation to be rather general.

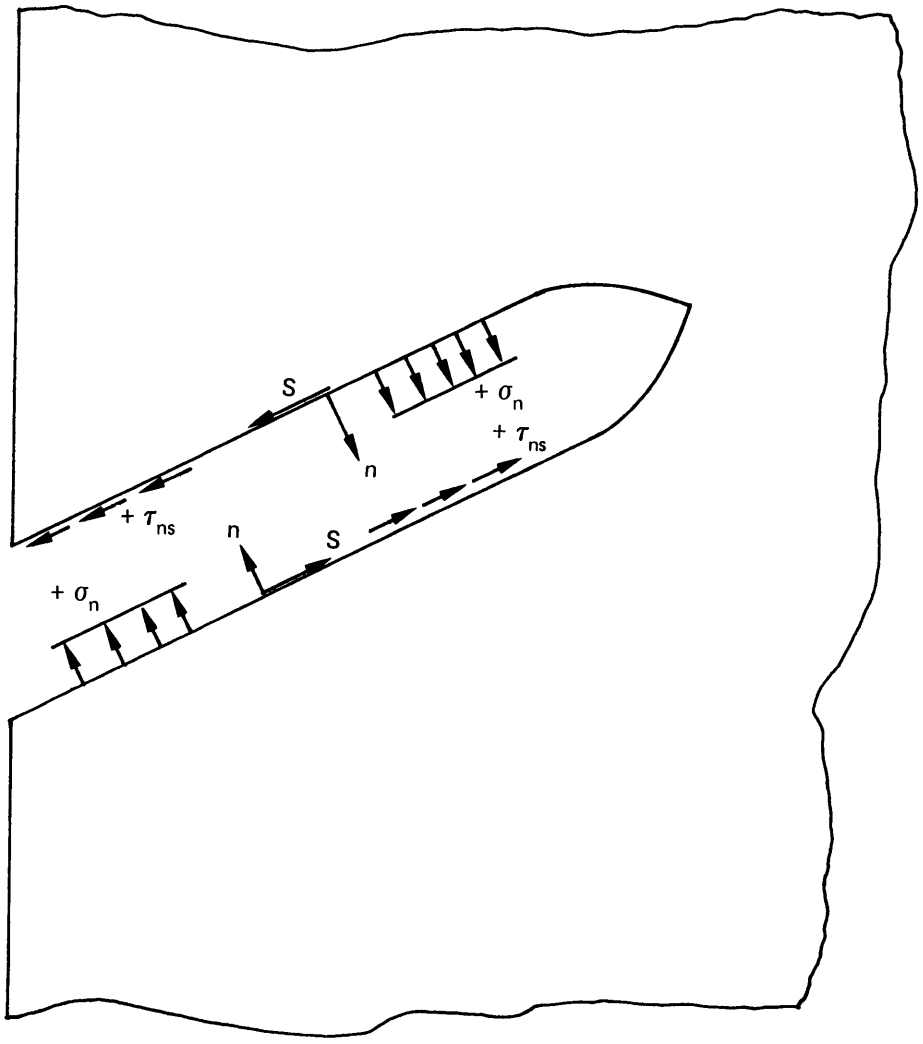

Figure 3 – Sign Convention and Local Coordinate System for Crack Loading

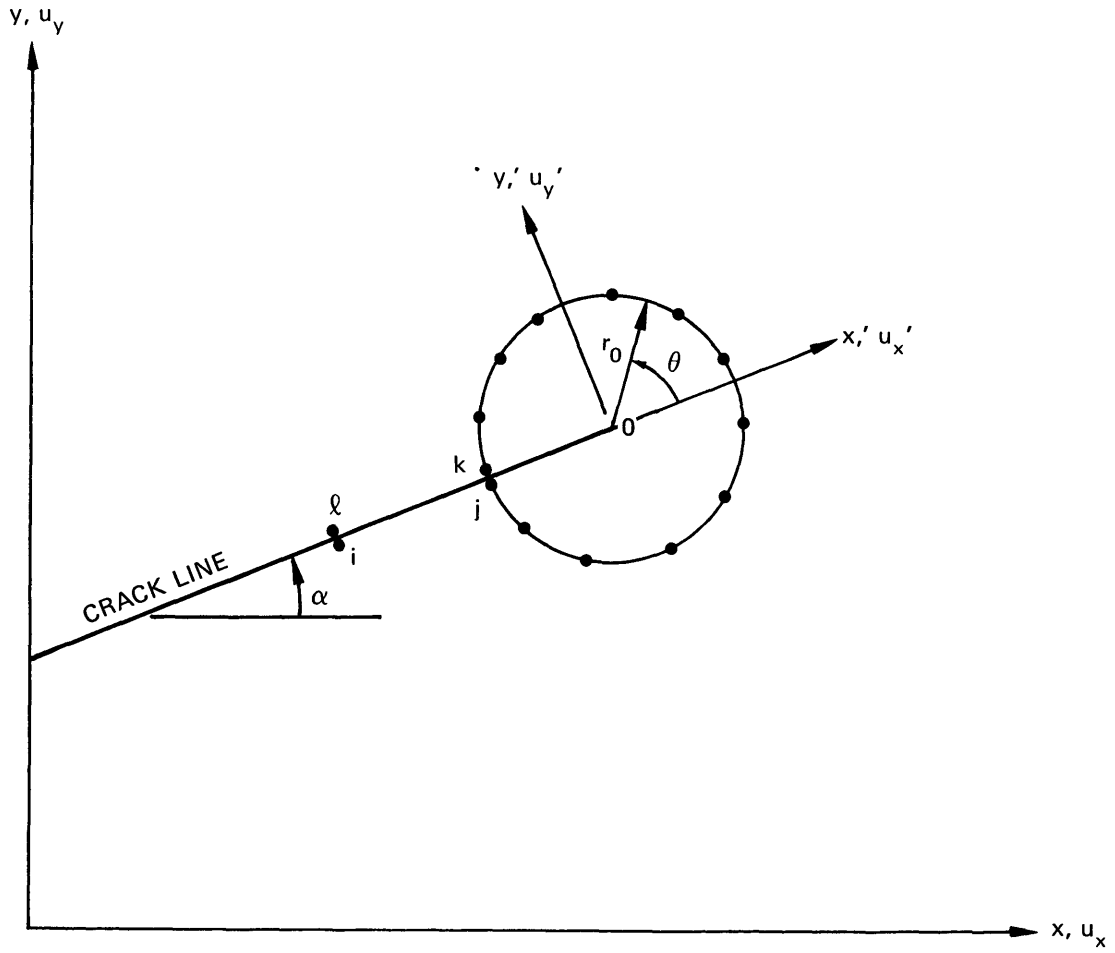

Figure 4 – Nodal Point Configuration in Vicinity of Crack Tip

$$\text{integral 3:} \begin{cases} u_n = -u_{y'}(r, \pi) = -u_{0y'} - k_1 (1+\nu) \sqrt{\dfrac{r}{2\pi}} \quad (\kappa + 1) \\ \\ u_s = -u_{x'}(r, \pi) = -u_{0x'} - k_2 (1+\nu) \sqrt{\dfrac{r}{2\pi}} \quad (\kappa + 1) \end{cases} \tag{15c}$$

$$\text{integral 4:} \begin{cases} u_n = \sin\alpha \, \Sigma \, N_i/_{SURF} \, u_{x_i} - \cos\alpha \, \Sigma \, N_i/_{SURF} \, u_{y_i} = \Sigma \, N_i/_{SURF} \, u_{n_i} \\ \\ u_s = -\cos\alpha \, \Sigma \, N_i/_{SURF} \, u_{x_i} - \sin\alpha \, \Sigma \, N_i/_{SURF} \, u_{y_i} = \Sigma \, N_i/_{SURF} \, u_{s_i} \end{cases} \tag{15d}$$

It would first appear the integrals 1 and 4 are independent of the parameters k_1, $u_{0x'}$, k_2, and $u_{0y'}$. However, the displacement components u_{x_i} and u_{y_i} which correspond to Nodes j or k of Figure 4 must be set equal to the values prescribed by the singular solution, Equations (3), evaluated at r_0 and $-\pi$ and $+\pi$, respectively. Thus these integrals also may contribute to nonhomogeneous "load" terms associated with k_1, $u_{0x'}$, k_2, and $u_{0y'}$.

Now, by substituting Equations (15) into Equations (14), an expression is obtained which may be integrated to give the work integral in terms of k_1, $u_{0x'}$, k_2, and $u_{0y'}$, as well as the nodal displacements associated with the crack face edges of the two elements adjacent to the singular core element. The exact form of this expression will depend on the standard finite element used in conjunction with the embedded singular element. Partial differentiation of this expression with respect to k_1, $u_{0x'}$, k_2, $u_{0y'}$, and the included element nodal displacements will then yield the consistent "load" or nonhomogeneous terms associated with each of these quantities for crack face loading. Special forms of these expressions for the standard finite elements considered in this report are presented in Appendix B for an assumed linear variation of crack face loading.

ELASTIC EXAMPLES

To this point, no mention has been made of the type of two-dimensional finite element to be employed with the singular core element because its formulation is independent of the conventional element type. For purposes of this study, three different finite elements have been examined: the familiar constant stress triangle (CST), a quadrilateral element composed of four constant stress triangles (QUAD-4), and a 12-node isoparametric quadrilateral with a quadratically varying strain field (QUAD-12). These elements are shown in Figure 5, where it must be remembered that the cross section of a full toroidal ring is implied for the axisymmetric case.

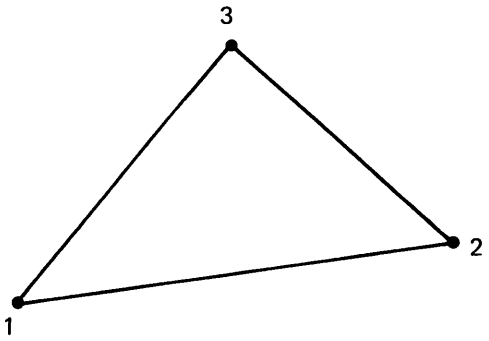

CONSTANT STRESS TRIANGLE (CST)

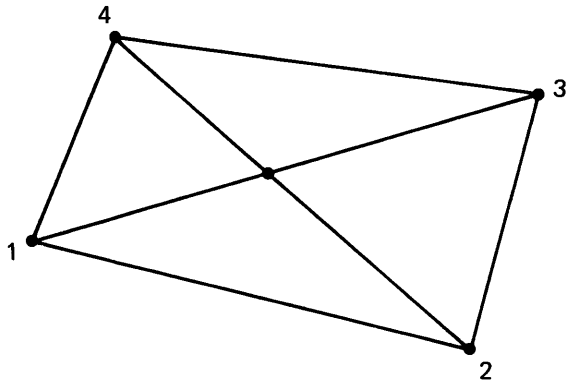

FOUR-NODE QUADRILATERAL (QUAD-4)

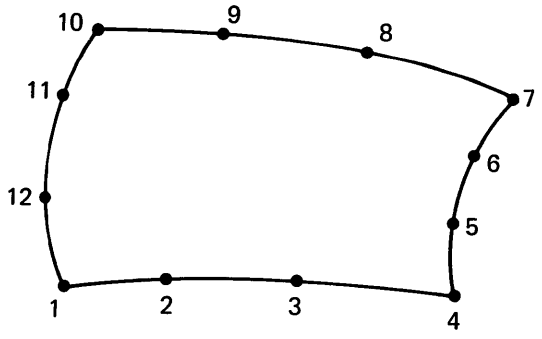

TWELVE-NODE QUADRILATERAL (QUAD-12)

Figure 5 – Finite Elements Employed with Singular Core Element

The QUAD-4 element, which actually has five nodes, is treated as a four-noded element by eliminating the degrees of freedom associated with the interior nodal point by means of static condensation,[14] resulting in a computationally economic formulation. Of the three element types considered, only the QUAD-12 element may have curved edges, assuring geometric continuity along the interface with the core element. However, as mentioned previously, such continuity is not a necessary requirement for good accuracy. The stiffness formulation for each of these elements may be found in Zienkiewicz.[12]

Figures 6–8 present typical idealizations of Mode I types of crack problems obtained by using the three different elements. Idealizations for combined mode problems, in which a full circle represents the singular element, may immediately be envisioned. The following elastic examples will be considered here:

1. Double-edge notched plate, Mode I
2. Single-edge notched plate, Mode I
   a. Accuracy study for remote tension
   b. Concentrated load at the crack face
3. Slant crack in tensile specimen, combined modes
4. Hollow cylinder with interior slant crack, combined modes

As will be discussed later, the QUAD-12 element has proven most convenient for calculations of this type. Pertinent details concerning idealization versus accuracy will be given along with various values calculated for the stress intensity factors in the examples that follow.

DOUBLE-EDGE NOTCHED PLATE

Representative results for three different geometries of double-edge notched plates are presented in Table 1 for idealizations using the three element types considered in this study. Reference values for K_I for the first two geometries, for which the half-length to width ratio is great enough to assume an infinitely long strip, were computed according to formulas derived from Bowie[15] as presented in Brown and Srawley.[16] For the third geometry, the length of the specimen is equal to its width and has a significant influence on K_I. The reference value for this case is taken from Pian.[17] In all cases, the reference values for K_I are considered to be within 1 to 2 percent of their exact values.

---

[14]Przemieniecki, J.S., "Theory of Matrix Structural Analysis," McGraw-Hill Book Company, New York (1968).

[15]Bowie, O.L., "Rectangular Tensile Sheet with Symmetric Edge Cracks," Am. Soc. Mech. Eng., Paper 64-APM-3 (1964).

[16]Brown, W.F. Jr. and J.E. Srawley, "Plane Strain Crack Toughness Testing of High Strength Metallic Materials," Am. Soc. Testing Mat STP-410 (1967).

[17]Pian, T.H.H., "Hybrid Models," International Symposium on Numerical and Computer Methods in Structural Mechanics, University of Illinois, Urbana (8–10 Sep 1971).

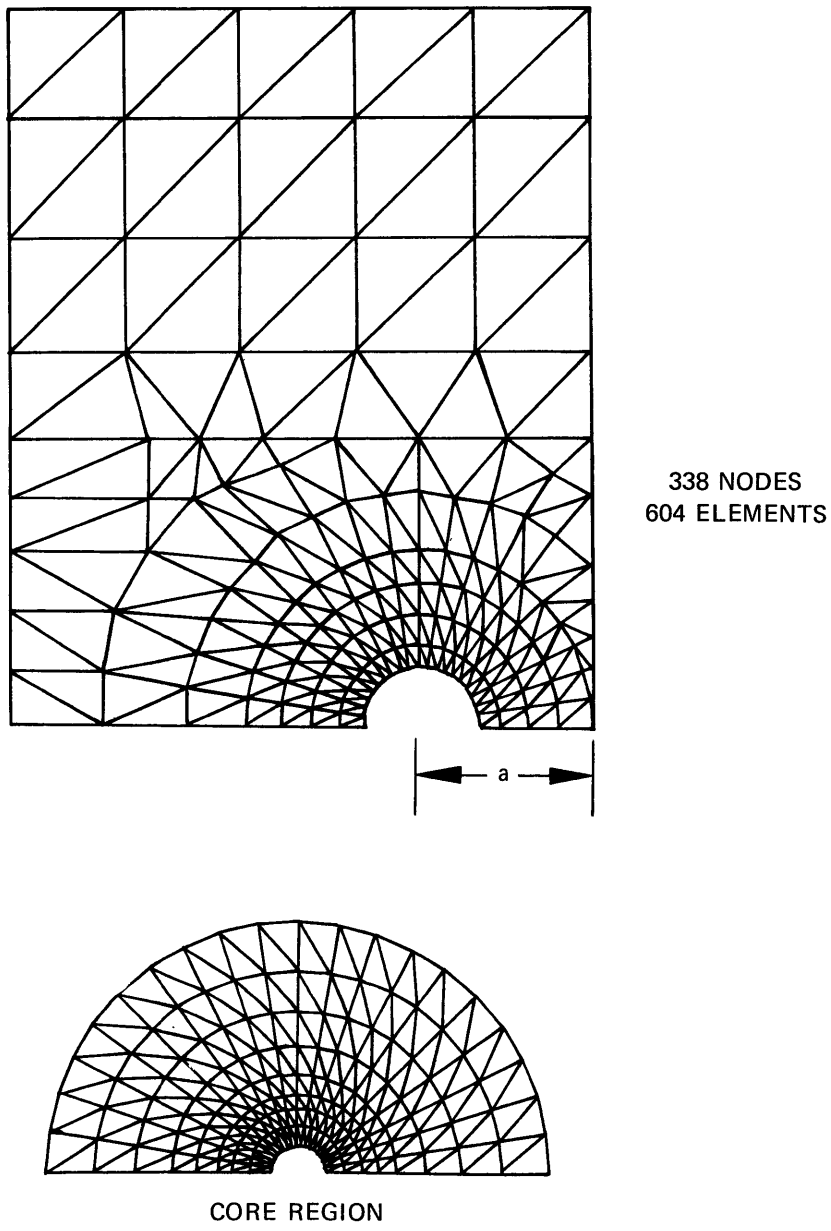

Figure 6 – Typical Mode I Crack Idealization Using CST Elements

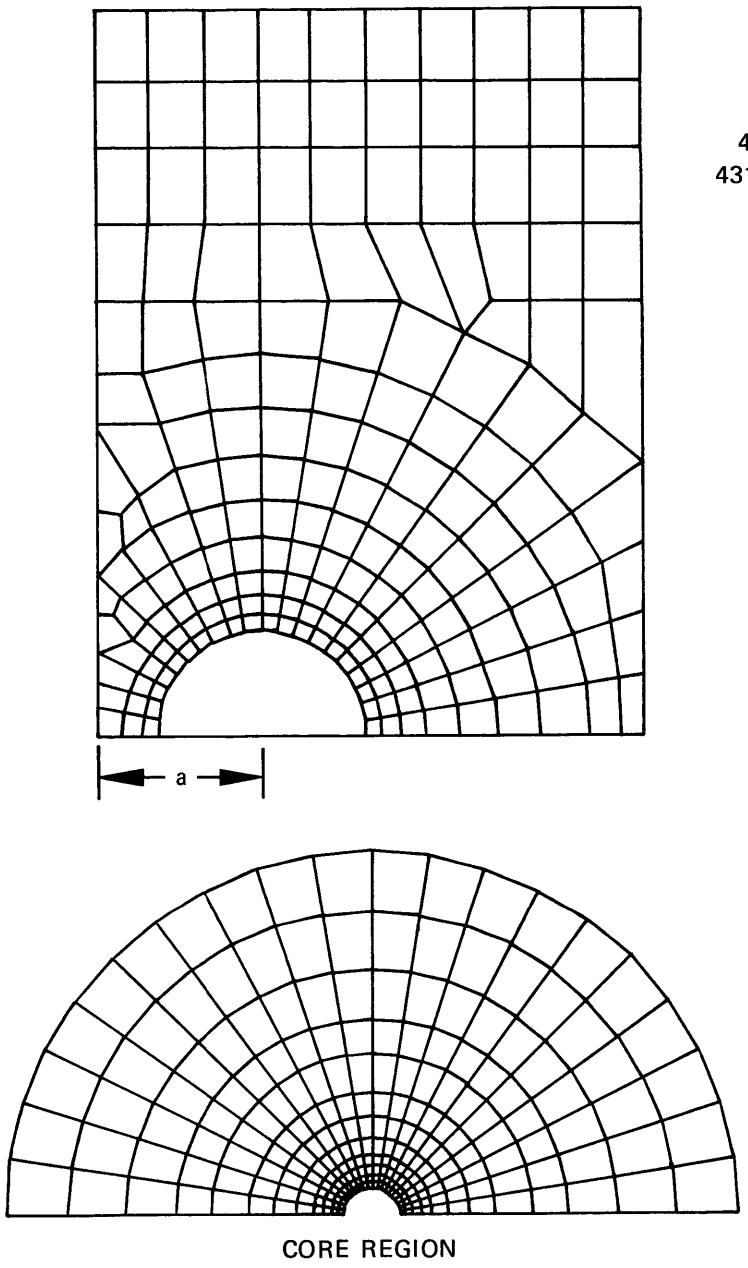

Figure 7 – Typical Mode I Crack Idealization Using QUAD-4 Elements

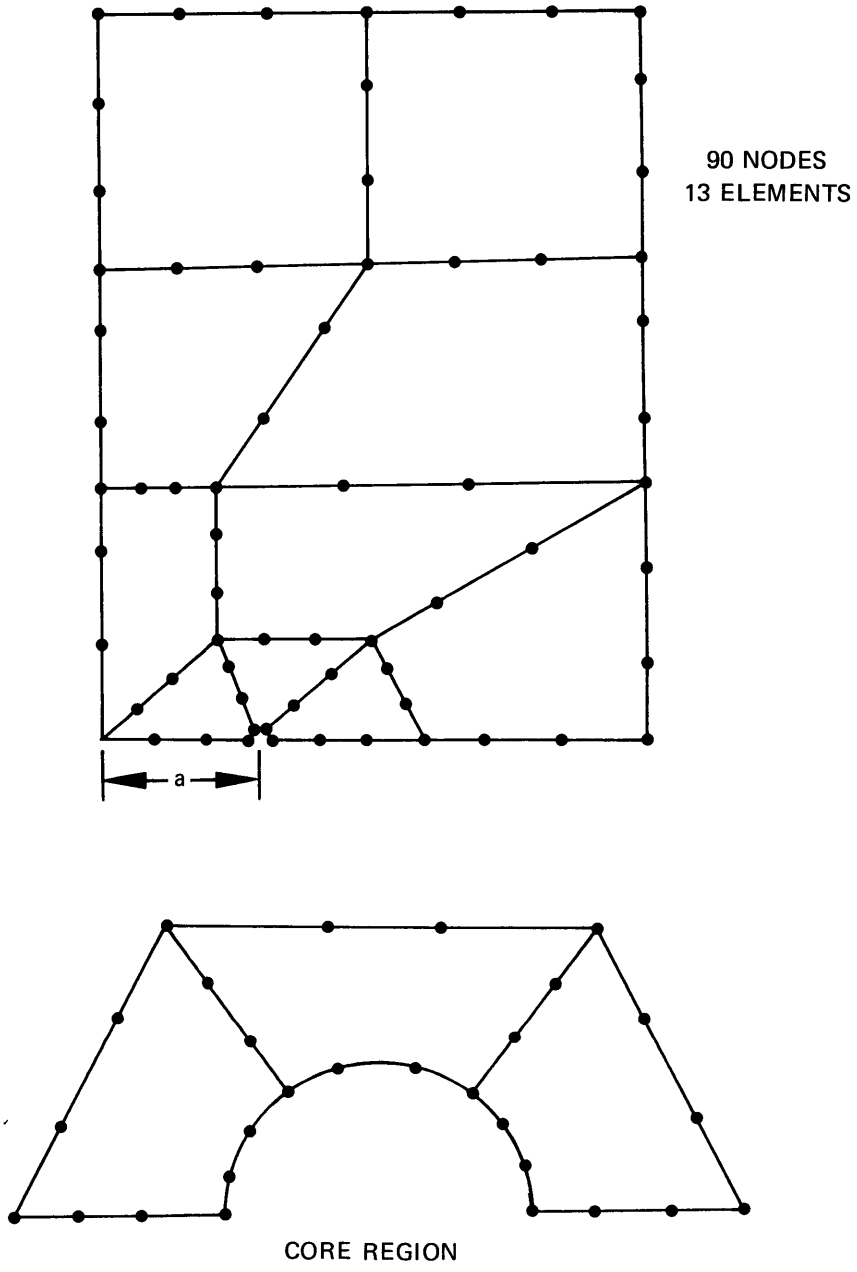

Figure 8 – Typical Mode I Crack Idealization Using QUAD-12 Elements

TABLE 1 - MODE I STRESS INTENSITY FACTORS FOR DIFFERENT ELEMENTS AND GEOMETRIES (DOUBLE-EDGE NOTCHED PLANE STRAIN SPECIMENS)

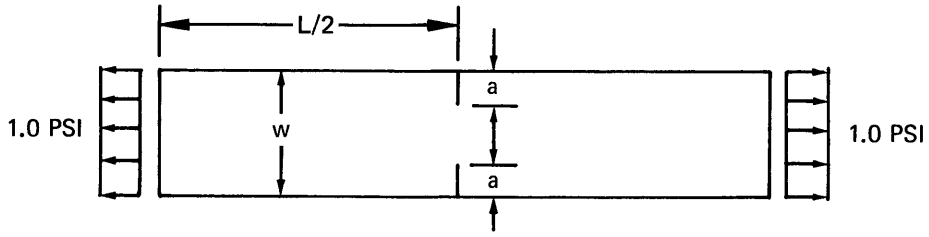

Case 1 – a = 1, W = 5, 2a/w = 0.4, w/L = 0.125, Ref. K_I = 2.00 [16]					
Element Type	Nodes on Core	Total Nodes	Total Elements	Computed K_I	Percent Error
CST	21	247	421	1.78	−11.0
QUAD- 4	13	226	190	1.97	− 1.5
QUAD-12	10	100	15	2.02	+ 1.0

Case 2 – a = 1.5, W = 5, 2a/w = 0.6, w/L = 0.125, Ref. K_I = 2.66 [16]					
Element Type	Nodes on Core	Total Nodes	Total Elements	Computed K_I	Percent Error
QUAD- 4	13	226	140	2.65	− 0.3
QUAD-12	10	100	15	2.71	+ 1.9

Case 3 – a = 0.4109, W = 2.1401, 2a/w = 0.384, w/L = 1, Ref. K_I = 1.405 [17]					
Element Type	Nodes on Core	Total Nodes	Total Elements	Computed K_I	Percent Error
CST	27	372	652	1.343	− 4.4
QUAD-12	13	126	19	1.445	+ 2.8

Notes: 1. Radius of the core element r_0 is taken as 2 percent of the crack length for all cases.

2. The number of nodes indicated for the QUAD-4 element refer to the four nodes per element achieved after static condensation for the interior node.

Table 1 is not intended to demonstrate or compare the relative accuracy and ability of each element type. Such an undertaking is beyond the scope of this work. It is included in the report to indicate that reasonable accuracy may be obtained by using any of the three element types considered here. However, it must be noted that for Case 1, a coarse mesh of CST elements (normally a necessity when considering combined mode problems with an augmented "standard" finite element program) can result in inaccuracies which may not be considered acceptable. Some time ago, the authors suspected—and later found—that the higher the "order" of the standard finite element, the more accurate would be the embedded singularity approach to crack problems. This has proven to be true despite the fact that in general, with a higher order element, fewer nodal points will join the boundary of the singular element. For these reasons, it is of interest to briefly discuss the merits of only the QUAD-4 and QUAD-12 elements, both of which have been shown capable of providing accuracy to 3 percent and less for Mode I problems.

The QUAD-4 element has been incorporated in a completely "in-core" program developed at Lehigh University expressly for the purpose of performing fracture mechanics computations. Fracture computations using the QUAD-12 element, on the other hand, have been incorporated at NSRDC in a new "out-of-core" program designed to minimize core storage requirements. These differing programming philosophies give the edge in computing time required for about the same degree of accuracy to the QUAD-4 element. Moreover, being a combination of four constant stress triangles and having a very small area compared to the overall structural dimensions, the QUAD-4 element makes a ready candidate for elastic-plastic calculations which will be discussed subsequently. On the bad side, the QUAD-4 grid pattern must be fairly fine, resulting in high manpower costs to construct (or generate) and verify a suitable element pattern. A suitable mesh and all necessary and verified input data for the QUAD-12 element, on the other hand, may usually be produced in about one or two man hours and run immediately on the computer, turnaround time being measured in minutes.

For these reasons, the QUAD-12 element has been pursued for elastic Mode I and combined mode calculations (the higher computer costs are more than offset by the lower engineering costs) and the QUAD-4 element will be reserved for elastic-plastic calculations (the lower computer costs for an iterative plastic solution tend to offset the higher cost of mesh generation) discussed later. These preferences, however, are not necessarily permanent. The QUAD-12 element has been implemented only recently and has not yet been extended to enable plastic calculations.* Neither is it certain at this time whether the computing time for

*Work is currently underway which will result in plastic capability for the QUAD-12 element.

the QUAD-12 will remain greater than that for the QUAD-4 for a given degree of accuracy. The QUAD-12 program is relatively new, but minor revisions have already cut computing time by a factor of 10.

SINGLE-EDGE NOTCHED PLATE

Since the isoparametric QUAD-12 element has been adopted for elastic fracture mechanics applications, the question arises as to what type of finite element grid about the singular crack tip region will yield desirable accuracy. Table 2 attempts to answer this question in a limited sense by examining results for a single notch, compact plane strain specimen under Mode I loading conditions. The reference value for K_I for this specimen is believed to be extremely accurate inasmuch as it was first published in 1965[18] and later republished in 1973.[1,19] For comparative purposes here, the reference value of 4.016 psi $\sqrt{\text{in.}}$ will be assumed to be "exact."

Assuming that the finite element grid is suitable elsewhere for proper representation of the problem, accuracy has been found to depend on three factors that are pertinent near the singular core element:

1. The radius of the core element as a percentage of the crack length.
2. The number of nodes along the boundary of the singular core element.
3. Somewhat surprisingly, the ratio of the basic dimension h of the standard QUAD-12 elements joined to the core to the radius r_0 of the singular core element.

For a value of r_0 of 2 percent of the crack length, accuracy is given for various values of h/r_0 for 7 core nodes in Table 2a, for 10 core nodes in Table 2b, and for 13 core nodes in Table 2c. In addition, Table 2b demonstrates the effect of changing the core radius over values of 1 to 3 percent of the crack length. The finite element grid corresponding to each tabulation of results is also shown. These grids were chosen so that nearly the same number of elements was required to model the complete problem for each case; accordingly, uniformity of the element pattern remote from the crack tip could be maintained only approximately. These differences are thought to have little or no bearing on the results of the accuracy study.

Table 2 brings out several rather surprising results and perhaps raises more questions than it answers. Nonetheless, some very important imformation and some useful (though not rigorously proven) conclusions can be drawn. Among the surprising results are:

---

[18] Bowie, O.L. and D.M. Neal, "Single Edge Crack in Rectangular Tensile Sheet," J. Appl. Mech., Vol. 32 (1965).

[19] Bowie, O.L., "Solutions of Plane Crack Problems by Mapping Techniques," in "Mechanics of Fracture," Vol. 1 Noordhoff, Leydon, Netherlands (1973).

TABLE 2 – ERROR IN K_I FOR SINGLE-EDGE NOTCHED COMPACT SPECIMEN AS A FUNCTION OF CRACK TIP GRID PATTERN

TABLE 2a WITH 7 CORE NODES

Reference K_I = 4.016 [1]

	r_0 = 0.02 a = 0.03	
h/r_0	K_I	Percent Error
1	4.075	+1.5
6	4.070	+1.3
12	4.098	+2.0

FIXED GRID PATTERN

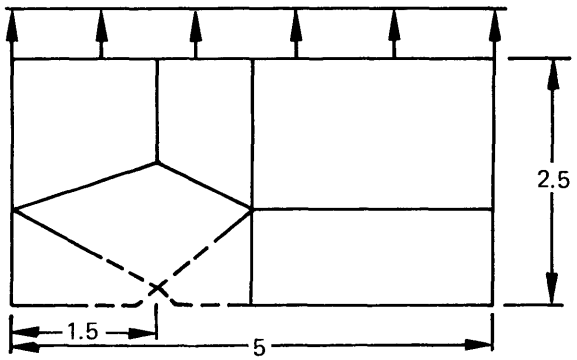

CORE REGION–VARIABLE GRID

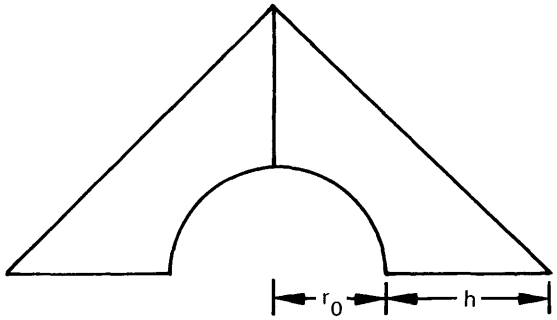

TABLE 2b WITH 10 CORE NODES

Reference K_I = 4.016 [1]

		r_0 = 0.01 a = 0.015		r_0 = 0.02 a = 0.03		r_0 = 0.03 a = 0.045	
Case	h/r_0	K_I	Percent Error	K_I	Percent Error	K_I	Percent Error
1	1	5.028	+25.2	4.357	+8.5	4.148	+3.3
2	2	4.652	+15.8	4.189	+4.3	4.063	+1.2
3	4	4.320	+ 7.6	4.068	+1.3	4.014	–0.05
4	6	4.189	+ 4.3	4.038	+0.5	4.012	–0.1
5	9	4.124	+ 2.7	4.040	+0.6	4.034	+0.4
6	12	4.122	+ 2.6	4.078	+1.5	4.071	+1.4
7	15	4.150	+ 3.3	4.122	+2.6	4.115	+2.5

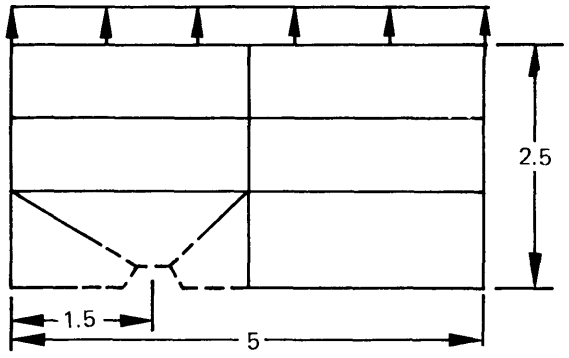

FIXED GRID PATTERN

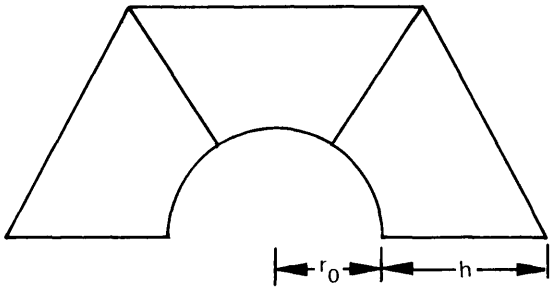

CORE REGION–VARIABLE GRID

TABLE 2c - WITH 13 CORE NODES

Reference K_I = 4.016 [1]

	r_0 = 0.02 a = 0.03	
h/r_0	K_I	Percent Error
1	4.332	+7.9
6	4.030	+0.3
12	4.071	+1.4

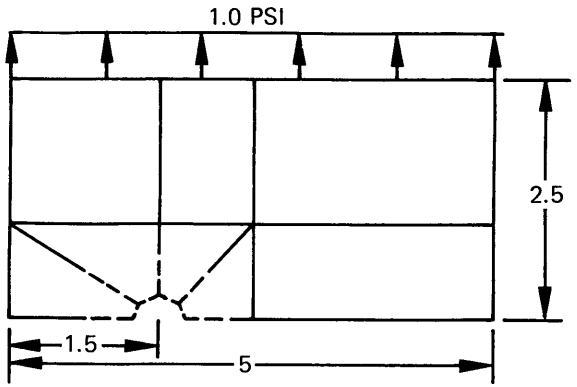

FIXED GRID PATTERN

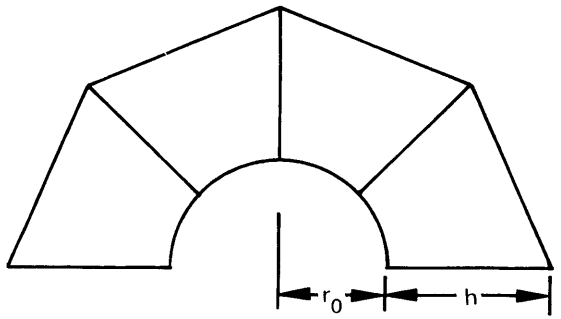

CORE REGION–VARIABLE GRID

1. Although the values predicted for K_I were generally quite accurate, they were persistently higher than the reference value. This is in contrast to predictions made by lower order standard finite elements and in conflict with what one would intuitively expect from a displacement finite element formulation. Such a result could be considered fortuitous, however, in that conservative predictions can be anticipated for K_I with the present formulation and within the range of parameters considered.

2. For a given value of r_0, the accuracy for 10-node and 13-node core elements showed a marked dependence on the ratio h/r_0, but such dependence was not found for the 7-node element. Further, such dependence increased as the value for r_0 decreased.

3. Accuracy of the 7-node core element was within 2 percent of the reference value for the complete range of h/r_0 studied. This unexpected result merits future study since, if verified as consistently true, some savings could result from using a coarser grid pattern. For present purposes, however, this strange result will be attributed to "happenstance."

4. As shown in Table 2b, where three different values of r_0 are compared, accuracy increased as r_0 increased from 1 to 3 percent of the crack length for any given value of h/r_0. This is opposite to the trend found with QUAD-4 elements, where K_I was found to be 2.1 percent low with r_0 equal to 2 percent of the crack length, and 1.9 percent low with r_0 equal to 1 percent of the crack length.

Despite these surprises, some rather positive, if tentative, conclusions can also be drawn from Tables 2:

1. Ten nodes on the singular element (19 for the combined mode case with a full core) are adequate for good accuracy. For constant r_0 and h/r_0, accuracy may be improved by the addition of more nodes on the core element.

2. The radius of the core element has a definite and major effect on accuracy. This is not surprising inasmuch as it dictates the distance from the crack tip at which the singular solution ends and the conventional finite element solution begins. It appears that the "best" value for r_0 lies in the range of 2 to 3 percent of the crack length.

3. The "best" value for the ratio h/r_0 (for no explainable reason) lies in the range of about 5 to 10.

In summary, it appears that if r_0 is taken between 2 and 3 percent of the crack length, if at least 10 nodes are assigned to the half-core element, and if the ratio h/r_0 is kept in the range of 5 to 10, accuracy to within 2 percent can be expected on the conservative side for problems similar to the one considered here. It does not appear at all unrealistic to expect accuracy, under the above-mentioned restrictions, to within a maximum of 5 percent (and probably considerably less) for other fracture problems. This conclusion is borne out in the QUAD-12 examples presented in Table 1, where 10 nodes were assigned to the core, r_0 was taken as 2 percent of the crack length, and h/r_0 was taken as 6.

CONCENTRATED LOAD ON CRACK FACE

Table 3 shows the results obtained for the case of a concentrated load applied at five different positions along the crack face for five different geometries of a single-edge notched plane strain specimen. In each case, the arrangement of nodes and elements about the core was similar to that shown in Table 2b, with r_0 taken as 2 percent of the crack length and h/r_0 taken as 5. Since an exact, closed-form reference solution was not available, an approximate asymptotic interpolation formula was derived for comparison purposes as presented in Appendix C. The formula is in the form of a polynomial approximation; it was found that the best agreement with the finite element solution was obtained for the fourth order polynomial. In addition, the table shows some comparisons with results generated at NSRDC by using the CHILES fracture mechanics code developed by Benzley and Beisinger at Sandia Laboratories[20] and with results for an infinitely wide plate as presented in Hartranft and Sih.[21]

SLANT CRACK IN TENSILE SPECIMEN

A slanted crack in a tensile specimen is one of only a very few combined mode problems for which reference solutions have been published. The reference values of K_I and K_{II}* for the geometry shown with Table 4 were taken from graphs presented by Bowie.[19] It is highly doubtful (even if the Bowie calculations are exact) that these reference values (1.86 and 0.88, respectively) are much more accurate than about 3 percent, inasmuch as this much error appeared inherent in reading the Bowie graphs.[19] For these reasons, only three calculations were performed for this specimen, one with 13 nodes about the full core element with $h/r_0 = 2$ and two with 19 nodes about the full core element with h/r_0 values of 1 and 6. In all cases, the radius r_0 of the core element was taken as 2 percent of the crack length.

---

[20]Benzley, S.E. and Z.E. Beisinger, "CHILES–A Finite Element Computer Program That Calculates the Intensities of Linear Elastic Singularities," Sandia Laboratories Report SLA-73-0894 (Sep 1973).

[21]Hartranft, R.J. and G.C. Sih, "Alternating Method Applied to Edge and Surface Crack Problems," in "Methods of Analysis and Solution of Crack Problems," Noordhoff, Leydon, Netherlands (1973).

[22]Sih, G.C., "Introductory Chapter: A Special Theory of Crack Propagation," in "Mechanics of Fracture," Noordhoff, Leydon, Netherlands (1973).

*Sih[22] presents an interesting theory of crack propagation under combined mode conditions.

TABLE 3 -- VALUES OF K_I COMPUTED BY VARIOUS METHODS FOR SINGLE-EDGE NOTCHED SPECIMEN WITH CONCENTRATED LOAD ON CRACK FACE

Case	P	b	QUAD-12	Chiles[20]	Asymp. Fourth Order	Ref. 21*
a/w = 0.05 L/w = 0.5	0.25	0	0.0747		0.0832	0.0817
	0.5	5	0.149		0.166	0.164
	0.5	10	0.156		0.174	0.171
	0.5	15	0.193		0.209	0.207
	0.5	18	0.323		0.300	0.299
a/w = 0.1 L/w = 1.0	0.25	0	0.0913		0.0882	
	0.5	5	0.177		0.176	
	0.5	10	0.179		0.182	
	0.5	15	0.209		0.216	
	0.5	18	0.333		0.306	
a/w = 0.2 L/w = 2.0	0.25	0	0.122	0.116	0.110	
	0.5	5	0.230	0.224	0.216	
	0.5	10	0.220	0.230	0.217	
	0.5	15	0.238	0.217	0.245	
	0.5	18	0.351		0.328	
a/w = 0.333 L/w = 3.33	0.25	0	0.189		0.173	
	0.5	5	0.336		0.329	
	0.5	10	0.304		0.318	
	0.5	15	0.292		0.330	
	0.5	18	0.384		0.396	
a/w = 0.4 L/w = 4.0	0.25	0	0.242		0.226	
	0.5	5	0.422		0.424	
	0.5	10	0.370		0.402	
	0.5	15	0.334		0.401	
	0.5	18	0.409		0.453	

*Independent of a/w.

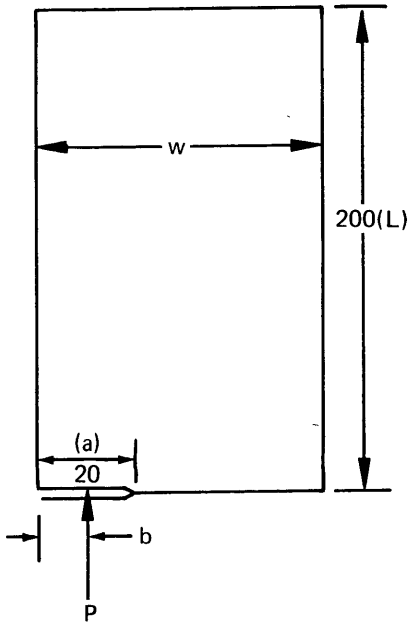

TABLE 4 RESULTS FOR SLANT CRACK IN TENSILE SPECIMEN

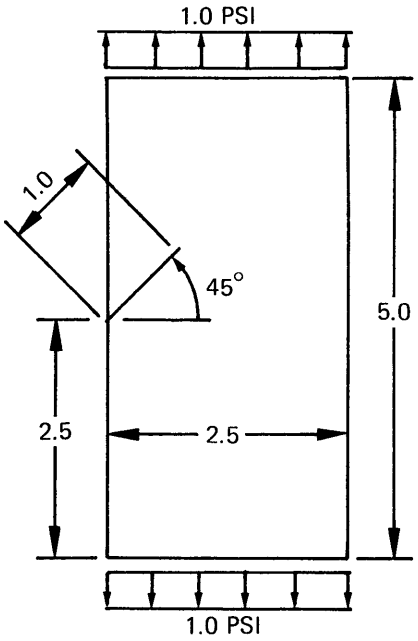

a/w = 0.4, L/w = 2, Ref. $K_I \approx 1.86$, Ref. $K_{II} \approx 0.88$ (Bowie[19])

Case	Total Nodes	Total Elements	Core Nodes	h/r_0	Cal. K_I	Percent Error	Cal. K_{II}	Percent Error
1	85	12	13	2	1.83	−1.6	0.91	+3.4
2	111	16	19	1	1.98	+6.5	0.94	+6.8
3	111	16	19	6	1.84	−1.1	0.89	+1.1

As will be observed from Table 4, results are less than 4 percent off the reference values if the guidelines to accuracy discussed previously are maintained. In any case, they are within 7 percent of the reference values. Based on the previous accuracy study, the underprediction of K_I in two cases raises the strong suspicion that the reference value derived from Bowie[19] was slightly in error on the high side. Irregardless, taking Case 3 of Table 4 as the recommended way of solving this problem (as dictated by the accuracy study), the results indicate that combined mode calculations can be performed with the same accuracy found for Mode I problems.

HOLLOW CYLINDER WITH INTERIOR SLANT CRACK

The final example is one of many interesting cases for which the authors were unable to find a previous solution—that of a hollow-cylinder under axial load containing an internal circumferential crack slanted at 22.5 degrees with respect to the normal to the cylinder surface. The geometry considered is shown in Figure 9. This is not an academic problem inasmuch as it represents a possible occurrence at a girth weld joining two similar cylinders.

Following the information gained from the accuracy tests, the core radius was taken as 2 percent of the crack length, 19 nodes were placed on the core element, and the ratio h/r_0 was taken as 8. The problem was modeled by using 139 nodes and 21 QUAD-12 elements. The element mesh was of the same order of refinement as used in the accuracy tests.

For a unit stress remote load, the values predicted for K_I and K_{II} were 1.135 and 0.2672, respectively. As a matter of curiosity, the same element mesh was run as a plane strain problem, resulting in values for K_I and K_{II} of 1.146 and 0.2781, respectively. These slightly higher values are in accord with expectations inasmuch as the ratio of ligament area to cracked area is slightly greater in the axisymmetric case. Based on the sum of previous experience with the QUAD-12 element, these values for the stress intensity factors are believed to be within 3 percent of their exact values.

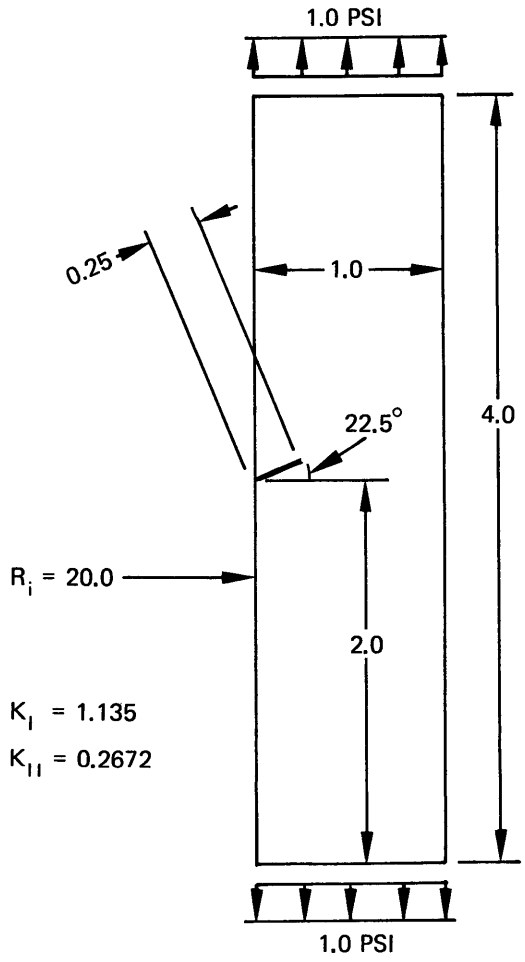

Figure 9 – Geometry of Hollow Cylinder with Interior Slant Crack

REVIEW OF PREVIOUS WORK

The applicability of elastic stress analysis to the prediction of crack propagation is limited to situations in which the plastic region surrounding the crack tip is relatively small.* Efforts to characterize the influence of plasticity on the fracture process have resulted in some significant accomplishments. Attention will be directed to planar and axisymmetric structures under Mode I loading conditions; relatively little research has been successful beyond this range although Shih has recently presented the combined mode plastic singular solution for plane strain[23] and for plane stress.[24]

Rice[25-27] and Hutchinson[28,29] have determined the character of the plastic stress and strain fields asymptotically close to the crack tip for a material obeying the Ramberg-Osgood tensile stress-strain relations, i.e.,

$$\epsilon = \begin{cases} \sigma & \sigma \leqslant 1 \\ \sigma^n & \sigma > 1 \end{cases} \tag{16}$$

where σ is the stress divided by the yield stress and ϵ is the strain normalized by its value at yield; n, the hardening coefficient, is an experimentally determined constant.** The asymptotic solution, which is based on the J_2, small strain, deformation theory of plasticity

---

*I.e., small with respect to crack length and the in-plane structural dimensions.

**Note that perfectly elastic and elastic-perfectly plastic (nonstrain hardening) material idealizations are respectively approached as $n \to 1$ and $n \to \infty$.

[23]Shih, C.F., "Small Scale Yielding Analysis of Mixed Mode Plane Strain Crack Problem," Harvard University Report DEAP S-1 (May 1973).

[24]Hutchinson, J.W. and C.F. Shih, "Plastic Analysis of Mixed Plane Stress Crack Problems," Harvard University Report DEAP S-4 (Sep 1973).

[25]Rice, J.R., "Mathematical Analysis in the Mechanics of Fracture," in "Fracture," Vol. 2, Academic Press (1968).

[26]Rice, J.R., "A Path Independent Integral and the Approximate Analysis of Strain Concentrations at Notches and Cracks," Brown University Report ARPA 50-80, E39 (1967).

[27]Rice, J.R. and G.F. Rosengren, "Plane Strain Deformation Near a Crack Tip in a Hardening Material," J. Mech. Physics and Solids, Vol. 16, No. 1 (1968).

[28]Hutchinson, J.W., "Singular Behavior at the End of a Tensile Crack in a Hardening Material," J. Mech. Physics and Solids, Vol. 16, No. 1 (1968).

[29]Hutchinson, J.W., "Plastic Stress and Strain Fields at a Crack Tip," J. Mech. Physics and Solids, Vol. 16 (1968).

can be expressed in the form

$$\sigma_{ij} = K_p \, r^{-1/n+1} \, \tilde{\sigma}_{ij}(\theta)$$

$$\epsilon_{ij} = (K_p)^n \, r^{-n/n+1} \, \tilde{\epsilon}_{ij}(\theta) \qquad i,j = r, \theta \tag{17}$$

where (r,θ) are polar coordinates centered at the crack tip as shown in Figure 1. The functions $\tilde{\sigma}_{ij}(\theta)$ and $\tilde{\epsilon}_{ij}(\theta)$ are governed by a nonlinear ordinary differential equation and have been determined numerically by Hutchinson[28] for a number of values of the hardening coefficient n. The plastic stress intensity factor K_p is dependent on the loading and geometry of the particular body under consideration. The resulting near-tip stress field is observed to be proportional, and thus it is also consistent with the flow theory of plasticity, provided there is no local unloading.

It is noticed that although the singular solution is based on an infinitesimal strain theory, it predicts infinite strains at the crack tip. This inconsistency is a consequence of the sharp crack tip model. Arguments analogous to the small-scale yielding concept (i.e., the plastic zone is relatively small) can be used to suggest that the plastic singular solution, Equation (17), will characterize the crack tip behavior provided the large strain region at the crack tip is sufficiently small. Such a "scale" argument clearly excludes application of the small strain, plastic singular solution to ductile fracture conditions where gross crack tip blunting is observed.

The plastic stress intensity factor K_p can be determined from the corresponding elastic intensity factor under the conditions of small-scale yielding through the application of a path-independent integral.[25,27,28] This integral, now known as the "J integral," was originally discovered by Eshelby[30] for use in dislocation theory and was first applied to elastic-plastic fracture mechanics by Rice.

The J integral is given by

$$J = \int_\Gamma (\text{SED})\, dy - \sigma_{ij} \, n_j \, \frac{\partial u_i}{\partial x} \, ds \tag{18}$$

In Equation (18), the summation convention is implied by repeated subscripts, i and j taking on values of x and y. SED is the strain energy density, i.e.,

---

[30]Eshelby, J.D., "Determination of the Elastic Field of an Ellipsoidal Inclusion, and Related Problems," Proc. Roy. Soc. London, Series A, Vol. 241 (1957).

$$\text{SED} = \int_0^{\epsilon_{ij}} \sigma_{ij}\, d\, \epsilon_{ij}$$

n_j is the j th component of the unit outward normal vector to the path Γ (see Figure 10), and $ds = \sqrt{dx^2 + dy^2}$. For situations in which the strain energy density is a unique function of the strain components ϵ_{ij}, the J integral has the following properties:

1. It has zero value for any closed path Γ_1 in the body which does not enclose any voids or singularities.

2. It has the same value (equal to the Griffith energy release rate G for linear elastic bodies) on all counterclockwise contours Γ_2 connecting the top and bottom surfaces of a traction-free crack directed parallel to the x axis.

3. The value of J on all contours Γ_3 enclosing the horizontal crack is equal to minus the derivative of the potential energy of the body with respect to the half-crack length a, i.e.,

$$J(\Gamma_3) = -\frac{d(PE)}{da} = 2J(\Gamma_2)$$

The J integral remains path independent in the sense described above for deformation theory plasticity with no unloading. Therefore, it is applicable to elastic-plastic fracture mechanics for situations in which this assumption is reasonable, i.e., the monotonic loading of a body containing a stationary crack.* The connection of J to K_I in the elastic range and to K_p in the plastic range will be discussed later.

Hilton and Hutchinson[7] have suggested using K_p to correlate unstable fracture results beyond the small-scale yielding range, i.e., the onset of rapid fracture is predicted to occur at a critical value of the plastic intensity factor K_{p_c} assumed to be a material constant.** Since the plastic singular solution is based on the assumption of increasing stresses at the crack tip, the failure criterion based on K_p can only be applied to predict fracture initiation for monotonic loading situations.

---

*This application is based on the *a priori* assumption that no local unloading occurs in the body during the loading process. Subsequent checks are necessary to ensure that this condition has not been violated for the particular problem under consideration.

**Analogous to elastic fracture mechanics, the failure predictions are based on the two-dimensional theories of plane strain and plane stress, and experimental values for K_{p_c} are expected to be thickness-dependent. Thus K_{p_c} cannot literally be a true material property.

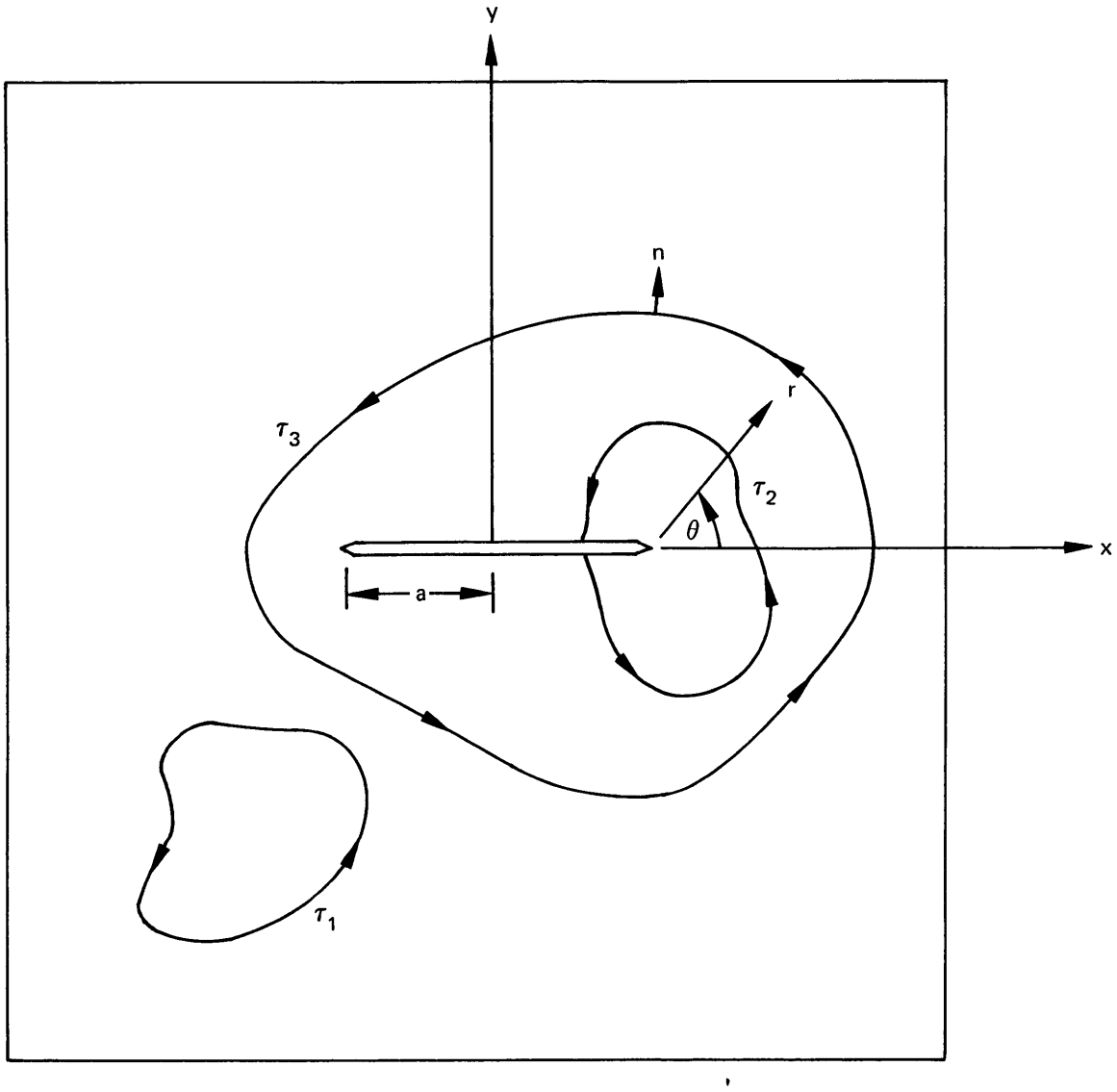

Figure 10 – Paths for the J Integral in a Cracked Body

Begley and Landes[31] have alternatively proposed the use of the J integral as a failure criterion. It will later be shown by Equation (37) that for deformation theory plasticity with no unloading at any point in the body, there is a one-to-one correspondence between J and K_p. Under these conditions, the J and K_p failure criteria are exactly equivalent. Further, both criteria are consistent with elastic fracture mechanics in the small-scale yielding range as will be shown later by Equation (40).

Hilton and Hutchinson[7] carried out embedded singularity finite element calculations to determine the load dependence of the plastic intensity factor for the plane stress problem of a crack in an infinite plate subjected to remote uniform tensile loading normal to the crack. In this example, the calculated values of the plastic intensity factor (based on deformation theory plasticity) were found to agree with the small-scale yielding result, Equation (40), for values of the applied stress up to approximately 50 percent of the yield stress. At higher values of applied stress, the calculated plastic intensity factor values became increasingly larger than the elastic prediction for them, and were found to depend on the material-hardening coefficient n. These numerical results were used in conjunction with the proposed plastic intensity factor failure criterion to predict the fracture initiation stress in terms of the elastic fracture toughness (K_{Ic}) of the material.

ELASTIC-PLASTIC EMBEDDED SINGULARITY FINITE ELEMENT PROCEDURE

Here the purpose is to augment a standard finite element computer program to enable calculations for elastic-plastic Mode I crack problems and to solve problems of fundamental interest. The procedure for changing an existing finite element program for this purpose is similar to the elastic case discussed earlier in that a semicircular crack tip element describing the singularity is embedded into the finite element grid pattern. The difference between the elastic-plastic and the elastic calculations arises from the following facts:

1. The stress-strain relations for the plastic problem are nonlinear.
2. The plastic rather than the elastic singular solution is used to describe the behavior of the crack tip element.
3. The resulting equations for the finite element idealization are nonlinear and must be solved iteratively.

---

[31] Begley, J. and J.A. Landes, "The J-Integral as a Failure Criterion," Westinghouse Research Laboratories Report 71-IE7-FMPWR-P3 (1971).

The new information required to carry out the elastic-plastic finite element calculations for crack problems is detailed in the following sections.*

Material Model – A total deformation theory of plasticity is employed for the calculations to be performed here. The plastic deformation is assumed to be independent of the hydrostatic component of stress σ_{kk} and completely determined by the first invariant of the stress deviator tensor

$$S_{ij} = \sigma_{ij} - 1/3\ \sigma_{kk}\ \delta_{ij} \quad ; \delta_{ij} = \begin{cases} 0 \text{ for } i \neq j \\ 1 \text{ for } i = j \end{cases}$$

where a repeated index indicates summation, i.e., $\sigma_{kk} = \sigma_x + \sigma_y + \sigma_z$. This invariant, usually called the "effective stress," is given by

$$\sigma_e^2 = 3/2\ S_{ij}\ S_{ij}$$

For simple tension, $\sigma_e = \sigma$ and the von Mises yield condition is $\sigma_e = 1$. The generalized strain-stress relations which reduce to Equation (16) for simple tension are

$$e_{ij} = \begin{cases} (1+\nu)\ S_{ij} & \sigma_e \leqslant 1 \\ [(1+\nu) + 3/2\ (\sigma_e^{n-1} - 1)]\ S_{ij} & \sigma_e > 1 \end{cases} \tag{19}$$

$$\epsilon_{pp} = (1-2\nu)\ \sigma_{pp}$$

where e_{ij} is the strain deviator tensor given by

$$e_{ij} = \epsilon_{ij} - 1/3\ \epsilon_{pp}\ \delta_{ij}$$

The effective strain e_e is given by

$$e_e^2 = 3/2\ e_{ij}\ e_{ij}$$

---

*These sections are based to a large extent on work published by Hutchinson;[7,28,29] this information is presented here for the convenience of the reader.

Determination of Plastic Singular Solution of Crack Tip[28] – The equilibrium equations for either plane stress or plane strain problems can be satisfied by introducing the airy stress function ϕ in the form

$$\sigma_r = \frac{1}{r}\frac{\partial \phi}{\partial r} + \frac{1}{r^2}\frac{\partial^2 \phi}{\partial \theta^2}$$

$$\sigma_\theta = \frac{\partial^2 \phi}{\partial r^2} \tag{20}$$

$$\sigma_{r\theta} = -\frac{\partial}{\partial r}\frac{1}{r}\frac{\partial \phi}{\partial \theta}$$

where (r, θ) are local polar coordinates centered at the crack tip as shown in Figure 10. The governing equation for the stress function ϕ can be obtained by substitution into the compatibility condition

$$\frac{1}{r}\frac{\partial^2}{\partial r^2}(r\epsilon_\theta) + \frac{1}{r^2}\frac{\partial^2}{\partial \theta^2}(\epsilon_r) - \frac{1}{r}\frac{\partial \epsilon_r}{\partial r} - \frac{2}{r^2}\frac{\partial}{\partial r}\left(r\frac{\partial \epsilon_{r\theta}}{\partial \theta}\right) = 0 \tag{21}$$

In the sequel, differential equations will be derived for the determination of the plastic singular solution for the core element, first for the plane stress case and then for the cases of plane strain and axial symmetry.

For the plane stress problem, the strain-stress relations are specialized as*

$$\epsilon_r = \sigma_r - \nu\sigma_\theta + (\sigma_e^{n-1} - 1)\left(\sigma_r - \frac{\sigma_\theta}{2}\right)$$

$$\epsilon_\theta = \sigma_\theta - \nu\sigma_r + (\sigma_e^{n-1} - 1)\left(\sigma_\theta - \frac{\sigma_r}{2}\right)$$

$$\epsilon_{r\theta} = (1+\nu)\sigma_{r\theta} + 3/2\,(\sigma_e^{n-1} - 1)\sigma_{r\theta}$$

with

$\sigma_e^2 = \sigma_r^2 + \sigma_\theta^2 - \sigma_r\sigma_\theta + 3\sigma_{r\theta}^2$. Substitution of these strain-stress relations into Equation (21) and then substitution of Equation (20) into the result yields the following differential

*The entire singular element at the crack tip is assumed to be within the plastic domain.

equation for the determination of ϕ for the plane stress case:

$$\nabla^4 \phi + \frac{1}{2}\left\{\frac{1}{r}\frac{\partial^2}{\partial r^2}\left[\sigma_e^{n-1}\left(2r\frac{\partial^2\phi}{\partial r^2} - \frac{\partial\phi}{\partial r} - \frac{1}{r}\frac{\partial^2\phi}{\partial\theta^2}\right)\right]\right.$$

$$+ \frac{6}{r^2}\frac{\partial^2}{\partial r\,\partial\theta}\left[\sigma_e^{n-1}\cdot r\frac{\partial}{\partial r}\left(\frac{1}{r}\frac{\partial\phi}{\partial\theta}\right)\right] + \frac{1}{r}\frac{\partial}{\partial r}\left[\sigma_e^{n-1}\left(-\frac{2}{r}\frac{\partial\phi}{\partial r} - \frac{2}{r^2}\frac{\partial^2\phi}{\partial\theta^2} + \frac{\partial^2\phi}{\partial r^2}\right)\right] \quad (22)$$

$$\left. + \frac{1}{r^2}\frac{\partial^2}{\partial\theta^2}\left[\sigma_e^{n-1}\left(-\frac{\partial^2\phi}{\partial r^2} + \frac{2}{r}\frac{\partial\phi}{\partial r} + \frac{2}{r^2}\frac{\partial^2\phi}{\partial\theta^2}\right)\right]\right\} = 0$$

The boundary conditions for Equation (22) on the crack edges are

$$\phi\,(r, \pm\pi) = \frac{\partial\phi}{\partial\theta}\,(r, \pm\pi) = 0 \quad (23)$$

and for symmetry of Mode I loading conditions are

$$\frac{\partial\phi}{\partial\theta}\,(r, 0) = \frac{\partial^2\phi}{\partial\theta^3}\,(r, 0) = 0 \quad (24)$$

Now, the purpose of this section is to obtain the singular portion of the solution in the immediate vicinity of the crack tip. This information will be used to develop the special crack tip plastic element, thereby enabling a finite element calculation procedure for elastic-plastic problems. Thus an asymptotic solution to Equation (22) is sought in the form

$$\phi\,(r, \theta) = f\,(r)\,\tilde{\phi}\,(\theta) + \text{h.o.t.}$$

where h.o.t. stands for "higher order terms." It can be shown that the $\nabla^4\,\phi$ term in Equation (22) does not contribute to the first term in the expansion and, further, that the singular solution reduces to

$$\phi\,(r, \theta) = r^s\,\tilde{\phi}\,(\theta)$$

The values of s for the first term of the expansion can be found through the use of the J integral described earlier. If the J integral is to remain path-independent on all paths Γ_2 from one crack surface to another, it is necessary that the strain energy density SED = $\int_0^{\epsilon_{ij}}$

$\sigma_{ij}\, d\, \epsilon_{ij}$ have a 1/r singularity at the crack tip. Referring to Equation (19) for the strain-stress relations, it is expected that σ_e will be large in the region immediately surrounding the crack tip and that asymptotically close to the tip, the elastic portions of the strain components will be negligible in comparison with the corresponding plastic portions, i.e., the strain components may be written

$$e_{ij} = \frac{3}{2}\, \sigma_e^{n-1}\, S_{ij}$$

Thus for a power hardening material, the 1/r singularity in the strain energy density implies an $(r)^{-1/n+1}$ singularity for the stress components and a corresponding $(r)^{-n/n+1}$ singularity for the plastic strain components. These arguments yield a value for s of

$$s = \frac{2n + 1}{n + 1}$$

Substitution of the assumed form for the asymptotic solution

$$\phi = r^{2n+1/n+1}\, \tilde{\phi}\,(\theta) + \text{h.o.t.}$$

into Equation (22) leads to the following nonlinear ordinary differential equation for $\tilde{\phi}\,(\theta)$:

$$\left[\frac{-n}{n+1} - \frac{d^2}{d\theta^2}\right]\left[\tilde{\sigma}_e^{n-1}\left(\frac{2n^2 + 5n + 2}{(n+1)^2}\,\tilde{\phi} + 2\,\frac{d^2\tilde{\phi}}{d\theta^2}\right)\right]$$

$$\frac{-n}{(n+1)^2}\,\tilde{\sigma}_e^{n-1}\left[\frac{2n^2 - n - 1}{(n+1)^2}\,\tilde{\phi} - \frac{d^2\tilde{\phi}}{d\theta^2}\right] \tag{25}$$

$$+\frac{6n}{(n+1)^2}\,\frac{d}{d\theta}\left[\tilde{\sigma}_e^{n-1}\,\frac{d\tilde{\phi}}{d\theta}\right] = 0$$

where

$$\sigma_e = K_p\, r^{-1/n+1}\, \tilde{\sigma}_e(\theta) = K_p\, r^{-1/n+1} \left[\tilde{\sigma}_r^2 + \tilde{\sigma}_\theta^{\,2} - \tilde{\sigma}_r\, \tilde{\sigma}_\theta + 3\, \tilde{\sigma}_{r\theta}^{\,2} \right]^{1/2}$$

$$\sigma_r = K_p\, r^{-1/n+1}\, \tilde{\sigma}_r(\theta) = K_p\, r^{-1/n+1} \left[\frac{2n+1}{n+1}\, \tilde{\phi} + \frac{d^2\, \tilde{\phi}}{d\theta^2} \right]$$

$$\sigma_\theta = K_p\, r^{-1/n+1}\, \tilde{\sigma}_\theta(\theta) = K_p\, r^{-1/n+1} \left[\frac{n(2n+1)}{(n+1)^2}\, \tilde{\phi} \right] \qquad (26)$$

$$\sigma_{r\theta} = K_p\, r^{-1/n+1}\, \tilde{\sigma}_{r\theta}(\theta) = K_p\, r^{-1/n+1} \left[\frac{-n}{n+1}\, \frac{d\, \tilde{\phi}}{d\theta} \right]$$

and where $\tilde{\sigma}_r$, $\tilde{\sigma}_\theta$, and $\tilde{\sigma}_{r\theta}$ represent the circumferential variation of the stress components σ_r, σ_θ, and $\sigma_{r\theta}$.

The plastic crack tip singular solution (for the stresses) for the plane stress crack problem is given by Equation (26); the θ dependence is found explicitly by numerical solution of Equation (25). Thus Equation (26) is analogous to Equation (1) of the elastic solution. The strain components can be found in terms of the stress components from the strain-stress relations following Equation (19). The asymptotic equations for the near-tip strain components are

$$\epsilon_r = K_p^{\,n}\, r^{-n/n+1}\, \tilde{\epsilon}_r = K_p^{\,n}\, r^{-n/n+1}\, \tilde{\sigma}_e^{\,n-1} \left[\frac{2n^2+5n+2}{2(n+1)^2}\, \tilde{\phi} + \frac{d^2\, \tilde{\phi}}{d\theta^2} \right]$$

$$\epsilon_\theta = K_p^{\,n}\, r^{-n/n+1}\, \tilde{\epsilon}_\theta = K_p^{\,n}\, r^{-n/n+1}\, \tilde{\sigma}_e^{\,n-1} \left[\frac{2\,n^2-n-1}{(n+1)^2}\, \tilde{\phi} - \frac{d^2\, \tilde{\phi}}{d\theta^2} \right] /2 \qquad (27)$$

$$\epsilon_{r\theta} = K_p^{\,n}\, r^{-n/n+1}\, \tilde{\epsilon}_{r\theta} = -\,3/2\, K_p^{\,n}\, r^{-n/n+1}\, \tilde{\sigma}_e^{\,n-1} \left(\frac{n}{n+1} \right) \frac{d\, \tilde{\phi}}{d\,\theta}$$

The components of displacement as measured relative to the crack tip are obtained from the strain-displacement relations as

$$u_r = K_p^{\,n}\, r^{1/n+1}\, \tilde{u}_r = (n+1)\, K_p\, r^{1/n+1}\, \tilde{\epsilon}_r$$

$$= K_p^{\,n}\, r^{1/n+1}\, \tilde{\sigma}_e^{\,n-1} \left[\frac{2n^2 + 5n + 2}{2(n+1)}\, \tilde{\phi} + (n+1)\, \frac{d^2 \tilde{\phi}}{d\theta^2} \right] \tag{28}$$

$$u_\theta = \int_0^\theta (r\, \epsilon_\theta - u_r)\, d\theta$$

or*

$$u_\theta = K_p^{\,n}\, r^{1/n+1}\, \tilde{u}_\theta$$

$$= -\, K_p^{\,n}\, r^{1/n+1} \int_0^\theta \tilde{\sigma}_e^{\,n-1} \left[\frac{2n^3 + 5n^2 + 8n + 3}{2(n+1)^2}\, \tilde{\phi} + \frac{2n+3}{2}\, \frac{d^2 \tilde{\phi}}{d\theta^2} \right] d\theta$$

Equations (28) for the plane stress displacements are analogous to Equations (2) of the elastic singular solution.

Equations (26) and (28) describe the plastic singular solution for the plane stress cases. The same approach may be carried out to determine the asymptotic solution for the plane strain case. Some simplifications arise if it is recognized at the outset that concern is only with the region in which the elastic strain components are negligible in comparison with the plastic components. Under this assumption, the strain-stress relations for the plane strain case become

$$\epsilon_r = 3/4\, \sigma_e^{\,n-1}\, (\sigma_r - \sigma_\theta)$$

$$\epsilon_\theta = 3/4\, \sigma_e^{\,n-1}\, (\sigma_\theta - \sigma_r) \tag{29}$$

$$\epsilon_{r\theta} = 3/2\, \sigma_e^{\,n-1}\, \sigma_{r\theta}$$

where $\sigma_e^{\,2} = 3/4\, (\sigma_r - \sigma_\theta)^2 + 3\, \sigma_{r\theta}^2$

---

*This result is obtained by substituting from Equations (27) and the first of Equations (28).

Substitution into the compatibility equation, Equation (21), yields the following equation for the stress function ϕ in the fully plastic domain:

$$\left[\frac{1}{r^2}\frac{\partial^2}{\partial\theta^2} - \frac{1}{r}\frac{\partial}{\partial r} - \frac{1}{r}\frac{\partial}{\partial r}\circ r\right]\left[\tilde{\sigma}_e^{n-1}\left(\frac{1}{r}\frac{\partial\phi}{\partial r} + \frac{1}{r^2}\frac{\partial^2\phi}{\partial\theta^2} - \frac{\partial^2\phi}{\partial r^2}\right)\right]$$

$$+ \frac{4}{r^2}\frac{\partial^2}{\partial r\,\partial\theta}\left[\tilde{\sigma}_e^{n-1} r \frac{\partial}{\partial r}\left(\frac{1}{r}\frac{\partial\phi}{\partial\theta}\right)\right] = 0 \tag{30}$$

As before, letting $\phi = r^{2n+1/n+1}\,\tilde{\phi}(\theta)$, one obtains the equation for $\tilde{\phi}(\theta)$ as

$$\left[\frac{d^2}{d\theta^2} + \frac{n(n+2)}{(n+1)^2}\right]\left[\tilde{\sigma}_e^{n-1}\left(\frac{2n+1}{(n+1)^2}\tilde{\phi} + \frac{d^2\tilde{\phi}}{d\theta^2}\right)\right]$$

$$+ \frac{4}{(n+1)^2}\frac{d}{d\theta}\left[\tilde{\sigma}_e^{n-1}\frac{d\tilde{\phi}}{d\theta}\right] = 0 \tag{31}$$

where

$$\sigma_e = K_p\, r^{-1/n+1}\,\tilde{\sigma}_e = K_p\, r^{-1/n+1}\left[3/4\,(\tilde{\sigma}_r - \tilde{\sigma}_\theta)^2 + 3\,\tilde{\sigma}_{r\theta}^{\,2}\right]^{1/2} \tag{32}$$

The relationship of the stress components to the stress functions $\tilde{\sigma}_r$ etc. (defined in Equation (26)) is the same as for the plane stress case.

The strain components asymptotically close to the crack tip are given in terms of the singular stress components in Equation (29) and can be expressed as a function of the stress function $\tilde{\phi}$ in the form

$$\epsilon_r = K_p^{\,n}\, r^{-n/n+1}\,\tilde{\epsilon}_r = K_p^{\,n}\, r^{-n/n+1}\,\tilde{\sigma}_e^{n-1}\left[\frac{2n+1}{(n+1)^2}\tilde{\phi} + \frac{d^2\tilde{\phi}}{d\theta^2}\right]$$

$$\epsilon_\theta = K_p^{\,n}\, r^{-n/n+1}\,\tilde{\epsilon}_\theta = -K_p^{\,n}\, r^{-n/n+1}\,\tilde{\sigma}_e^{n-1}\left[\frac{2n+1}{(n+1)^2}\tilde{\phi} + \frac{d^2\tilde{\phi}}{d\theta^2}\right] \tag{33}$$

$$\epsilon_{r\theta} = K_p^{\,n}\, r^{-n/n+1}\,\tilde{\epsilon}_{r\theta} = -\frac{3}{2}K_p^{\,n}\, r^{-n/n+1}\,\tilde{\sigma}_e^{n-1}\cdot\frac{n}{n+1}\frac{d\tilde{\phi}}{d\theta}$$

The displacement components relative to the crack tip corresponding to the plane strain asymptotic solution are

$$u_r = K_p^n r^{1/n+1} \tilde{u}_r = K_p^n r^{1/n+1} \tilde{\sigma}_e^{n-1} \left[\frac{2n+1}{n+1} \tilde{\phi} + (n+1) \frac{d^2 \tilde{\phi}}{d\theta^2} \right]$$

$$u_\theta = K_p^n r^{1/n+1} \tilde{u}_\theta = - K_p^n r^{1/n+1} \int_0^\theta \tilde{\sigma}_e^{n-1} \left[\frac{(2n+1)(n+2)}{(n+1)^2} \tilde{\phi} + (n+2) \frac{d^2 \tilde{\phi}}{d\theta^2} \right] d\theta \quad (34)$$

It should be noted that the function $\tilde{\sigma}_e(\theta)$ involved in these equations is different for the plane strain and plane stress problems, given respectively by Equations (32) and (26) for the two problem types.

Attention is now directed to consideration of axisymmetric problems involving either internal penny-shaped cracks or exterior circumferential cracks. In this case, x, y, and z represent a cylindrical coordinate system with y the axis of symmetry, x the radial distance from the axis of symmetry, and z the circumferential coordinate. The circumferential strain component ϵ_z is related to the radial displacement component by

$$\epsilon_z = u_x / x$$

The condition that u_x remains finite requires ϵ_z to be nonsingular at the crack tip and thus negligible in comparison with the strain components ϵ_x, ϵ_y, and ϵ_{xy} in the region immediately surrounding the crack tip, and thus also negligible with respect to the polar components of strain ϵ_r, ϵ_θ, and $\epsilon_{r\theta}$. This means that the equations which govern the plane strain problem are asymptotically correct for axisymmetric crack problems in the immediate vicinity of the crack tip. Thus the plastic singular solution for the axisymmetric case is identical to the plane strain result and is given by Equations (26) and (31) through (34).

In all the cases for plane stress, plane strain, and axial symmetry, the plastic singular solution $\tilde{\phi}(\theta)$ is governed by a nonlinear differential equation which must be solved numerically. Appendix D describes the numerical procedures employed in the solution of this equation.

RELATION BETWEEN THE PLASTIC INTENSITY FACTOR AND THE J INTEGRAL

Following the notation shown in Figure 10, the J integral given by Equation (18) also applies to the deformation theory plasticity with no unloading. Thus J can be determined

in terms of K_p by choosing the contour Γ_2 asymptotically close to the crack tip. The explicit functional dependence of J on K_p is developed in the following, i.e., the integrand of the J integral will be determined from the plastic singular solution in terms of K_p.

Under the assumption that the elastic strain components are small in comparison with the corresponding plastic components, the asymptotic calculation for the strain energy density in the vicinity of the crack tip yields

$$\text{SED} = \int \sigma_{ij}\, d\,\epsilon_{ij} = \int S_{ij}\, d\, e_{ij} \quad + \text{h.o.t.}$$

Substituting into the fully plastic strain-stress relations ($e_{ij} = 3/2\ \sigma_e^{\,n-1}\ S_{ij}$), one obtains

$$\text{SED} = \frac{n}{n+1}\ \sigma_e^{\,n+1} + \text{h.o.t.} = \frac{n}{n+1}\ K_p^{\,n+1}\ \frac{1}{r}\ \tilde{\sigma}_e(\theta) + \text{h.o.t.} \tag{35}$$

where σ_e is given by Equations (26) and (32) for the plane stress and plane strain cases, respectively. The second part of the integrand, $\sigma_{ij}\ n_j\ \partial\, u_i/\partial x$, can also be expressed in terms of the singular solution as

$$\begin{aligned}\sigma_{ij}\ n_j\ \partial\ u_i/\partial x = K_p^{\,n+1}\ \frac{1}{r}\ \Bigg\{ \sin\theta \Bigg[\tilde{\sigma}_r \left(\tilde{u}_\theta - \frac{d\,\tilde{u}_r}{d\theta} \right) \\ - \tilde{\sigma}_{r\theta} \left(\tilde{u}_r + \frac{d\,\tilde{u}_\theta}{d\theta} \right) \Bigg] + \frac{1}{n+1}\ \cos\theta \left[\tilde{\sigma}_r\ \tilde{u}_r + \tilde{\sigma}_{r\theta}\ \tilde{u}_\theta \right] \Bigg\}\end{aligned} \tag{36}$$

where $\tilde{\sigma}_r$, $\tilde{\sigma}_\theta$, $\tilde{\sigma}_{r\theta}$, $\tilde{u}_r$, and $\tilde{u}_\theta$ are given in terms of the circumferential variation of the stress function $\tilde{\phi}(\theta)$ in Equations (26), (28), (32), and (34).

Thus the J integral can be expressed in terms of the plastic intensity factor in the form

$$J = \int \left[(\text{SED})\ dy - \sigma_{ij}\ n_j\ \frac{\partial\, u_i}{\partial x}\ ds \right] = K_p^{\,n+1}\ I \tag{37}$$

where

$$I = \int_{-\pi}^{\pi} \left\{ \frac{n}{n+1} \tilde{\sigma}_e^{n+1} \cos\theta - \sin\theta \left[\tilde{\sigma}_r \left(\tilde{u}_\theta - \frac{d\tilde{u}_r}{d\theta} \right) - \tilde{\sigma}_{r\theta} \left(\tilde{u}_r + \frac{d\tilde{u}_\theta}{d\theta} \right) \right] + \frac{\cos\theta}{n+1} \left(\tilde{\sigma}_r \tilde{u}_r + \tilde{\sigma}_{r\theta} \tilde{u}_\theta \right) \right\} d\theta$$

Values of the integral I have been recorded by Hutchinson[28] for material-hardening coefficients of n = 3, 5, 9, and 13.

Under the assumption of small-scale yielding, the J integral can be calculated from the elastic singular solution, Equations (1) and (2), thereby relating the plastic intensity factor to the elastic stress intensity factor in that range. For linear elasticity, the J integral on paths Γ_2 surrounding the crack tip reduces to the Griffith energy release rate and can be expressed in terms of the elastic stress intensity factor. To make the result consistent with the normalized plastic singular solution under consideration here, a nondimensionalized J integral J_{ND} is defined in the form

$$J_{ND} = \frac{JE}{\sigma_y^2} \tag{38}$$

In the small-scale yielding range

$$(J_{ND})_{SSY} = \begin{cases} (K_I/\sigma_y)^2 & \text{plane stress} \\ (1-\nu^2)(K_I/\sigma_y)^2 & \text{plane strain} \end{cases} \tag{39}$$

In the special case of small-scale yielding, J can be calculated directly from the elastic singular solution, Equation (1), by choosing a contour sufficiently far from the crack tip that it describes the solution. In such a contour, J_{ND} can be calculated from Equation (39). On the other hand, J can also be evaluated on the contour asymptotically close to the crack tip, in which case J_{ND} can be calculated from Equations (37) and (38). By equating these two values of J_{ND} and designating $K_{p_{SSY}}$ as the value of K_p in the small-scale yielding (SSY) range, one obtains

$$K_{p_{SSY}} = \begin{cases} [(K_I/\sigma_y)^2/I]^{1/n+1} & \text{plane stress} \\ [(1-\nu^2)(K_I/\sigma_y)^2/I]^{1/n+1} & \text{plane strain or axisymmetric} \end{cases} \quad (40)$$

For situations where the small-scale yielding conditions are violated, Equation (40) no longer holds and it is necessary to make independent calculations for K_p or J. These calculations are of interest for at least two purposes:

1. A comparison of calculated K_p values with $K_{p_{SSY}}$ from Equation (40) yields a measure of the errors involved in applying elastic fracture mechanics to elastic-plastic problems.

2. The plastic intensity factor is a measure of the amplitude of the near-tip stress and strain fields and thus a rational failure criterion beyond the small-scale yielding range.

The following section describes an embedded singularity finite element procedure for determining K_p values.

PLASTIC FINITE ELEMENT GOVERNING EQUATIONS

The specialized finite element procedure for elastic-plastic crack problems is similar to the elastic approach described earlier in that an asymptotic description [Equations (26), (28), (32), and (34)] is employed for the displacement field in a semicircular core element centered on the crack tip. Since the plastic singular solution is based on the assumption that the elastic portions of the strain components are small in comparison with the plastic portions, the core element for this procedure must be contained within the plastic zone. This additional constraint implies that the allowable radius of the core element is related to the loading conditions as well as to the geometric dimensions of the problem under consideration. Thus the procedure to be described here is not suitable for performing calculations in the small-scale yielding range for which Equation (40) can be used.* For this reason, the embedded singularity method cannot be used in a straightforward manner to

*This statement does not contradict the discussion in the preceding section. It simply implies that the magnitude of the applied load must be great enough (say, $>0.3\ \sigma_y$) so that the plastic solution is applicable. The numerical results obtained by Hilton and Hutchinson[7] as well as those presented in this report demonstrate the existence of an intermediate size plastic zone; within its range, close agreement is observed between the small-scale yielding result, Equation (40), and the finite element large-scale yielding results for the plastic intensity factor.

carry out incremental plasticity theory calculations because the early loading stages will violate the assumed conditions on the core element. Thus deformation theory calculations are performed and an *a posteri* check for unloading of the core element is necessitated.* These calculations, in fact, reduce to a nonlinear elastic analysis based on the assumption of no unloading. The governing equations for this embedded singularity finite element procedure can therefore be developed from the variational principle of minimum potential energy.

Here only Mode I elastic-plastic crack problems will be considered.** For this case, symmetry conditions make it possible to consider only half the body, and the singular core element becomes a half-disk as indicated in Figure 11. The potential energy for the half specimen can be approximated by the embedded singularity finite element as

$$PE = SE_{CORE} + \Sigma\, SE_{EL.} - \Sigma\, R_i\, u_i \tag{41}$$

The strain energy of the core element is obtained from Equation (35) as

$$SE_{CORE} = K_p^{\,n+1}\, B = k_\epsilon^{\,n+1/n}\, B \;;\; K_p = (k_\epsilon)^{1/n} \tag{42}$$

where k_ϵ is the amplitude of the plastic strain singularity and will be referred to as the plastic strain intensity factor.*** The constant B is given by

$$B = \frac{n}{n+1}\, r_0 \int_0^{\pi} \tilde{\sigma}_e^{\,n+1}(\theta)\, d\theta \tag{43}$$

where $\tilde{\sigma}_e(\theta)$ is given in Equations (26) and (32) for plane stress and plane strain problems, respectively. For the axisymmetric case,

$$B_{AXI} = 2\pi\, \bar{R}\, B_{(PLANE\ STRAIN)} \tag{44}$$

where $\bar{R}$ is the radial (x) distance from the axis of symmetry to the crack tip.

The displacement components at the NI nodes along the boundary of the core element are given by the plastic singular solution in terms of the plastic strain intensity factor

---

*Such a check may be accomplished by showing that for successive solutions under increasing load, the old plastic zone is completely contained within the new plastic zone.

**The plastic singular solution for combined mode crack problems has only recently been developed.[23,24]

***Here k_ϵ is introduced in order to simplify the formulation which follows.

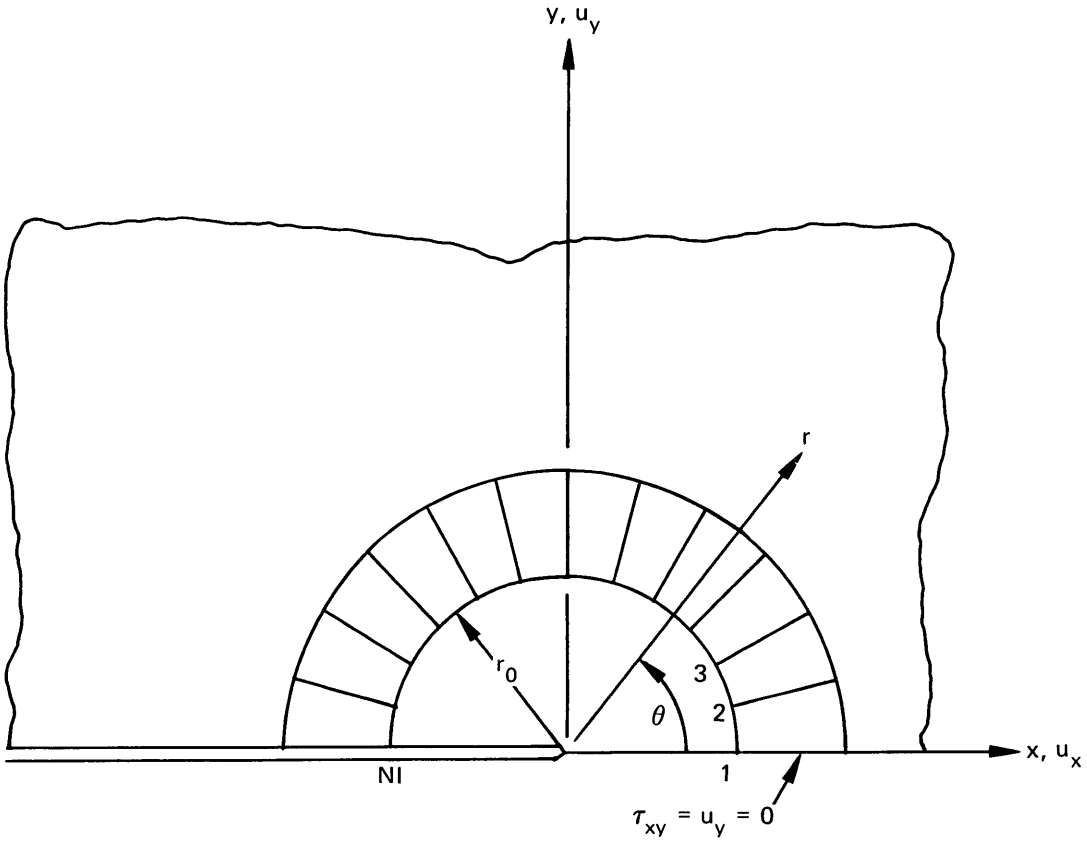

Figure 11 – Half-Core Singular Element for Symmetric Mode I Cracked Body

$k_\epsilon = K_p^n$ and the crack tip displacement u_{0x}. (The y component of the crack tip displacement is zero by symmetry of the Mode I problem.) These nodal displacement components can be expressed in the form

$$u_i = a_{1i}\, k_\epsilon + a_{2i}\, u_{0x} \tag{45}$$

where i goes from 1 to 2 N1, N1 being the number of nodes on the singular element. Referring to Figure 11 for cracks propagating in the positive x direction,

$$a_{1i} = r_0^{1/n+1} \begin{cases} \tilde{u}_r\,(\theta_{i+1/2}) \cos\theta_{i+1/2} - \tilde{u}_\theta(\theta_{i+1/2}) \sin\theta_{i+1/2} & \text{i odd} \\ \tilde{u}_r(\theta_{i/2}) \sin\theta_{i/2} + \tilde{u}_\theta(\theta_{i/2}) \cos\theta_{i/2} & \text{i even} \end{cases}$$

$$a_{2i} \quad \begin{cases} 1 & \text{i odd} \\ 0 & \text{i even} \end{cases} \tag{46}$$

On the other hand, for externally cracked axisymmetric bodies, the crack propagates in the negative x direction. In this case, the nodes about the core are numbered clockwise and θ is measured positive clockwise from the x axis, giving

$$a_{1i} = r_0^{1/n+1} \begin{cases} -\tilde{u}_r\,(\theta_{i+1/2}) \cos\theta_{i+1/2} + \tilde{u}_\theta(\theta_{i+1/2}) \sin\theta_{i+1/2} & \text{i odd} \\ u_r\,(\theta_{i/2}) \sin\theta_{i/2} + \tilde{u}_\theta(\theta_{i/2}) \cos\theta_{i/2} & \text{i even} \end{cases}$$

$$a_{2i} = \begin{cases} -1 & \text{i odd} \\ 0 & \text{i even} \end{cases} \tag{47}$$

With the strain energy of the core element established by Equations (42)–(44) and the displacements of the core nodes by Equations (45)–(47), the governing equations for the elastic-plastic finite element procedure can be obtained in the same way as for the elastic case. Minimization of the potential energy with respect to the unknown parameters k_ϵ, u_{0x}, and u_L (L varies over degrees of freedom not associated with core nodes) leads to

$$\frac{\partial PE}{\partial k_\epsilon} = \frac{n+1}{n} k_\epsilon^{1/n} B + \sum_{EL} \left[\sum_i \sum_j k_{ij} u_i \frac{\partial u_j}{\partial k_\epsilon} \right] = 0$$

$$\frac{\partial PE}{\partial u_{0x}} = \sum_{EL} \left[\sum_i \sum_j k_{ij} u_i \frac{\partial u_j}{\partial u_{0x}} \right] = 0 \qquad (48)$$

$$\frac{\partial PE}{\partial u_L} = \sum_{EL} \left(\sum_i k_{iL} u_i \right) - R_L = 0$$

The dependence of the nodal displacement components on the crack tip parameters k_ϵ and u_{0x} is obtained from Equations (45), (46), and (47). Substitution of these results into Equation (48) yields the governing equations for the elastic-plastic embedded singularity finite element calculation in the form

$$\frac{\partial PE}{\partial k_\epsilon} = \left[\frac{n+1}{n} B k_\epsilon^{1-n/n} + \sum_{EL} \left(\sum_{i=1}^{2(N1)} \sum_{j=1}^{2(N1)} k_{ij} a_{1i} a_{1j} \right) \right] k_\epsilon$$
$$+ \left[\sum_{EL} \left(\sum_{i=1}^{2(N1)} \sum_{j=1}^{2(N1)} k_{ij} a_{2i} a_{1j} \right) \right] u_{0x} \qquad (49a)$$
$$+ \sum_{EL} \sum_{i=2(N1)+1}^{N} \left[\sum_{j=1}^{2(N1)} k_{ij} a_{1j} \right] u_i = 0$$

$$\frac{\partial PE}{\partial u_{0x}} = \left[\sum_{EL} \left(\sum_{i=1}^{2(N1)} \sum_{j=1}^{2(N1)} k_{ij} a_{1i} a_{2j} \right) \right] k_\epsilon + \left[\sum_{EL} \left(\sum_{i=1}^{2(N1)} \sum_{j=1}^{2(N1)} k_{ij} a_{2i} a_{2j} \right) \right] u_{0x}$$
$$+ \sum_{EL} \sum_{i=2(N1)+1}^{N} (k_{ij} a_{2j}) u_i = 0 \qquad (49b)$$

In the standard finite element manner, the remainder of the governing equations may be expressed

$$\frac{\partial PE}{\partial u_L} = \left[\sum_{EL} \sum_{i=1}^{2(N1)} k_{iL}\, a_{1i} \right] k_\epsilon + \left[\sum_{EL} \sum_{i=1}^{2(N1)} k_{iL}\, a_{2i} \right] u_0 + \sum_{EL} \sum_{i=2(N1)+1}^{N} k_{iL}\, u_i - R_L = 0 \tag{49c}$$

In Equations (49), N is twice the number of nodes used to define the plastic finite element problem. The first two terms are nonzero only for elements which contain one or more nodes on the core periphery.

Equations (49) are nonlinear in k_ϵ and the stiffness terms k_{ij}. The stiffness matrix of the conventional finite elements is given by

$$[k] = \int_{VOL.} [B]^T [D] [B]\, dv \tag{50}$$

where [D] is defined by

$$\{\sigma\} = [D] \{\epsilon\}$$

and [B] is defined by (51)

$$\{\epsilon\} = [B] \{u\}$$

In the present formulation, the [B] matrix contributes no nonlinearities; however, the [D] matrix is no longer a constant for the elastic-plastic problem, but rather is a function of the element stresses. The [D] matrix must be obtained through the inversion of the strain-stress relations, Equations (19), which will be carried out for the cases of plane stress, plane strain, and axial symmetry in the following.

ELASTIC-PLASTIC STRESS-STRAIN RELATIONS

The normalized strain-stress relations employed in the present calculations are defined in Equations (19) as

$$e_{ij} = \begin{cases} (1+\nu)\, S_{ij} & \sigma_e \leq 1 \\ [(1+\nu) + 3/2\,(\sigma_e^{\,n-1} - 1)]\, S_{ij} & \sigma_e > 1 \end{cases} \qquad (52)$$

$$\epsilon_{pp} = (1 - 2\nu)\, \sigma_{pp}$$

Solution of these equations for the stress components in terms of the strain components to determine [D] of Equation (50) is straightforward for the elastic range. In the plastic region, the effective strain can be found from Equation (52) as

$$e_e = [(1+\nu) + 3/2\,(\sigma_e^{\,n-1} - 1)]\, \sigma_e \qquad (53)$$

This equation may be considered as a nonlinear algebraic equation for σ_e as a function of e_e. By using this equation, the strain-stress relations can be rewritten in the form

$$e_{ij} = \begin{cases} (1+\nu)\, S_{ij} & \sigma_e \leq 1 \\ e_e/\sigma_e\, S_{ij} & \sigma_e > 1 \end{cases} \qquad (54)$$

$$\epsilon_{pp} = (1-2\nu)\, \sigma_{pp}$$

Inversion of the strain-stress relations in this form is straightforward, yielding

$$S_{ij} = \begin{cases} e_{ij}/(1+\nu) & e_e \leq (1+\nu) \\ \sigma_e/e_e\, e_{ij} & e_e > (1+\nu) \end{cases}$$

$$\sigma_{pp} = \frac{\epsilon_{pp}}{1-2\nu} \qquad (55)$$

where σ_e is known in terms of e_e through Equation (53). It is convenient to rewrite these equations in terms of the usual stress and strain components, i.e.,

$$\sigma_{ij} = \begin{cases} \dfrac{\epsilon_{ij}}{1+\nu} + \dfrac{\nu}{(1+\nu)(1-2\nu)} \epsilon_{pp}\, \delta_{ij} & e_e \leqslant (1+\nu) \\ \sigma_e/e_e\ \epsilon_{ij} + 1/3 \left(\dfrac{1}{1-2\nu} - \sigma_e/e_e\right) \epsilon_{pp}\, \delta_{ij} & e_e > (1+\nu) \end{cases} \tag{56}$$

Specialization of the plastic stress-strain relations to the cases of plane strain ($\epsilon_z = \gamma_{xz} = \gamma_{yz} = 0$) and axial symmetry ($\gamma_{xz} = \gamma_{xy} = 0$) is as follows:

Plane strain plastic:

$$\sigma_x = \left[\frac{2}{3}\frac{\sigma_e}{e_e} + \frac{1}{3(1-2\nu)}\right]\epsilon_x + \frac{1}{3}\left[\frac{1}{1-2\nu} - \frac{\sigma_e}{e_e}\right]\epsilon_y$$

$$\sigma_y = \left[\frac{2}{3}\frac{\sigma_e}{e_e} + \frac{1}{3(1-2\nu)}\right]\epsilon_y + \frac{1}{3}\left[\frac{1}{1-2\nu} - \frac{\sigma_e}{e_e}\right]\epsilon_x \tag{57}$$

$$\tau_{xy} = \frac{\sigma_e}{e_e}\gamma_{xy}$$

Axial symmetry plastic (z is circumferential direction):

$$\sigma_x = \left[\frac{2}{3}\frac{\sigma_e}{e_e} + \frac{1}{3(1-2\nu)}\right]\epsilon_x + \frac{1}{3}\left[\frac{1}{1-2\nu} - \frac{\sigma_e}{e_e}\right]\left[\epsilon_y + \epsilon_z\right]$$

$$\sigma_y = \left[\frac{2}{3}\frac{\sigma_e}{e_e} + \frac{1}{3(1-2\nu)}\right]\epsilon_y + \frac{1}{3}\left[\frac{1}{1-2\nu} - \frac{\sigma_e}{e_e}\right]\left[\epsilon_x + \epsilon_z\right] \tag{58}$$

$$\sigma_z = \left[\frac{2}{3}\frac{\sigma_e}{e_e} + \frac{1}{3(1-2\nu)}\right]\epsilon_z + \frac{1}{3}\left[\frac{1}{1-2\nu} - \frac{\sigma_e}{e_e}\right]\left[\epsilon_x + \epsilon_y\right]$$

$$\tau_{xy} = \frac{\sigma_e}{e_e}\gamma_{xy}$$

The case for plane stress is complicated by the fact that the specialization condition, $\sigma_z = 0$, must be applied before inversion of the strain-stress relations. It is thus advantageous to make use of the extended Michell theorem[32] which states that for all homogeneous isotropic structures with tractions prescribed on all boundaries, the stress state is independent of Poisson's ratio. Therefore, in the plane stress elastic-plastic crack problems under consideration, the plastic intensity factor K_p, the plastic strain intensity factor $k_\epsilon = K_p{}^n$, and the elastic-plastic boundaries do not depend on Poisson's ratio. Therefore, one may choose $\nu = 0.5$, resulting in the simplified strain-stress relations

$$e_e = \frac{3}{2}\ \sigma_e{}^n$$

$$e_{ij} = \epsilon_{ij} = \begin{cases} \frac{3}{2}\ S_{ij} & \sigma_e \leqslant 1 \\ e_e/\sigma_e\ S_{ij} & \sigma_e > 1 \end{cases} \tag{59}$$

Inversion of Equation (59) gives

$$S_{ij} = \begin{cases} 2/3\ \epsilon_{ij} & e_e \leqslant 3/2 \\ \sigma_e/e_e\ \epsilon_{ij} & e_e > 3/2 \end{cases} \tag{60}$$

Substitution of the condition $\sigma_z = 0$ into this equation results in the desired stress-strain relations for plane stress:

$$\sigma_x = \begin{cases} 2/3\ (2\ \epsilon_x + \epsilon_y) & e_e \leqslant 3/2 \\ \sigma_e/e_e\ (2\ \epsilon_x + \epsilon_y) & e_e > 3/2 \end{cases}$$

$$\sigma_y = \begin{cases} 2/3\ (2\ \epsilon_y + \epsilon_x) & e_e \leqslant 3/2 \\ \sigma_e/e_e\ (2\ \epsilon_y + \epsilon_x) & e_e > 3/2 \end{cases} \tag{61}$$

$$\tau_{xy} = \begin{cases} 2/3\ \gamma_{xy} & e_e \leqslant 3/2 \\ \sigma_e/e_e\ \gamma_{xy} & e_e > 3/2 \end{cases}$$

[32] Budiansky, B., "Extension of Michell's Theorem to Problems of Plasticity and Creep," Q. Appl. Math., Vol. 16 (1958).

SOLUTION PROCEDURE FOR ELASTIC-PLASTIC CALCULATIONS

The nonlinear governing equations for the embedded singularity finite element representation of the elastic-plastic crack problem are Equations (49) where the stiffness terms k_{ij} contain the nonlinear stress-strain relations, Equations (57), (58), and (61), for the plane strain, axisymmetric, and plane stress cases, respectively. The solution procedure employed here is iterative in character; initial values are estimated for the quantity $k_\epsilon^{1-n/n}$ arising in the first equation and for the effective strains e_e in each element. At present, each of these values is initialized at 1.0 for simplicity, but more accurate initial values could be chosen (based on experience) to reduce the number of iterations required for convergence. The resulting set of linearized equations are then solved, $k_\epsilon^{1-n/n}$ and e_e are recalculated for each element, and the procedure is repeated until convergence is attained. The stabilized value of k_ϵ is then used to calculate K_p and J by means of Equations (42) and (37).

Adequate convergence for problems in which the plastic zone is relatively small is normally obtained in five or less iterations. For problems in which the applied load is high enough to produce larger plastic regions, convergence becomes increasingly slow with increasing load. In such cases, it may be found advantageous to iterate to convergence at smaller but progressively higher load steps until the desired load level is reached, using the plastic solution at the previous load level as the initial "guess" for k_ϵ and e_e in the elements for the next higher load. Thus a number of solutions may be calculated economically for a single geometry at different load levels.

ELASTIC-PLASTIC EXAMPLES

Calculations have been performed at NSRDC for two double-edge notched tensile specimens, a hollow cylinder with an external circumferential crack, and several single-edge-notched bend specimens. The four-node quadrilateral element (QUAD-4) was used in all calculations. The results of the computations are presented in Tables 5–8 and in Figures 12–20. They include the plastic strain intensity factor k_ϵ along with the small-scale yielding prediction for its magnitude as obtained from Equation (40) and the elastic stress intensity factor K_I. Elastic intensity factors have been calculated for this purpose by using the identical grid pattern employed for the elastic-plastic computations. Nondimensionalized J-integral values ($J_{ND} = JE/\sigma_y^2$) are also presented in the tables. Crack face separation at the free surface (COD) is shown therein in the nondimensionalized form $COD_{ND} = (E/\sigma_y) \cdot COD$; elastic COD values are included for comparison. Finally, the average displacement $u_{ND} = uE/\sigma_y$ of the loaded boundary is included in several of the tables.

DOUBLE-EDGE NOTCHED TENSILE SPECIMENS

The double-edge notched tensile specimen geometry is shown in Figure 12. Because of double symmetry of the problem, only one quadrant of the specimen was idealized using 226 nodes and 190 QUAD-4 elements. Plane strain conditions were assumed. The radius of the half-disk core element was taken as 0.02 inches, and 13 nodes were placed at 15-degree intervals about the core. Crack lengths a of 1.0 and 1.5 inches were considered.

The influence of load magnitude, hardening coefficient n, and crack length were studied as indicated in Table 5. The plastic zones corresponding to the tabulated results are shown in Figures 13 and 14.* Notice that for all the cases in which the plastic zone is contained within an elastic region (Cases 1–4, 7, 8, and 10), the small-scale yielding prediction for the plastic strain intensity factor is within about 10 percent of the calculated value. The same may be said about the reported COD values. Convergence of the iterative procedure for most of the cases studied was rapid and generally required less than five iterations. However, cases corresponding to plastic zones that traverse the specimen required larger numbers of iterations, with Cases 6 and 11 not quite converging after 10 iterations. Here, large differences are observed between elastic predictions for and calculated values of both k_ϵ and COD. Note also the rapid increase of average load point displacement when the yield zone traverses the specimen. The implications of this result are that if one considers a displacement-controlled test (or displacement-constrained crack growth in a structural component), the magnitude of k_ϵ will increase less quickly with displacement than predicted by elastic stress analysis. This may be an important consideration for components in structural applications where because of redundancies, a cracked member may, in effect, be subjected to deformation-controlled loading. In this situation, an elastic analysis for K_I will tend to give overly conservative predictions for failure.

It is interesting to observe that an average net section stress of at least $3/2\ \sigma_y$ was required to cause unconstrained yielding for this specimen. This elevated yield appears to be the result of large tensile stresses observed parallel to the crack direction in the ligament. Even in Cases 5, 6, 8, and 10 where the plastic zone traverses the specimen, an elastic region is observed directly between the crack tips.

The displaced shape of the crack face as computed here is illustrated in Figure 15 for the double-edge notched specimen with a 1-inch crack and a hardening coefficient of n = 9. Curves are given for applied stress to yield stress ratios of 0.6 and 0.9. The elastic prediction

---

*Plastic zones shown in this report have nonsmooth boundaries because of the discontinuous nature of stresses in the finite elements. Thus the plastic zones must be interpreted as qualitative, giving only an approximation to the actual plastic regions.

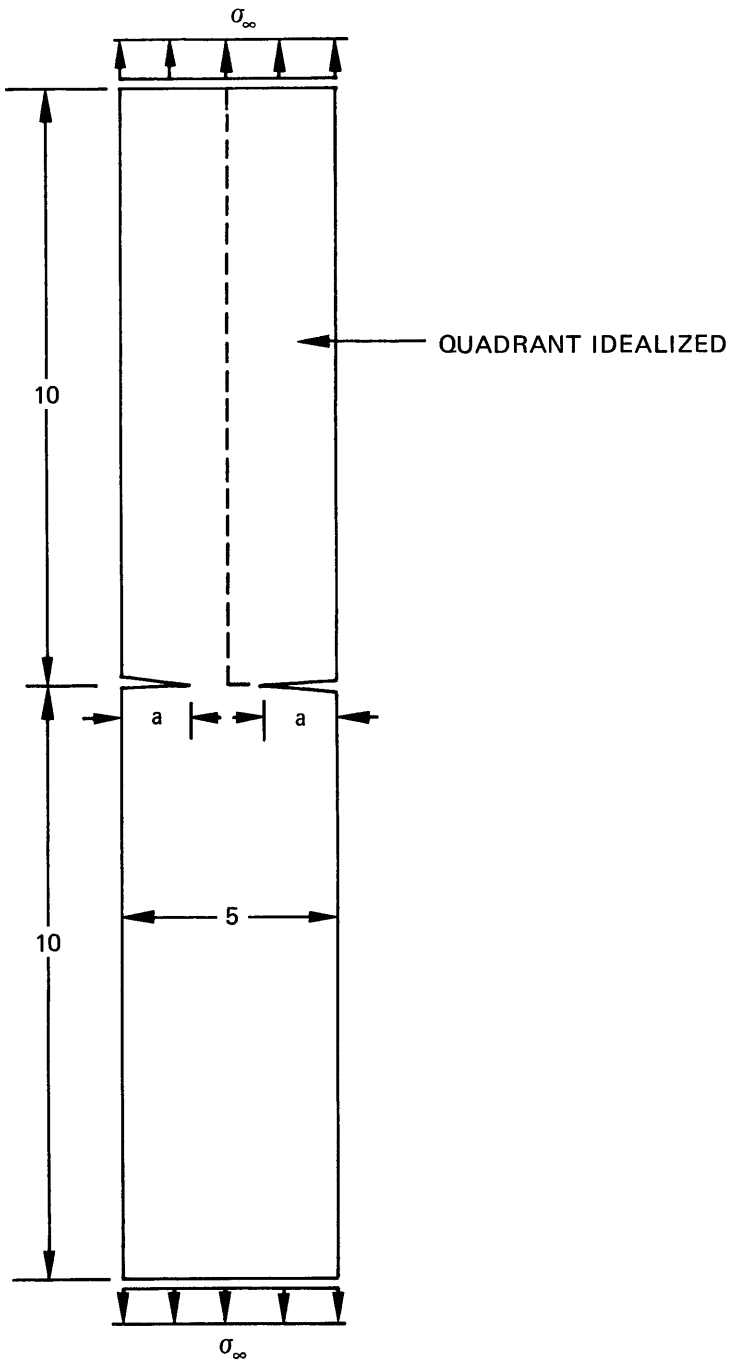

Figure 12 – Geometry of Double-Edge Notched Specimen

TABLE 5 – PLASTIC RESULTS FOR DOUBLE-EDGE NOTCHED TENSILE SPECIMEN

TABLE 5a - a = 1, 2a/w = 0.4

Case	$\frac{\sigma_\infty}{\sigma_y}$	n	k_ϵ SSY	k_ϵ CAL.	J_{ND}	COD_{ND}	COD_{ND} (ELAS)	Average Load Point Displacement
1	0.3	3	0.118	0.137	0.389	0.76	0.76	2.94
2	0.6	3	0.334	0.360	1.412	1.53	1.51	5.90
3	0.8	3	0.514	0.560	2.54	2.08	2.01	7.90
4	0.6	9	0.313	0.318	1.28	1.55	1.51	5.91
5	0.8	9	0.526	0.550	2.35	2.13	2.01	7.95
6	0.9	9	0.650	0.880*	4.0*	2.8*	2.26	9.39*

TABLE 5b - a = 1.5, 2a/w = 0.6

Case	$\frac{\sigma_\infty}{\sigma_y}$	n	k_ϵ SSY	k_ϵ CAL.	J_{ND}	COD_{ND}	COD_{ND} (ELAS)	Average Load Point Displacement
7	0.3	3	0.188	0.205	0.67	1.18	1.17	3.23
8	0.6	3	0.521	0.570	2.60	2.41	2.34	6.53
9	0.8	3	0.802	1.06	5.90	3.68	3.12	9.27
10	0.6	9	0.534	0.56	2.40	2.46	2.34	6.59
11	0.8	9	0.897	1.85*	8.5*	4.7*	3.12	10.53*

*Extrapolated-results not completely converged.

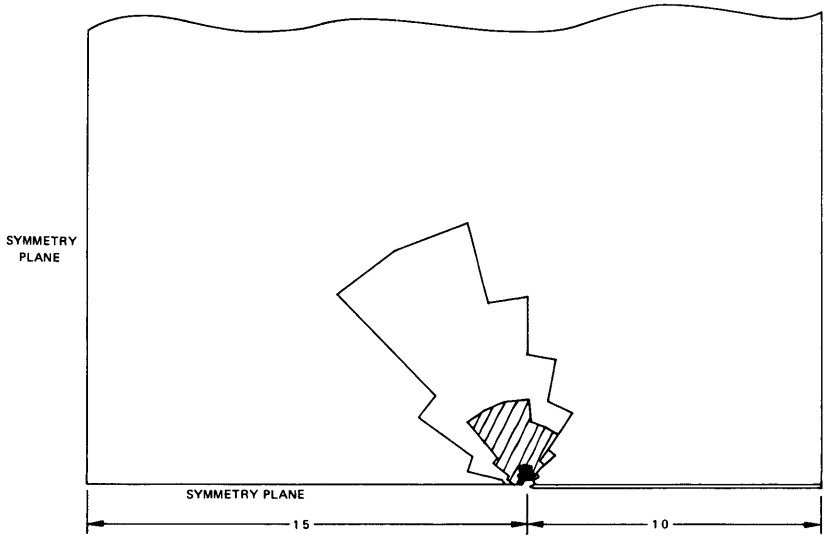

Figure 13a – For n = 3 and σ_∞ / σ_y = 0.3, 0.6, and 0.8 (Cases 1, 2, and 3)

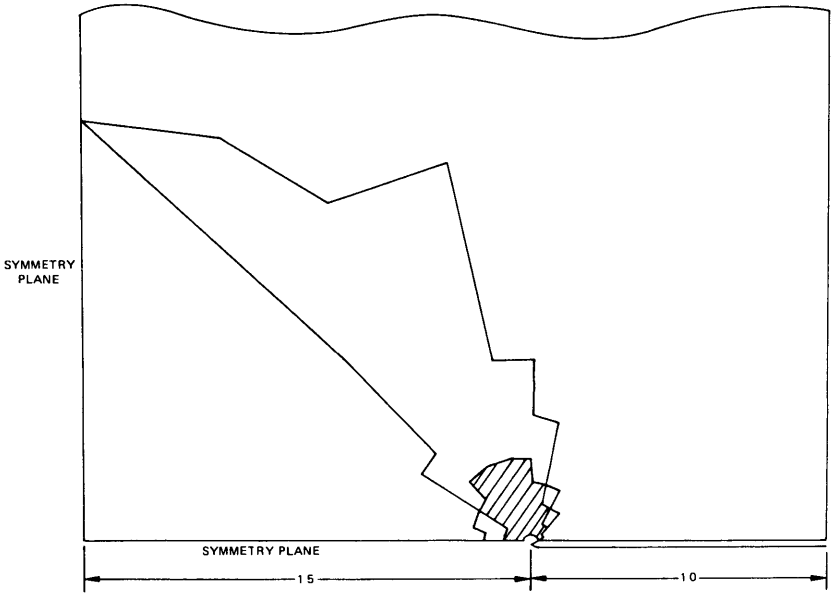

Figure 13b – For n = 9 and σ_∞ / σ_y = 0.6 and 0.8 (Cases 4 and 5)

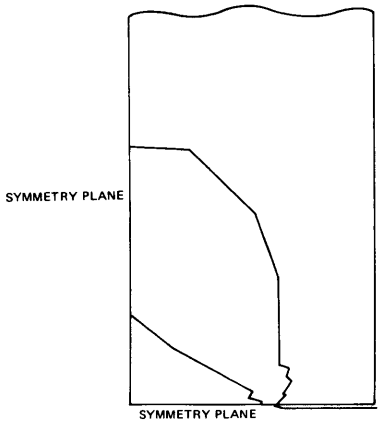

Figure 13c – For n = 9 and σ_∞ / σ_y = 0.9 (Case 6)

Figure 13 – Plastic Zones for Double-Edge Notched Specimen, 2a/w = 0.4

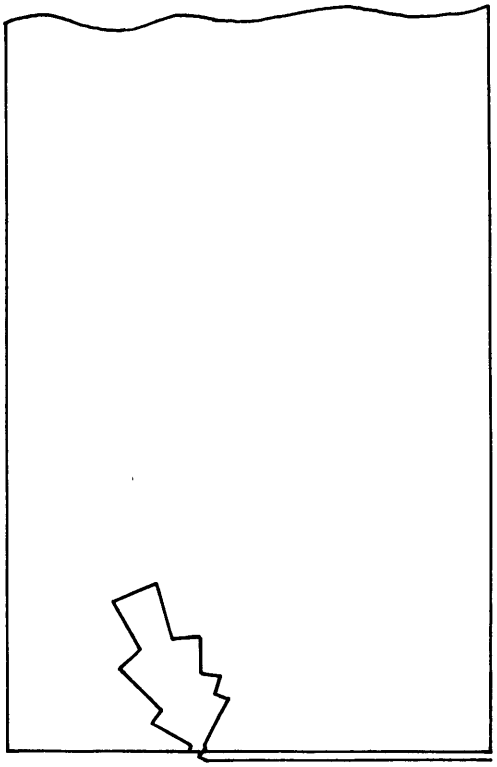

Figure 14a – For n = 3, σ_∞ / σ_y = 0.6 (Case 8)

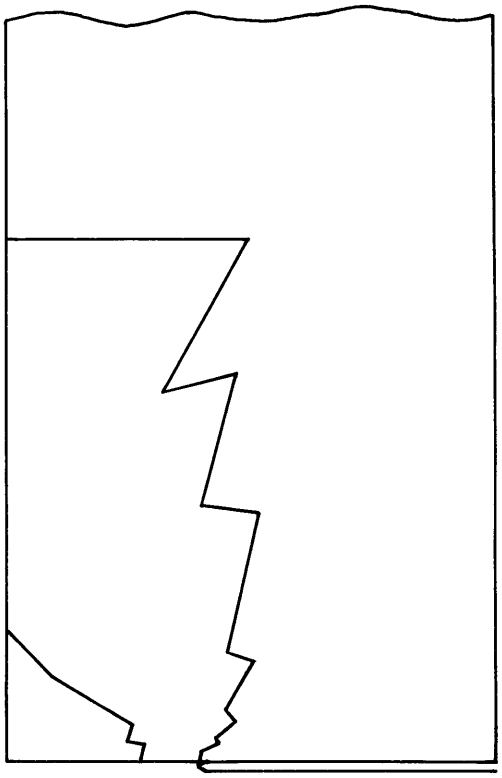

Figure 14b – For n = 3, σ_∞ / σ_y = 0.8 (Case 9)

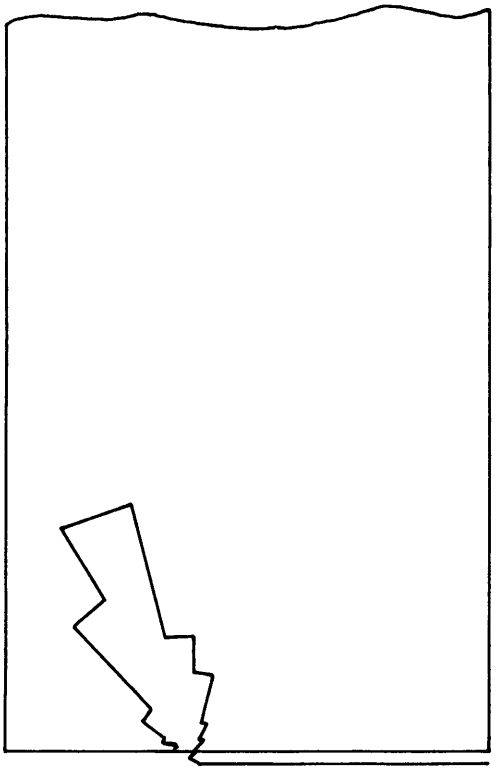

Figure 14c – For n = 9, σ_∞ / σ_y = 0.6 (Case 10)

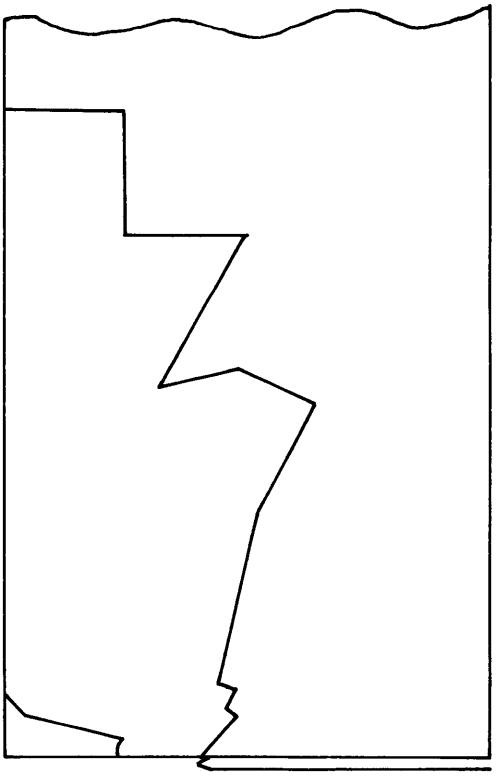

Figure 14d – For n = 9, σ_∞ / σ_y = 0.8 (Case 11)

Figure 14 – Plastic Zones for Double-Edge Notched Specimen, 2a/w = 0.6

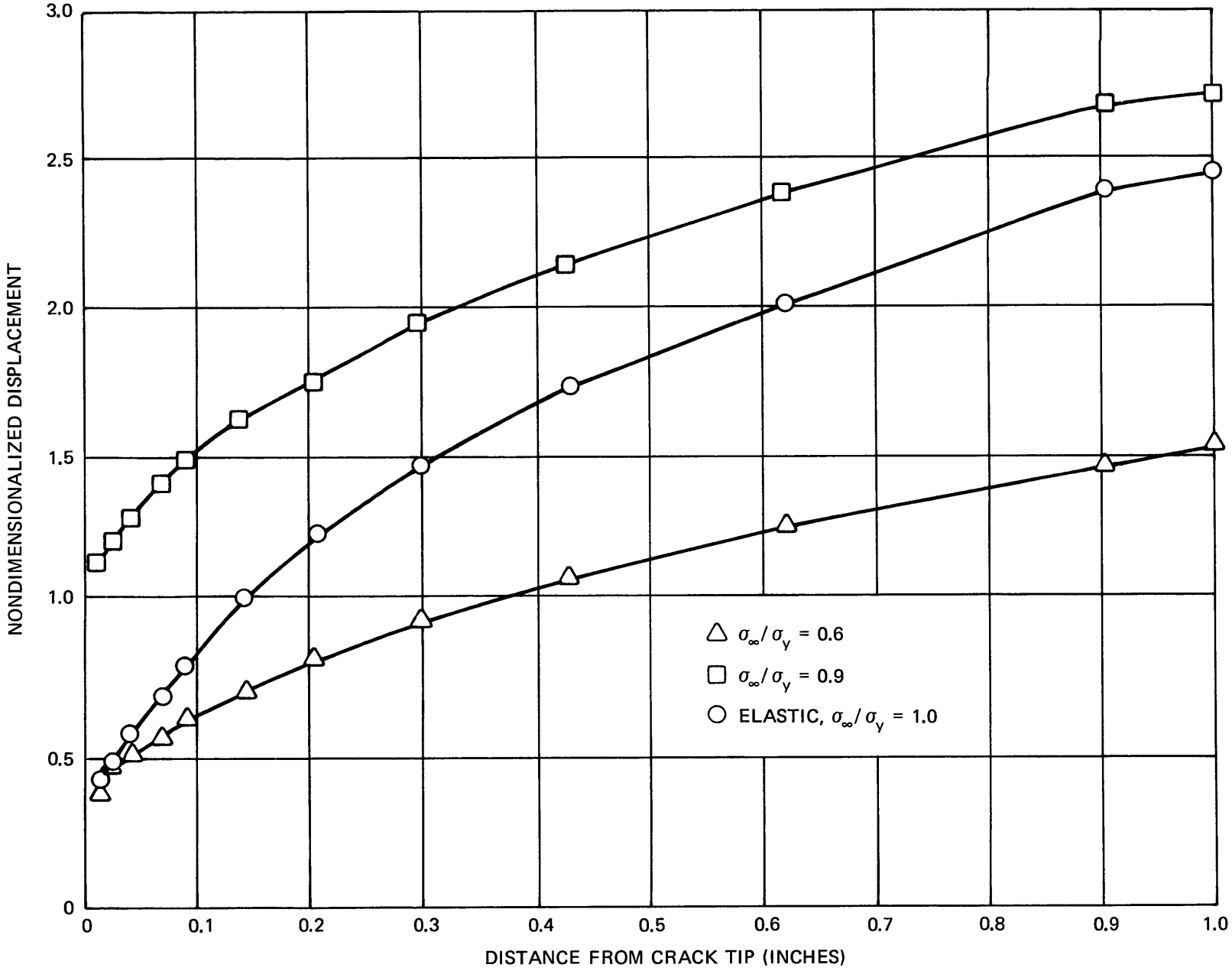

Figure 15 – Displacement along Crack Face for 2a/w = 0.4 and n = 9

for an applied stress to yield stress of 1.0 is also shown for comparison. Note that considerable "crack tip blunting" occurred and also that a significant increase in COD was obtained for $\sigma_\infty/\sigma_y = 0.9$ but not for $\sigma_\infty/\sigma_y = 0.6$.

AXISYMMETRIC HOLLOW CYLINDERS

Consider next the problem of an axisymmetric hollow cylinder containing an exterior circumferential crack subjected to remote axial tensile stress σ_∞ and internal (P_i) or external (P_0) pressure. The intent here is to examine the effect of curvature on the elastic-plastic solution and on the amplitude of the plastic singularity. This problem also demonstrates the effects of triaxial loading (which results from the applied pressure) on elastic-plastic fracture predictions. The occurrence of such loading conditions is typical for components of submerged vessels. It should be recalled that loadings which do not cause stresses normal to the crack face, such as the pressure situation to be considered here, do not influence the elastic stress intensity factor and thus are not accounted for in elastic fracture predictions. The fact that this type of loading does influence the elastic-plastic solution and the associated plastic intensity factor has been demonstrated by Hilton[33] for a plate subjected to biaxial tension.

The axisymmetric cases considered here are listed in Table 6. In all cases, the crack depth was chosen as 1.5 inches and the cylinder thickness was taken as 2.5 inches. Inside radii of 25 and 18.5 inches were considered for values of the hardening coefficient n of 3 and 9. Various combinations of axial and pressure loads were analyzed as indicated in the table. Elastic-plastic boundaries for some of these calculations are shown in Figure 16.

Similar to the double-edge notched plane strain specimen, the calculated amplitude of the plastic singularity k_ϵ and the displacement of the crack surface at the exterior of the cylinder were only slightly above the elastic predictions for these quantities at relatively small values of the applied load (Cases 1–5). In this load range, the plastic zones are observed to be contained within an elastic region. The more interesting observation to be made here is that the addition of external pressure to the cylinder increased the values for the plastic singularity parameter k_ϵ, the J_{ND} integral, the COD, and the average load point displacement. Further, the percentage increase in these parameters with the addition of external pressure increased rapidly with increasing axial load. These results are consistent with the biaxial

---

[33]Hilton, P.D., "Plastic Intensity Factors for Cracked Plates Subjected to Biaxial Loading," Int. J. Fract., Vol. 9, No. 2 (Jun 1973).

TABLE 6 – PLASTIC RESULTS FOR EXTERNAL CIRCUMFERENTIAL CRACK IN HOLLOW CYLINDER

Case	R_i	R_0	σ_∞/σ_y	P_i/σ_y	P_0/σ_y	n	$k_{\epsilon_{SSY}}$	k_ϵ	J	COD	COD (Elas.)	Average Load Point Displacement
1	25	27.5	0.3	0	0	3	0.51	0.55	2.50	3.55	3.36	3.55
2	25	27.5	0.3	0	0	9	0.52	0.53	2.30	3.70	3.36	3.68
3	18.5	21.0	0.3	0	0	↓	0.43	0.44	1.86	3.11	2.89	4.26
4	↓	↓	0.3	0.075	0	↓	0.43	0.45	1.87	3.10	2.89	2.69
5	↓	↓	0.3	0	0.09	↓	0.43	0.53	2.25	3.48	2.89	7.18
6	↓	↓	0.45	0	0	↓	0.90	1.08	5.04	5.42	4.32	6.91
7	↓	↓	0.45	0.075	0	↓	0.90	1.24	5.85	5.90	4.32	5.64
8	↓	↓	0.45	0	0.09	↓	0.90	3.32	17.5	15.6	4.32	24.0
9	↓	↓	0.6	0	0	↓	1.5	3.06*	16.0*	10.3*	5.77	11.7*
10	18.5	21.0	0.6	0.075	0	9	1.5	4.25*	23.0*	13.5*	5.77	12.5*

*Extrapolated value, results not converged.

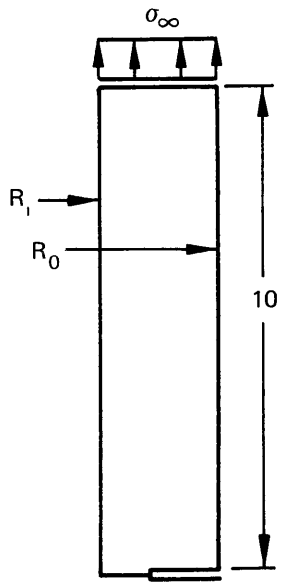

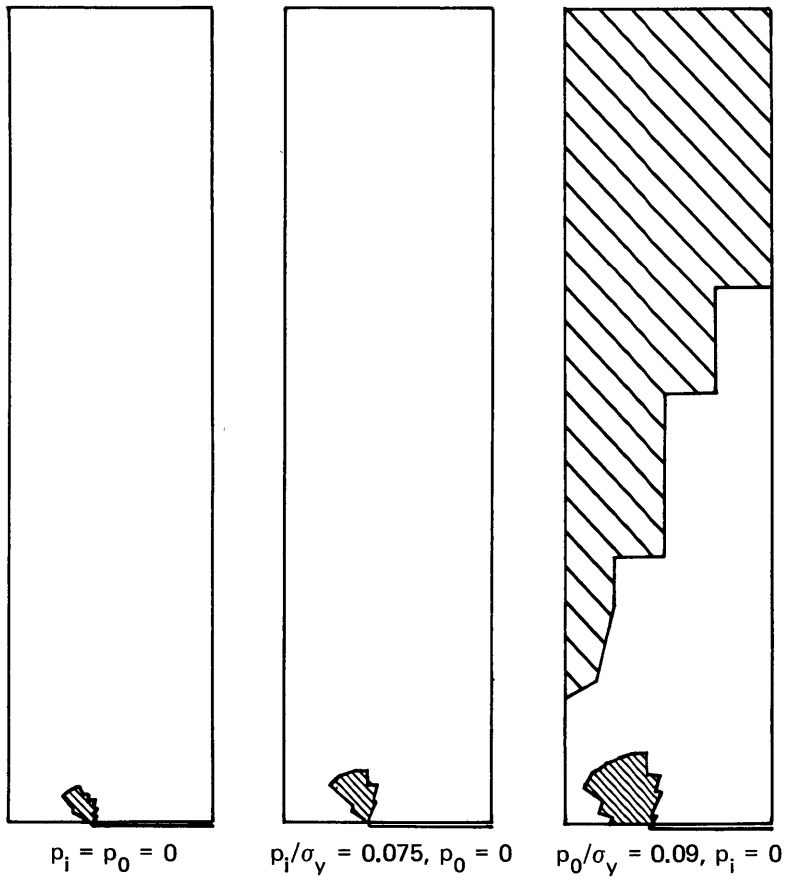

Figure 16a – For $\sigma_\infty/\sigma_y = 0.3$

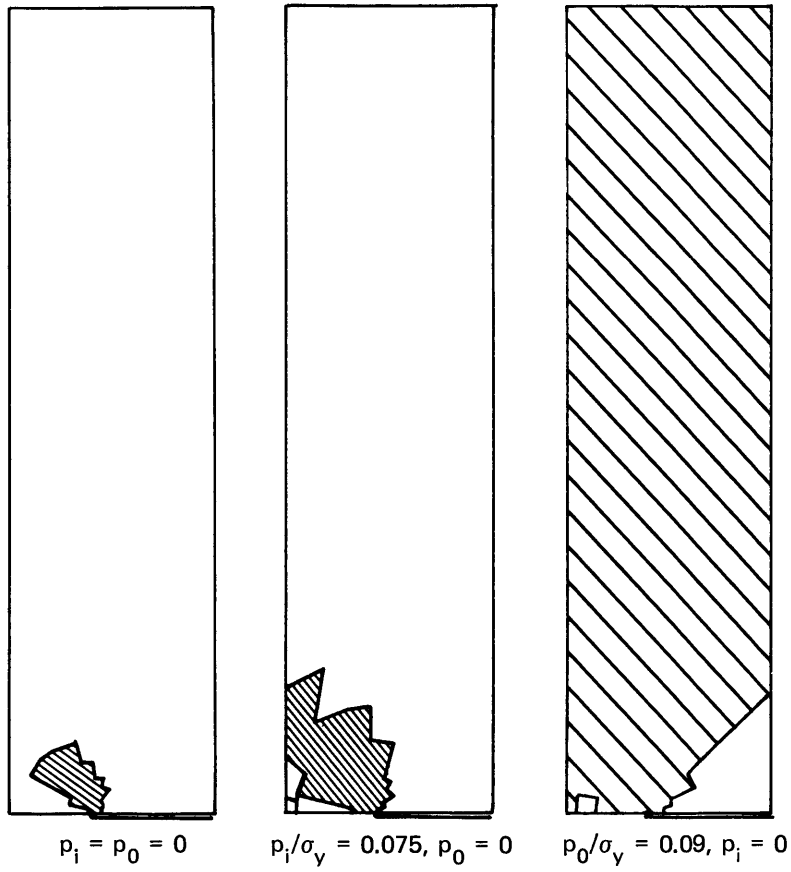

Figure 16b – For $\sigma_\infty/\sigma_y = 0.45$

Figure 16 – Plastic Zones in Hollow Cylinder Wall for Various Loading Conditions

results reported in Hilton.[33] This effect appears to be related to the plastic yield condition (von Mises), i.e., the addition of external pressure loading causes compressive circumferential stresses in the cylinder, thereby reducing the axial stress at which an element of material will yield. The increased size of the yield zones associated with the external pressure is clearly observable in Figure 16. Further, the earlier results reported here and by Hilton[7,33] indicated that the elastic-plastic predictions for the amplitude of the plastic singularity deviate increasingly from the elastic (small-scale yielding) predictions with increasing plastic zone size. Since the effect of external pressure is to increase the plastic zone size, it consequently also increases the singularity parameters k_ϵ and J. On the other hand, the effect of internal pressure on the elastic-plastic predictions is much less pronounced, as shown in Table 6 and Figure 16.

SINGLE-EDGE NOTCHED BEND SPECIMENS

Elastic-plastic finite element analyses have been performed for plane strain bend specimens containing edge cracks frequently used in fracture toughness testing. The purpose of these calculations is to determine the plastic strain intensity factor k_ϵ, the J integral, etc. at loads which correspond to K_{I_c} as estimated from elastic fracture analysis. The comparison of calculated k_ϵ values with $k_{\epsilon_{SSY}}$ results at these load levels is expected to provide a measure of the inaccuracy which results from application of elastic fracture mechanics for these specimens.

For this purpose, specimens with cracks of length 2.0, 0.4, and 0.1875 inches were analyzed. (The other pertinent geometrical data for the calculations are summarized in Table 7.) The material properties were approximated as

$$\sigma_y = 112.5 \text{ ksi}$$
$$n = 9$$
$$K_{I_c} = 125 \text{ ksi}\sqrt{\text{in.}}$$

Elastic stress analyses were performed to determine the elastic stress intensity factor; values for K_I/σ_∞ are given in Table 7. Here, σ_∞ corresponds to the applied bending stress at the outer surface of the beam ($\sigma_\infty = 6M/BW^2$). These results were used to estimate (based on elastic fracture mechanics) the value of σ_∞/σ_y at which failure should occur ($\sigma_\infty/\sigma_y = K_{I_c}/(K_I\ \sigma_y)$) leading to values of σ_∞/σ_y = 0.3, 1.0, and 1.45 for crack lengths a = 2.0, 0.4, and 0.1875 inches, respectively.

The results of the elastic-plastic stress analyses for the bend specimens are given in Table 7 and the corresponding plastic zones indicated in Figures 17–19. In each case, the loading

TABLE 7 – ELASTIC-PLASTIC RESULTS FOR BEND SPECIMENS

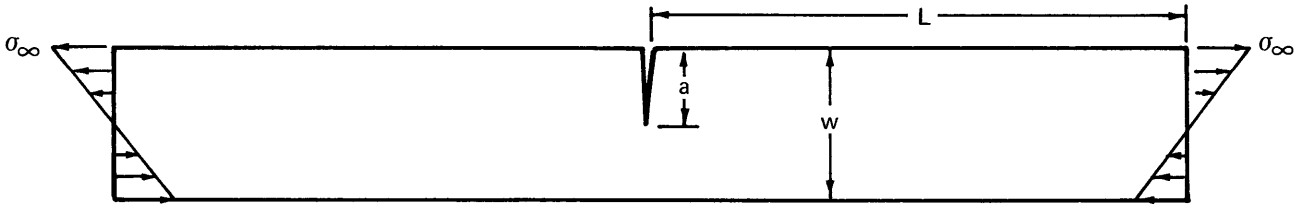

Specimen	a	w	L	σ_∞/σ_y	n	$k_{\epsilon_{SSY}}$	k_ϵ	J_{ND}	COD_{ND}	$COD_{(Elas.)_{ND}}$	$\frac{K_I}{\sigma_\infty}$
1	2.0	4.0	12.0	0.3	9	0.277	0.296	1.19	3.10	3.0	3.665
2	0.4	4.0	8.0	1.0	9	0.286	0.310	1.25	1.13	1.00	1.123
3	0.1875	2.0	4.0	1.45	9	0.281	0.351	1.43	0.891	0.675	0.763

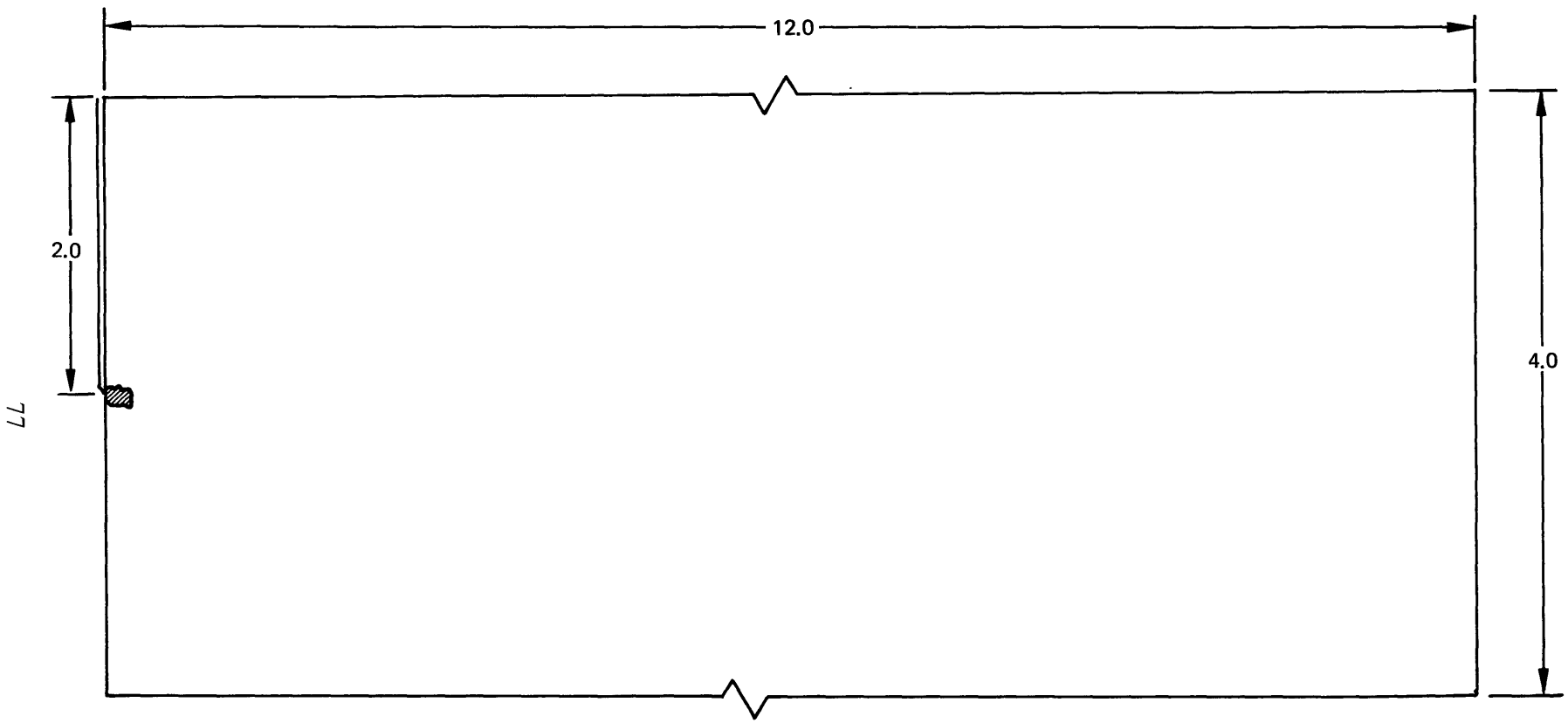

Figure 17 – Plastic Zone for Bend Specimen 1 (σ_∞/σ_y = 0.3)

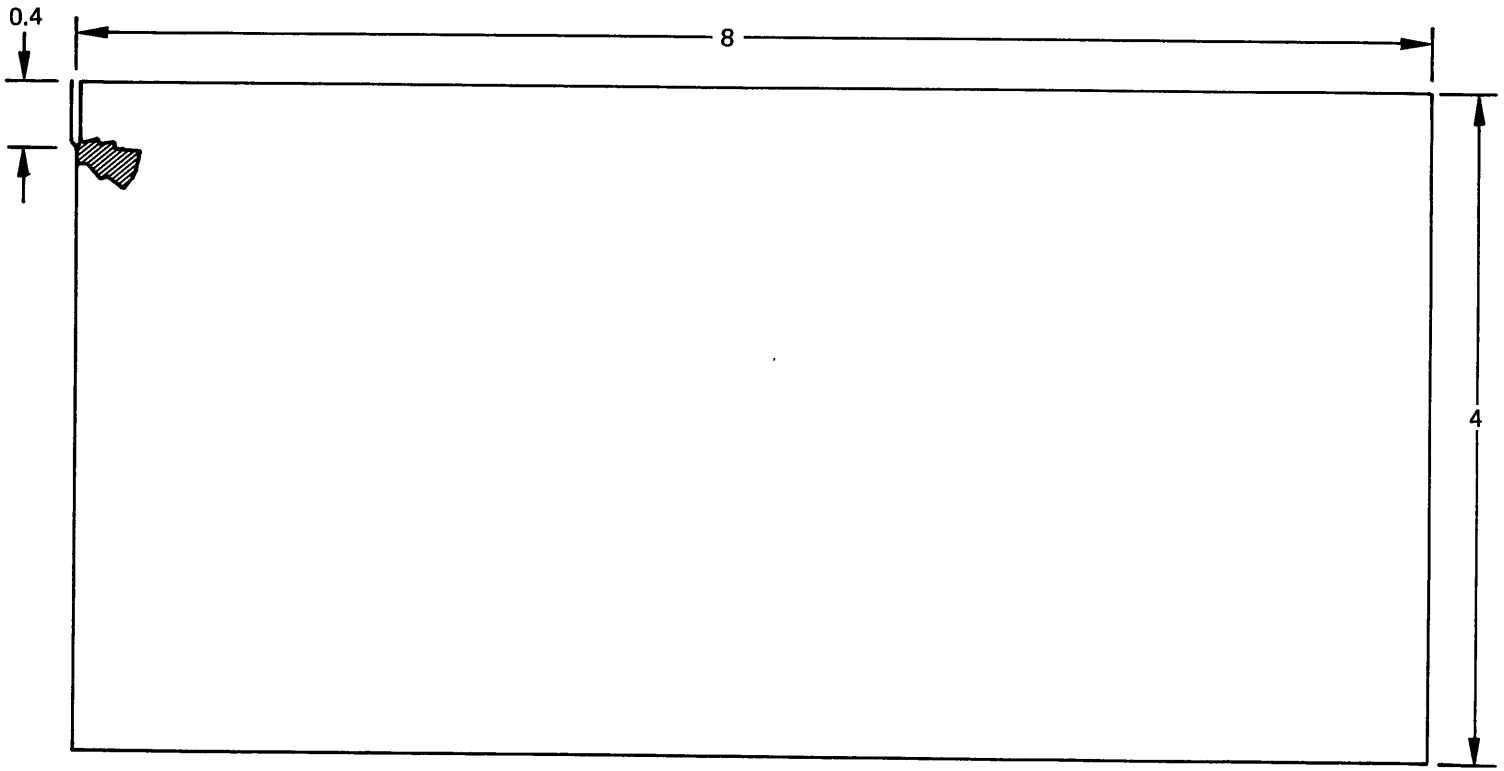

Figure 18 – Plastic Zone for Bend Specimen 2 (σ_∞ / σ_y = 1.0)

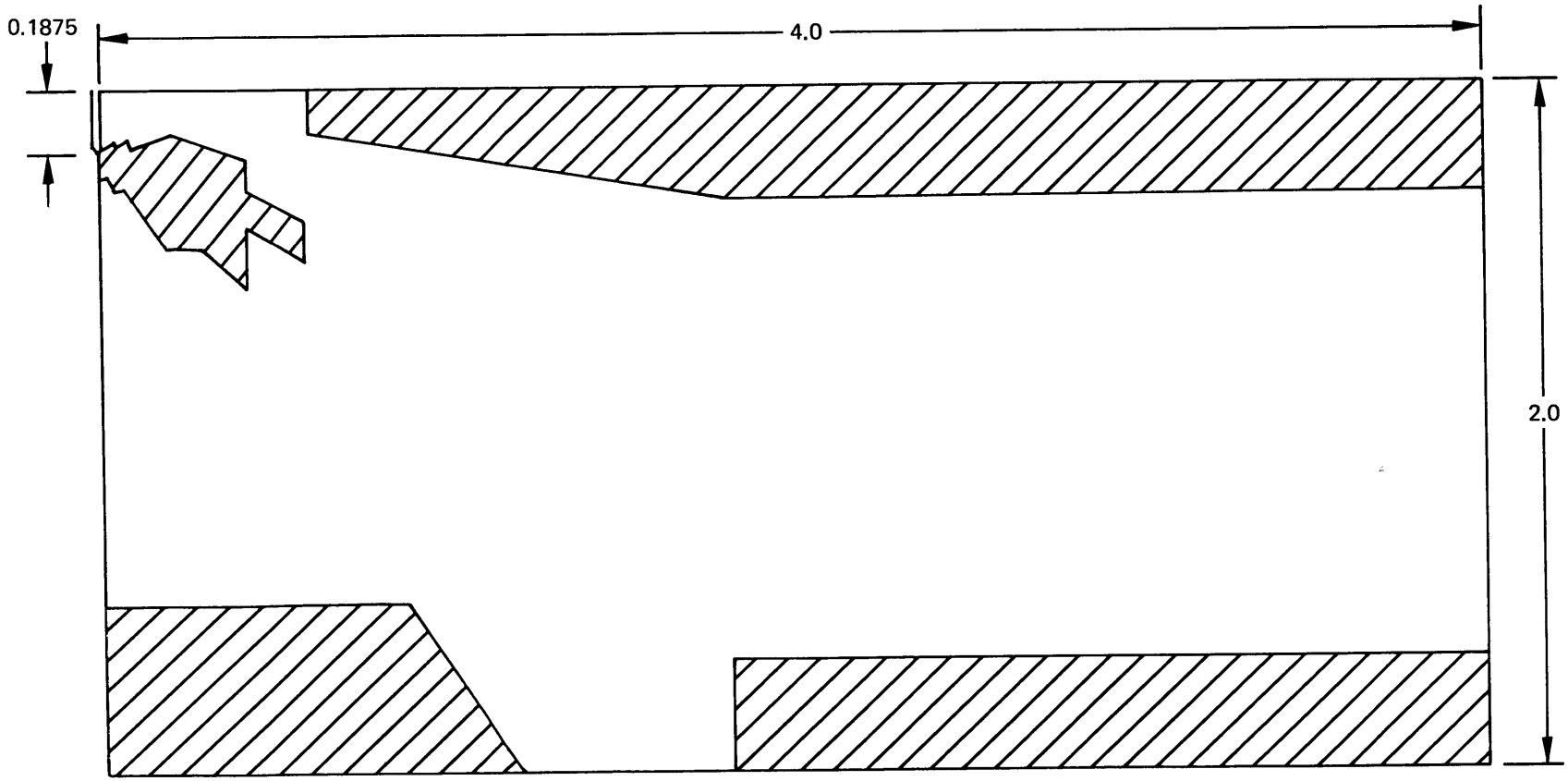

Figure 19 – Plastic Zones for Bend Specimen 3 (σ_∞ / σ_y = 1.45)

corresponds to the same value of the elastic stress intensity factor K_{I_c}. Notice that as the crack length is decreased, larger bending stresses must be applied to reach this state. As a result, both the relative and absolute sizes of the plastic zones increase with decreasing crack length, i.e., the elastic-plastic solution deviates further from the elastic solution. This is demonstrated by comparing the plastic strain intensity factors with their corresponding small-scale yielding values. It also shows up in comparing the ratios of the plastic crack opening displacement to its elastic value. Figure 20 indicates the variation of net section stress σ_n (nondimenisonalized by the remote fiber stress σ_∞) ahead of the crack tip for Specimen 3. It was assumed that σ_∞ = 163 ksi. The results of an elastic analysis based on QUAD-12 elements are also given. In the immediate vicinity of the crack tip, the effect of crack tip blunting[34] precludes the determination of peak plastic stress by means of existing analytical methods.

In addition to the elastic-plastic calculations described above, it was deemed appropriate for comparison purposes to perform calculations for a specimen which had been analyzed by another author. The four-point bend specimen of Wilson and Begley,[35] analyzed by the finite element method without the use of a singular element, was chosen for this purpose. The specimen geometry is shown in Table 8 and the original material stress-strain curve is reproduced as Figure 21. The analysis procedure used here requires a modeling of that curve by the equation

$$\epsilon/\epsilon_y = \begin{cases} \sigma/\sigma_y & \sigma \leqslant \sigma_y \\ (\sigma/\sigma_y)^n & \sigma > \sigma_y \end{cases}$$

where n and σ_y are to be adjusted to fit the curve. As shown in Figure 21, the material model chosen incorporated an artificially reduced yield stress to account for the yield point instability and more closely approximates the experimentally obtained material curve.

Calculations were performed with this model for normalized load values ($F = P/2B\,\sigma_y$) corresponding to Figure 17 of Reference 35 in order to compare the results with numerically obtained J values. A supplementary elastic analysis was carried out to obtain the elastic stress intensity factor, giving the result $K_I = 5.5\,F$. For small-scale yielding, the nondimensionalized J value for plane strain is given by Equation (39). Here, the calculated

---

[34]Rice, J.R. and M.A. Johnson, "The Role of Large Crack Tip Geometry Changes in Plane Strain Fracture," Brown University Report NYO-2394-38 (Sep 1969).

[35]Wilson, W.K. and J.A. Begley, "Heavy Section Steel Technology Program Technical or Programmatic Manuscript No. 25–Variable Thickness Study of the Edge Cracked Bend Specimen," Westinghouse Electric Corporation Report WCAP-8237 (Nov 1973).

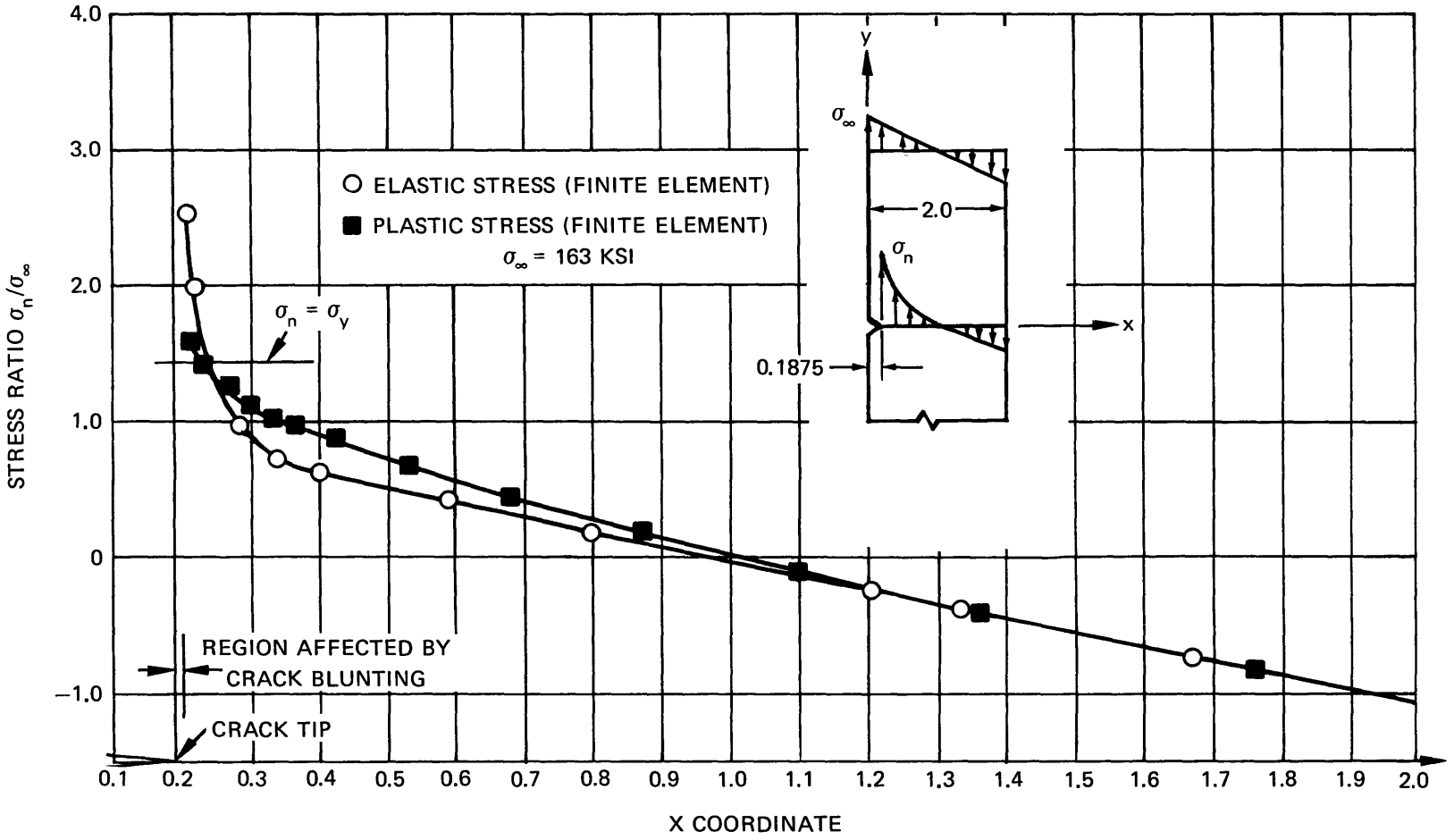

Figure 20 – Net Section Stress Variation ahead of Crack for Bend Specimen 3

TABLE 8 – COMPARISON OF PLASTIC J VALUES FOR WILSON AND BEGLEY BENDING SPECIMEN

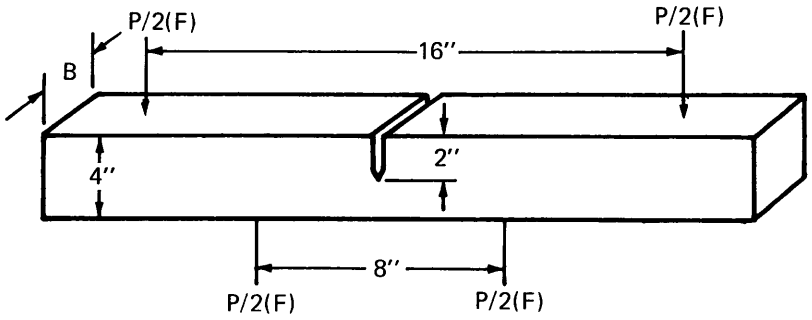

P/B ksi	Normalized Point Load F	$[J_{ND}/(J_{ND})_{SSY}]^{1/2}$ (This Analysis)	$[J_{ND}/(J_{ND})_{SSY}]^{1/2}$ (Reference 35)
57.1	0.492	1.56	1.5
64.6	0.551	2.01	2.1

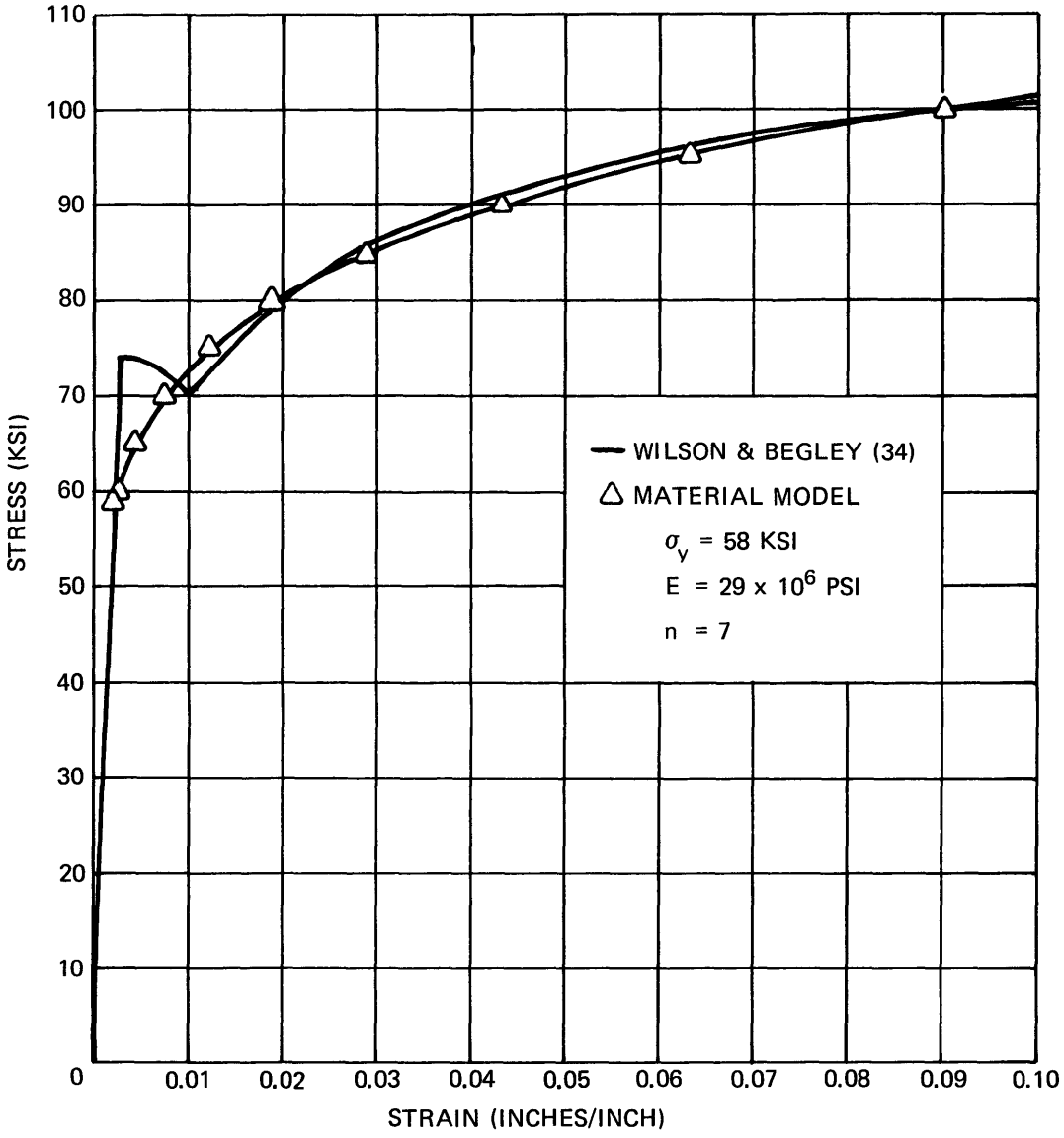

Figure 21 – Stress-Strain Curves for Four-Point Bend Specimen
(From Wilson and Begley[35])

(elastic-plastic) J values have been normalized by taking Young's modulus E = 1.0. Thus

$$[J_{ND}/(J_{ND})_{SSY}]^{1/2} = \left(\frac{J}{1-\nu^2}\right)^{1/2} \cdot \frac{1}{5.5\,F}$$

Comparative values of $[J_{ND}/(J_{ND})_{SSY}]^{1/2}$ from this analysis and from the Wilson and Begley[35] incremental finite element results are in good agreement as shown in Table 8.

Computationally, the method presented here is more advantageous in that once convergence on k_ϵ has been obtained, the J integral is evaluated directly via Equations (37) and (42), thus bypassing the need for numerical contour integration. It should be noted, however, that results obtained here are rather sensitive to the choice of parameters n and σ_y which characterize the stress-strain curve of the material in accordance with the Ramburg-Osgood model, Equation (16).

SUMMARY AND CONCLUSIONS

Recognition of the effects of notches and cracks on structural performance is a basic prerequisite for the successful application of new materials to high performance structures. Invariably, one complicating factor is the relationship of various specimens to fatigue and fracture performance of full-scale structures. The concepts of fracture mechanics have emerged in recent years as one of the most promising analytical tools for bridging the gap between laboratory specimens and full-scale structural details. As in all engineering disciplines, the utilization of new analytical techniques requires a thorough understanding of their limitations. Nevertheless, the usefulness of the stress intensity factor as a correlating parameter for fracture in the linear elastic range applicable to brittle materials is now well recognized. The range of applicability to fatigue crack propagation is even wider; for a broad range of materials, crack growth rates have been successfully calculated by means of the range of the stress intensity factor.

By contrast, the framework of elastic-plastic fracture mechanics is at a much earlier stage of development. Progress is being made in applying such concepts as the J integral and crack opening displacement not only to characterize material but also to evaluate structural performance. The application of elastic-plastic fracture mechanics is expected to be to materials in the intermediate toughness range. Here, within the context of high localized stresses (applied or fabrication induced) and material nonlinearity, the concepts of linear elastic fracture mechanics are no longer adequate for elucidating many aspects of fatigue and

fracture. These include stress biaxiality, thickness effects, deflection vis-a-vis load-controlled crack growth, sustained load cracking from prestrained notches, and sequence effects in low-cycle fatigue.

One factor that hampers the use of fracture mechanics to evaluate structural performance is the difficulty of calculating governing stress-flaw size parameters for full-scale structural details with highly localized and complex applied or fabrication-induced stress fields. Without the capability for such calculations, fracture mechanics methodology can be used only as a sophisticated tool for screening materials; its potential as a quantitative method for evaluating structural performance cannot be exploited. Even in the linear elastic fracture mechanics range, where stress intensity factor K_I plays the dominant role, recourse must often be made to numerical methods. These are required, for example, for the evaluation of the J integral and crack opening displacement even for many of the simple laboratory type specimens.

Within this framework, this report represents an essential phase of the NSRDC effort to develop quantitative methods for fatigue and fracture of high performance structures. The major elements of the report as well as some general conclusions are outlined below.

In the first part of the report, a method has been demonstrated whereby accurate elastic stress intensity factors can be calculated by using the finite element method for arbitrary two-dimensional and axisymmetric structures under Mode I or combined Modes I and II loading conditions. The mathematical presentation has been made with the modification of standard finite element program in mind. The introduction of a special singular crack tip element, which is independent of the conventional finite element used, enables stress intensity factors to be calculated directly rather than being merely deduced later on the basis of some arbitrary extrapolation of conventional finite element results.

The introduction of the high order, 12-node isoparametric element as a "conventional" element results in very high accuracy throughout the cracked structure. It also enables the idealization of practical problems in a small fraction of the time ordinarily required in the past when less sophisticated elements were used. The incorporation of this element into an "out-of-core" computer program requiring less than 20,000 decimal words of computer storage for execution of large problems makes it possible to obtain results in a matter of minutes on any third-generation computer.* These two approaches, in combination, enable the rapid solution of large numbers of problems, including parametric studies, which would have been prohibitive in the past. It appears reasonable to state that the oldest and most

*Calculations at NSRDC are presently performed on the CDC 6700 computing system. Results are obtained on a "while-you-wait" basis at a remote terminal only steps away from the author's working area.

valid objection to the finite element method—the manpower and costs required for its use—has been largely overcome in the context of elastic problems considered here.

In the second part of the report, the combination of a plastic singular crack tip core element with four-noded conventional elements extends the fracture mechanics analysis into the elastic-plastic (strain-hardening) range. Previous work of Rice and Hutchinson was utilized to develop the stiffness properties of the core element. Solutions were obtained for a number of conventional cracked specimen configurations; integral parts of these solutions are the J integral, plastic zone size, and crack opening displacement. This approach can now be used as a valuable technique for the interpretation of experimental data on fracture (including stress corrosion cracking) in situations where linear elastic fracture mechanics is not considered to be applicable. Conversely, it can be helpful in setting limits of applicability of linear elastic fracture mechanics. A combined experimental/analytical approach is essential in the development of rational fracture criteria in the elastoplastic range.

FUTURE STUDIES

On the basis of the results obtained in this report and in the context of the broad requirements for analytical methodology in fracture and fatigue, the following studies appear warranted:

1. Although the combination of standard finite elements with a circular singular element of the type described in this report is a good method, it is only one of several possible approaches to the direct computation of stress intensity factors by the finite element method. Several alternative methods are described by Wilson.[11] A method described by Benzley and Beisinger[20] may prove superior to the embedded singular element approach and warrants exploration. Here, the conventional finite element displacement assumption is "enriched" with the singular displacements of Equation (2) for elements having a nodal point which coincides with a crack tip. The advantage of this approach is that problems may be modeled in terms of one element type only without concern for local crack tip modeling; moreover displacement continuity is maintained in the region near the crack tip. More importantly, the approach appears capable of modeling arbitrary notch geometries and may be used for stress concentration as well as stress intensity factor solutions, thus providing the necessary information for crack initiation analysis. The only disadvantages of the approach appear to be (1) the need for more expensive and complicated computations in forming enriched element stiffness matrices and (2) the greater difficulty and effort inherent in modifying a standard finite element program to incorporate the method. The accuracy of the approach compared

to that of the embedded singular element is unknown at this time. Plans have been made to modify the NSRDC QUAD-12 program to permit fracture calculations with this method as a program option.

2. Parametric studies should be initiated on typical welded details containing cracks. For best efficiency in such studies, it is essential that additional work be conducted to automate the local grid generation in the vicinity of the crack tip and to otherwise further reduce the computer costs associated with such studies. Although computer costs are fairly reasonable already, it is clear that they can be reduced still more. It is not yet clear, however, how much additional reduction can be achieved without major program revisions. These would entail a sacrifice of the modest core requirements now enjoyed in problem solution.

3. The combination of singular crack tip and high order isoparametric elements should be extended to the plastic regime. As in the case of elastic analysis, an alternate approach based on "enriched" isoparametric elements should be explored.

4. Finally, the use of finite elements should be investigated for modeling the growth of cracks in residual stress fields induced by fabrication processes.

ACKNOWLEDGMENTS

The authors are indebted to Dr. C.F. Shih of Harvard University for supplying numerical input necessary for the plastic calculations, to Dr. S.E. Benzley of Sandia Laboratories, Albuquerque, for providing a copy of his CHILES fracture mechanics computer program, and to Ms. L.P. Massaro of NSRDC for her continued technical support in this work.

APPENDIX A

AUGMENTATION OF A STANDARD FINITE ELEMENT PROGRAM FOR ELASTIC ANALYSIS

The embedded singularity finite element approach discussed here can be rather easily implemented into a standard two-dimensional, plane strain/plane stress/axisymmetric computer program, provided one is careful and familiar with the computational setup of the particular program. The modification is most easily accomplished if the first N1 nodal points are required to lie on the singular core element,* node 1 corresponding to $\theta = -\pi$ and node N1 corresponding to $\theta = \pi$. (For Mode I only, node 1 corresponds to $\theta = 0$ and node N1 corresponds to $\theta = \pi$, and the core element is a half-disk.) In this manner, the only additional input data required for the embedded singular element is the x coordinate of the crack tip (for the axisymmetric case), the angle α of the crack, the radius r_0 of the core element, the number of nodes on the core element, and—if the program is to be capable of handling the symmetric case of Mode I only—** a flag indicating whether the problem is Mode I only or combined mode.

The description given here assumes that the master stiffness matrix is contained "out-of-core" on a peripheral storage unit*** (say, TAPE 3) and that another peripheral storage unit (say, TAPE 7) is available for "scratch" storage. The nodal displacement vector and the load vector are assumed to be in-core, and enough core storage is assumed to be available for holding the first four rows of the master stiffness matrix from the diagonal terms to the end of the nonzero band. The procedure to be followed is then as follows:

1. The singular element is modeled as an unconstrained "hole," and the master stiffness matrix (including modification for constrained nodes) and load matrix for this "auxiliary" problem are formed in the standard manner. As assumed above, the rows of the master stiffness matrix are written one row at a time onto TAPE 3 as they are formed.

2. The master stiffness matrix is then copied from TAPE 3 to TAPE 7.

3. Equations (10) are now treated as if the stiffness terms k_{ij} are master stiffness values, i.e., the summation over the elements is disregarded since this has already been accomplished in constructing the master stiffness matrix. The first 2(N1) rows of the master stiffness matrix are then read from TAPE 3 (one row at a time), from which the first four specialized equations, Equations (10a) through (10d), are constructed. Note that because the master stiffness matrix is symmetric, all necessary stiffness terms are contained in the first 2(N1) rows.

---

*It is assumed here for simplicity that only one crack tip is to be permitted in the structure. Generalization to multiple singular points becomes more complicated but may be implemented in a manner analogous to the method outlined here.

**This option is easily implemented and will be discussed in the following.

***If the master stiffness matrix is contained "in-core," the steps outlined here become especially easy to implement.

4. TAPE 3 is then rewound and the first four special rows of the augmented stiffness matrix are written onto it. Beginning with Row 2(N1) + 1, TAPE 7 is then read and written onto TAPE 3 to complete the specialized master stiffness matrix.

5. The order of the master stiffness matrix is thus reduced by the quantity [2(N1) −4], and the load matrix is shifted accordingly.

6. Nonhomogeneous terms associated with crack face loading as calculated by minimization of Equation (14) are then added, if necessary, into the master load vector.

7. This modified system is then solved by an out-of-core equation solver to give k_1, $u_{0x'}$, k_2, $u_{0y'}$, and the displacements of all nodes except those on the singular element. The stress intensity factors are then given by $K_I = E\, k_1$ and $K_{II} = E\, k_2$.

8. The displacements of nodes on the core element are recovered by evaluation of Equation (5). From this point on, the finite element program operates in its standard fashion. The procedure described above is for a specific program structure, but it should be easily applicable to any program organization. Although the modification described above is conceptually easy, it should not be taken lightly, particularly in programs where compact storage schemes result in rather complex bookkeeping operations. In such cases, there are many subtle areas and ways for introducing errors which can lead the unwary into "rebugging" a checked-out program.* Modifications of the type described here should be undertaken only by an individual who is completely familiar with the notation, storage, and operation of the finite element program to be modified.

Finally, it should be pointed out that symmetric, Mode I computations may be made economically by using the procedure described here. For this case, the core element becomes a half-disk about which all nodes are again unconstrained. Now the nodes on the half-disk are numbered counterclockwise from 1 at $\theta = 0$ to N1 at $\theta = \pi$. The exact same procedure is then followed with but two exceptions:

1. The quantity B_1 of Equation (7) is multiplied by 1/2.

2. The unknowns k_2 and $u_{0y'}$ are constrained to be zero in the standard finite element manner.**

---

*This is popularly called "program regression."

**Thus the specialized equations corresponding to k_2 and $u_{0y'}$ do not even need to be calculated.

APPENDIX B
SPECIALIZED FORMS FOR CONSISTENT CRACK FACE LOADING

Figure B.1 shows the region about the singular core element which must be considered in evaluating the special nonhomogeneous "loading" terms R_1, R_2, R_3, and R_4 which respectively correspond to the unknowns k_1, $u_{0x'}$, k_2, and $u_{0y'}$. These terms result from tractions σ_{ns} and τ_{ns} on the crack face as shown in their positive directions in the figure; σ_{ns} and τ_{ns} are assumed to vary linearly with respect to distance along the crack in the sequel.

The standard finite elements in Figure B.1 are intended to represent both the QUAD-4 and QUAD-12 elements in their isoparametric forms* in order that both element types can be treated simultaneously. Midside nodes such as b and c or f and g should be disregarded for the QUAD-4 element. In accordance with the usual isoparametric notation,[12] the geometry and displacement assumptions may be written

$$\left.\begin{aligned} x &= \sum_{i=1}^{M} N_i(\alpha, \beta)\, x_i \\ y &= \sum_{i=1}^{M} N_i(\alpha, \beta)\, y_i \end{aligned}\right\} \text{geometry} \qquad \text{(B1)}$$

$$\left.\begin{aligned} u_x &= \sum_{i=1}^{M} N_i(\alpha, \beta)\, u_{x_i} \\ u_y &= \sum_{i=1}^{M} N_i(\alpha, \beta)\, u_{y_i} \end{aligned}\right\} \text{displacement}$$

where α** and β are dimensionless isoparametric coordinates having the value ± 1 at the various element edges, and where M is the number of nodes associated with the element (4 or 12 here). For simplicity of presentation, the element edges corresponding to $\beta = 1$ have been

---

*Consistent "loading" terms for the four-node isoparametric element are identical to those for the constant stress triangle from which the QUAD-4 element of this report is developed.

**α is not to be confused with its earlier usage as the crack angle.

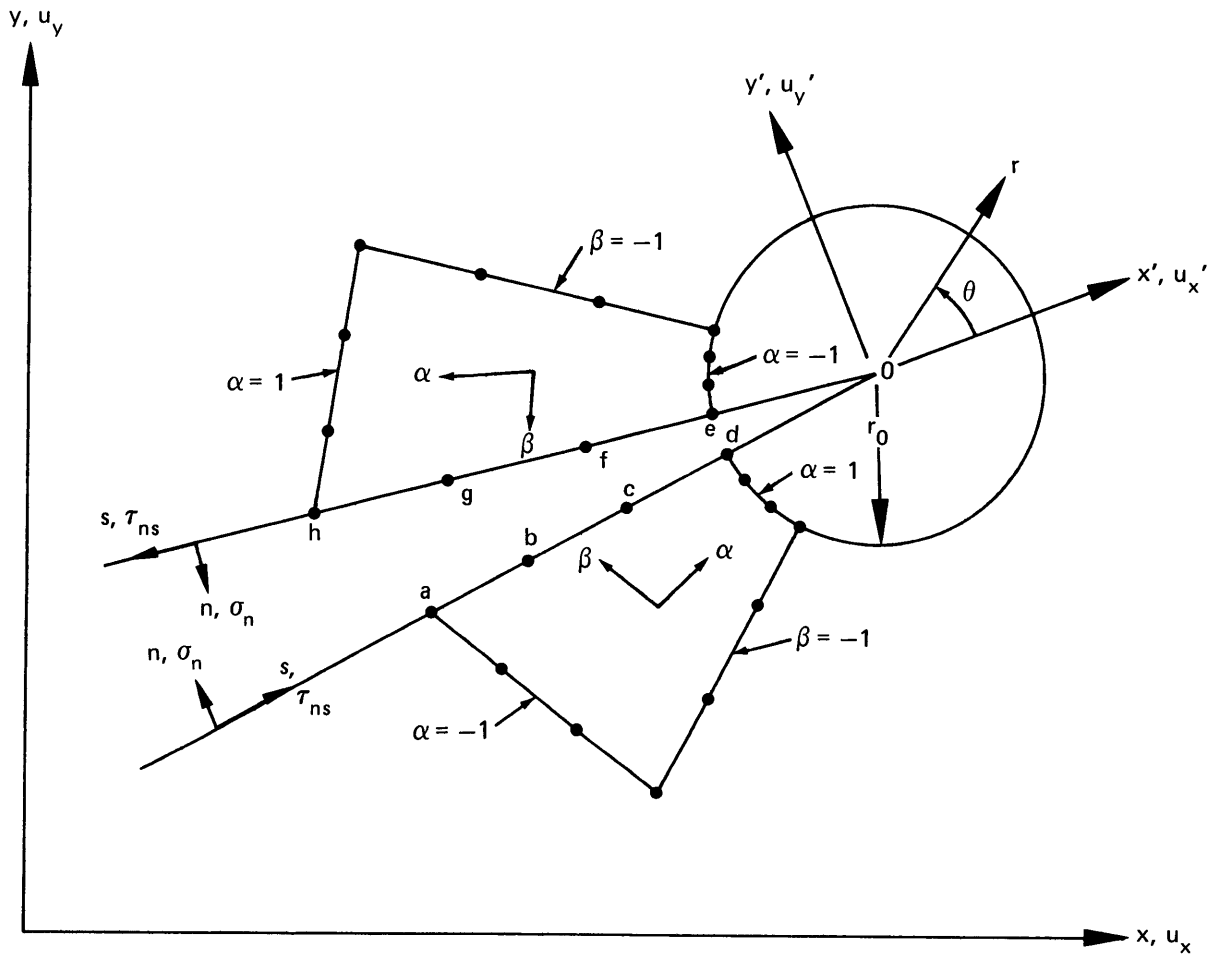

Figure B.1 – Elements Adjoining Core under Crack Face Loading

assigned to the crack face as shown in Figure B.1. The "shape functions" or interpolating polynomials N_i for both the QUAD-4 and QUAD-12 elements are given by Zienkiewicz[12] along with additional details on the formulation of isoparametric elements.

With these preliminaries aside, the work integral, Equation (14), may be written in terms of Figure B.1 as follows:

$$w = \int_a^d (\sigma_n u_n + \tau_{ns} u_s)\, dA + \int_d^0 (\sigma_n u_n + \tau_{ns} u_s)\, dA + \int_0^e (\sigma_n u_n + \tau_{ns} u_s)\, dA + \int_e^h (\sigma_n u_n + \tau_{ns} u_s)\, dA \tag{B2}$$

where, from Equation (15),

$$\text{integral 1} \begin{cases} u_n = \sum_{i=1}^{M} N_i/_{\beta=1}\, u_{n_i} \\ u_s = \sum_{i=1}^{M} N_i/_{\beta=1}\, u_{s_i} \end{cases} \tag{B3a}$$

$$\text{integral 2} \begin{cases} u_n = u_{0y'} - k_1\, c_1 \sqrt{r} \\ u_s = u_{0x'} - k_2\, c_1 \sqrt{r} \end{cases} \tag{B3b}$$

$$\text{integral 3} \begin{cases} u_n = -\, u_{0y'} - k_1\, c_1 \sqrt{r} \\ u_s = -\, u_{0x'} - k_2\, c_1 \sqrt{r} \end{cases} \tag{B3c}$$

$$\text{integral 4} \begin{cases} u_n = \sum_{i=1}^{M} N_i/_{\beta=1}\, u_{n_i} \\ u_s = \sum_{i=1}^{M} N_i/_{\beta=1}\, u_{s_i} \end{cases} \tag{B3d}$$

where $c_1 = (1 + \nu)\ (\kappa + 1)/\sqrt{2\pi}$.

It can now be shown by inspection of the element shape functions N_i given in Zienkiewicz[12] that these quantities vanish at $\beta = 1$ unless the local node number i lies on the surface $\beta = 1$. Furthermore, local node numbers i corresponding to any of the nodes a, b, c, f, g, or h of Figure B.1 lead to nonhomogeneous loading terms for these nodes which may be found by the usual finite element procedure. Consequently, these portions of u_n and u_s may be subtracted out of the first and fourth displacements in Equation (B3), leaving the "special" forms for the displacements in the work integral (B2) as:

$$\text{integral 1} \begin{cases} u_n = N_d/_{\beta=1}\ u_{n_d} = N_d/_{\beta=1}\ (u_{0y'} - k_1\ c_1\ \sqrt{r_0}) \\ u_s = N_d/_{\beta=1}\ u_{s_d} = N_d/_{\beta=1}\ (u_{0x'} - k_2\ c_1 \sqrt{r_0}) \end{cases} \tag{B4a}$$

$$\text{integral 2} \begin{cases} u_n = u_{0y'} - k_1\ c_1\ \sqrt{r} \\ u_s = u_{0x'} - k_2\ c_1\ \sqrt{r} \end{cases} \tag{B4b}$$

$$\text{integral 3} \begin{cases} u_n = -\ u_{0y'} - k_1\ c_1\ \sqrt{r} \\ u_s = -\ u_{0x'} - k_2\ c_1\ \sqrt{r} \end{cases} \tag{B4c}$$

$$\text{integral 4} \begin{cases} u_n = N_e/_{\beta=1}\ u_{n_e} = N_e/_{\beta=1}\ (-\ u_{0y'} - k_1\ c_1\ \sqrt{r_0}) \\ u_s = N_e/_{\beta=1}\ u_{s_e} = N_e/_{\beta=1}\ (-\ u_{0x'} - k_2\ c_1\ \sqrt{r_0} \end{cases} \tag{B4d}$$

In Equations (B4a) and (B4d), the shape functions N_d and N_e are given by

$$\left.\begin{aligned} N_d/_{\beta=1} &= \frac{1}{16}\ (1 + \alpha)\ (9\ \alpha^2 - 1) \\ N_e/_{\beta=1} &= \frac{1}{16}\ (1 - \alpha)\ (9\ \alpha^2 - 1) \end{aligned}\right\} \text{QUAD-12} \tag{B5a}$$

$$\left.\begin{aligned} N_d/_{\beta=1} &= \frac{1}{2}\ (\alpha + 1) \\ N_e/_{\beta=1} &= \frac{1}{2}\ (1 - \alpha) \end{aligned}\right\} \text{QUAD-4} \qquad \text{(B5b)}$$

Finally, the linearly varying stresses over each of the integrals of Equation (B2) are given by:

$$\text{integral 1:} \quad \sigma(\alpha) = \frac{(\sigma_d - \sigma_a)}{2}\ \alpha + \frac{(\sigma_d + \sigma_a)}{2} \qquad \text{(B6a)}$$

$$\text{integral 2:} \quad \sigma(r) = \frac{(\sigma_d - \sigma_0)}{r_0}\ r + \sigma_0 \qquad \text{(B6b)}$$

$$\text{integral 3:} \quad \sigma(r) = \frac{(\sigma_e - \sigma_0)}{r_0}\ r + \sigma_0 \qquad \text{(B6c)}$$

$$\text{integral 4:} \quad \sigma(\alpha) = \frac{(\sigma_h - \sigma_e)}{2}\ \alpha + \frac{(\sigma_e + \sigma_h)}{2} \qquad \text{(B6d)}$$

where σ stands for σ_n or τ_{ns}.

By substituting from Equations (B4) into Equation (B2), an explicit form for the specialized work integral may be written in terms of the unknowns k_1, $u_{0x'}$, k_2, and $u_{0y'}$:

$$\begin{aligned} w = &\int_a^d [\sigma_n(\alpha)\, N_d(\alpha)\, (u_{0y'} - k_1\, c_1 \sqrt{r_0}) + \tau_{ns}(\alpha)\, N_d(\alpha)\, (u_{0x'} - k_2\, c_1 \sqrt{r_0})]\ dA \\ &+ \int_d^0 [\sigma_n(r)\, (u_{0y'} - k_1\, c_1 \sqrt{r}) + \tau_{ns}(r)\, (u_{0x'} - k_2\, c_1 \sqrt{r})]\ dA \\ &+ \int_0^e [\sigma_n(r)\, (-u_{0y'} - k_1\, c_1 \sqrt{r}) + \tau_{ns}(r)\, (-u_{0x'} - k_2\, c_1 \sqrt{r})]\ dA \\ &+ \int_e^h [\sigma_n(\alpha)\, N_e(\alpha)\, (-u_{0y'} - k_1\, c_1 \sqrt{r_0}) + \tau_{ns}(\alpha)\, N_e(\alpha)\, (-u_{0x'} - k_2\, c_1 \sqrt{r_0})]\ dA \end{aligned} \qquad \text{(B7)}$$

Equation (B7) is the most general expression for the special form for the work done by prescribed tractions in the vicinity of the singular core element. It reflects the fact that the tractions could conceivably vary in a different manner over each of the integrals. However, it is difficult to imagine tractions near a crack tip which would not be self-equilibrating, and it is a simple matter to require the distances a–d and e–h of the first and fourth integrals to be the same. Under both of these conditions, the special work integral may be simplified to

$$w = -2c_1\sqrt{r_0}\left\{\int_a^d \sigma_n(\alpha)\,N_d(\alpha)\,dA\right\}k_1 - 2c_1\sqrt{r_0}\left\{\int_a^d \tau_{ns}(\alpha)\,N_d(\alpha)\,dA\right\}k_2$$
$$-2c_1\left\{\int_d^0 \sigma_n(r)\sqrt{r}\,dA\right\}k_1 - 2c_1\left\{\int_d^0 \tau_{ns}(r)\sqrt{r}\,dA\right\}k_2 \tag{B8}$$

This form leads to the following nonhomogeneous terms corresponding to k_1, $u_{0x'}$, k_2, and $u_{0y'}$:

$$R_1 = \frac{\partial w}{\partial k_1} = -2c_1\left\{\sqrt{r_0}\int_a^d \sigma_n(\alpha)\,N_d(\alpha)\,dA + \int_d^0 \sigma_n(r)\sqrt{r}\,dA\right\} \tag{B9a}$$

$$R_2 = \frac{\partial w}{\partial u_{0x'}} = 0 \tag{B9b}$$

$$R_3 = \frac{\partial w}{\partial k_2} = -2c_1\left\{\sqrt{r_0}\int_a^d \tau_{ns}(\alpha)\,N_d(\alpha)\,dA + \int_d^0 \tau_{ns}(r)\sqrt{r}\,dA\right\} \tag{B9c}$$

$$R_4 = \frac{\partial w}{\partial u_{0y'}} = 0 \tag{B9d}$$

The integrals of Equation (B9) are most readily evaluated numerically within a finite element program at the same time that the "standard" nodal loads are calculated.

APPENDIX C

ASYMPTOTIC INTERPOLATION SOLUTION FOR A SINGLE-EDGE NOTCHED STRIP UNDER CRACK OPENING LOADS

Consider an edge-cracked semi-infinite strip subjected to a concentrated load on the crack face as shown in Figure C.1. By using an asymptotic interpolation procedure described by Benthem and Koiter,[36] an expression for the stress intensity factor K_I may be obtained based on the existing solutions for two limiting cases: (1) an edge-loaded semi-infinite plate as represented by $a/w \to 0$ and (2) a semi-infinite crack approaching a free boundary as represented by $a/w \to 1$.

For an edge-loaded semi-infinite plate, the Mode I stress intensity factor is given by Hartranft[21] as:

$$K_I = 2P \sqrt{\frac{a}{\pi (a^2 - b^2)}} \; [1 + f(\beta)] \tag{C1}$$

for $a/w \to 0$, and where

$$\beta = \frac{b}{a} \tag{C2}$$

and where

$$f(\beta) = (1 - \beta^2)\,(0.2945 - 0.3912\,\beta^2 + 0.7685\,\beta^4 - 0.9942\,\beta^6 + 0.5094\,\beta^8) \tag{C3}$$

For a semi-infinite crack approaching a free boundary, one may obtain by superimposing axial tension and bending solutions[22]

$$K_I = 1.122\,P\sqrt{\pi}\;\frac{w}{(w-a)^{2/3}}\left[\frac{3-\beta}{2} - 0.736\left(1 - \frac{a}{w}\right) + 0\left(1 - \frac{a}{w}\right)^n\right] \tag{C4}$$

where $0\left(1 - \frac{a}{w}\right)^n$ are higher order terms in $(1 - a/w)$.

---

[36] Benthem, J.P. and W.T. Koiter, "Asymptotic Approximations to Crack Problems," in "Mechanics of Fracture," Vol. 1, Noordhoff, Leydon, Netherlands (1973).

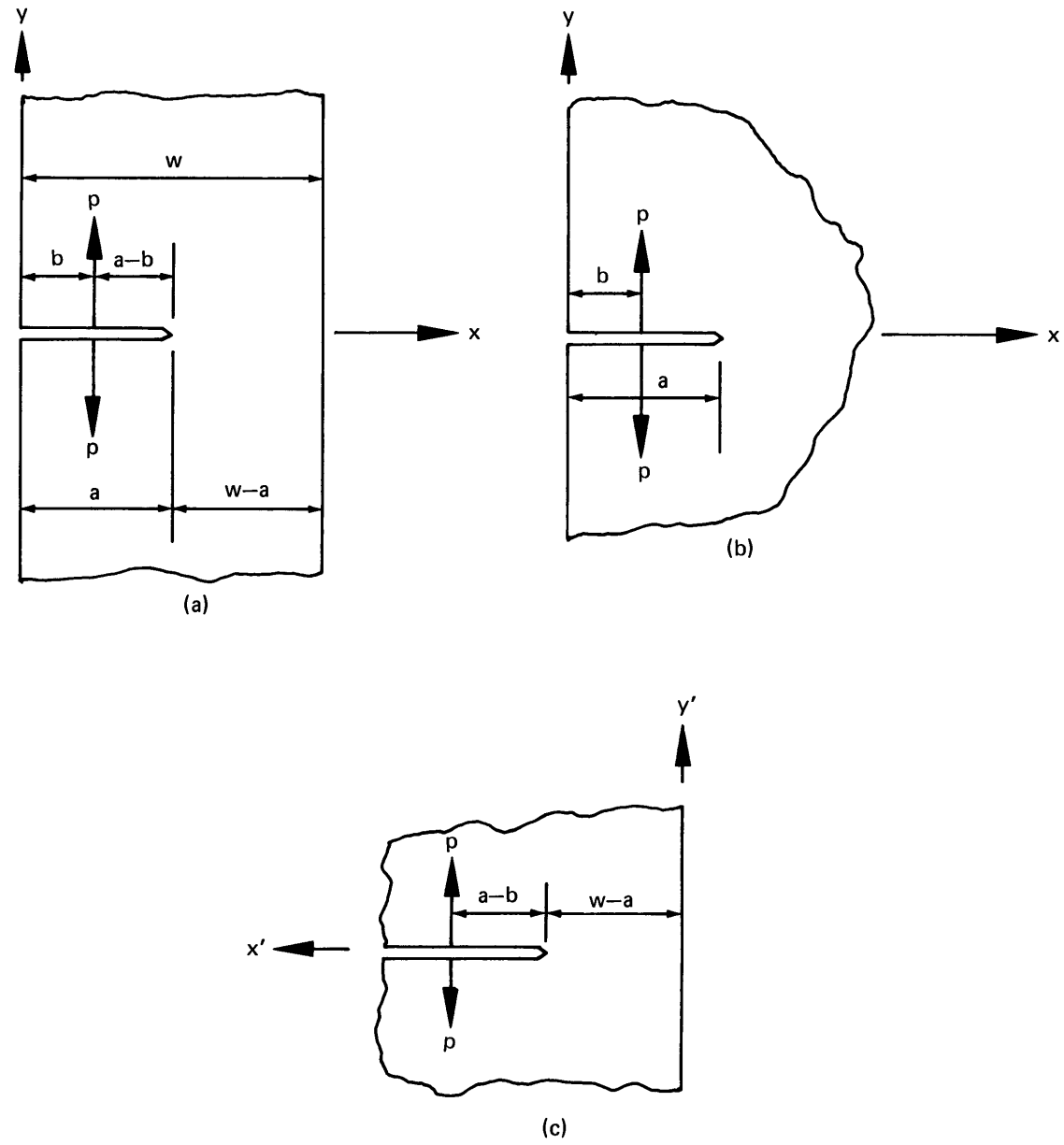

Figure C.1 – Edge Crack Loading Configurations

(Solution for a finite width strip (a) is obtained from two limiting cases represented by an edge cracked semi-infinite plate (b) and an infinite crack approaching a free boundary (c)).

Following Benthem and Koiter, an expression for K_I is assumed in the following form:

$$K_I = K \left[\frac{P[3w - 2(w-a)]\sqrt{\pi a}}{(w-a)\sqrt{(w-a)}\ w} \right] \tag{C5}$$

where the expression for K is to be obtained as a function of $\frac{a}{w}$ and $\beta = \frac{b}{a}$.

By comparing Equation (C5) with (C1) and (C4), the asymptotic form of $K\left(\frac{a}{w}, \beta\right)$ can be determined for the two limiting cases of $a/w \to 0$ and $a/w \to 1$ as follows:

$$K \to \frac{2}{\pi} \left[\frac{1 + f\left(\beta \frac{a}{w}\right)}{\sqrt{\left(\frac{a}{w}\right)^2 - \left(\frac{d}{2}\right)^2}} \right] \left[1 - 3.5 \frac{a}{w} + 7.375 \left(\frac{a}{w}\right)^2 \right] \tag{C6}$$

for $\frac{a}{w} \to 0$

$$K \to 0.374 \left\{ \left(\frac{3-\beta}{2} \right) + [0.583(3-\beta) - 0.736] \left(1 - \frac{a}{w}\right) + \left[1.153 \left(\frac{3-\beta}{2}\right) - 0.859\right] \left(1 - \frac{a}{w}\right)^2 \right\} \tag{C7}$$

for $\frac{a}{w} \to 1$

Since Equations (C5), (C6), and (C7) permit K_I calculations only near the ends of the interval $0 \leqslant \frac{a}{w} \leqslant 1$, an interpolation function is introduced in the form

$$K_I = \frac{2P}{\sqrt{\pi a}} F(\alpha, \beta) \tag{C8}$$

where

$$\alpha = \frac{a}{w} \tag{C9}$$

and where

$$F(\alpha, \beta) = \frac{g_N(\alpha, \beta)}{(1-\alpha)^{3/2}} \tag{C10}$$

and

$$g_N(\alpha, \beta) = \sum_{n=0}^{N} c_n \alpha^n \tag{C11}$$

The coefficients $c_n = c_n(\beta)$ are to be determined by curve fitting of the polynomial $g_N(\alpha, \beta)$ to the asymptotic forms given by Equations (C6) and (C7). For example, selecting a fourth degree polynomial (N = 4) and equating the values of g_4 and $\partial g_4/\partial \alpha$ at $\alpha = 1$ and $\frac{\partial^2 g_4}{\partial \alpha^2}$ at $\alpha = 1$ to the corresponding asymptotic forms, five simultaneous linear equations for c_0, c_1, c_2, c_3, and c_4 are obtained which lead to

$$c_0 = \frac{1 + f(\beta)}{\sqrt{1 - \beta}}$$

$$c_1 = -\frac{3}{2} c_0$$

$$c_2 = 6 A_2 - 2 A_3 + A_4/4 \tag{C12}$$

$$c_3 = -8 A_2 + 5 A_3 - A_4$$

$$c_4 = 3 A_2 - 2 A_3 + A_4/2$$

where $A_2 = 0.561\ \pi(2 - \beta) - c_0 - c_1$

$A_3 = 0.187\ \pi(5.207 - 4.5\ \beta) - c_1$

$A_4 = 0.187\ \pi(0.704 - 2.25\ \beta)$

This formula was used to compute the results shown in Table 3.

Lower or higher degree polynomials can be obtained by decreasing or increasing the number of matching conditions at the ends of the interval. For example, a third degree polynomial can be obtained by omitting the matching condition on $\partial^2 g_3/\partial \alpha^2$ at $\alpha = 1.0$, and the fifth degree polynomial can be obtained by adding the condition $\partial^2 g_5/\partial \alpha^2$ at $\alpha = 0$.

Where a solution has been obtained for the single concentrated load, the problem of an arbitrary pressure loading can be handled by integration. Table C.1 compares the results obtained in this fashion (using the fourth order polynomial) with theoretical results[37] based on the solution of integral equations for the special case of a strip with an edge crack opened by a uniform pressure. The comparison indicates that the accuracy of the fourth order polynomial is within 5 percent for a/w ratios less than 0.4.

[37]Chatterjee, S.N. and S.N. Prasad, "On Papkovich–Fadle Solutions of Crack Problems Relating to an Elastic Strip," Int. J. Eng. Sci., Vol. II (1973).

TABLE C.1 – COMPARISON OF K_I VALUES AS CALCULATED BY THEORY AND ASYMPTOTIC INTERPOLATION FOR DISTRIBUTED CRACK FACE LOADING

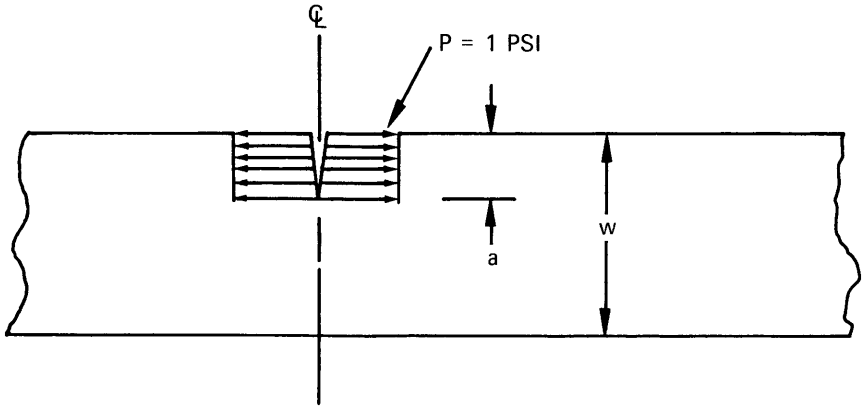

a/w	K_I (Theory, [37])	K_I (Fourth Order Polynomial)	Percent Difference
0.05	2.0178	2.0089	−0.4
0.1	2.1030	2.0754	−1.3
0.15	2.2409	2.1931	−2.1
0.20	2.4189	2.3700	−2.0
0.25	2.6495	2.6162	−1.3
0.30	2.9353	2.9458	+0.4
0.35	3.2887	3.3778	+2.7
0.40	3.7248	3.9391	+5.6
0.45	4.2688	4.6619	+9.3

APPENDIX D
CALCULATIONS OF PLASTIC SINGULAR SOLUTIONS

The equations which govern the circumferential variation of the airy stress function $\tilde{\phi}(\theta)$ asymptotically close to the crack tip within the plastic region are given by Equation (25) for plane stress and by Equation (31) for plane strain and axisymmetric cases. These are

$$\left[\frac{-n}{n+1} - \frac{d^2}{d\theta^2}\right]\left[\tilde{\sigma}_e^{n-1}\left(\frac{2n^2+5n+2}{(n+1)^2}\tilde{\phi} + 2\ddot{\tilde{\phi}}\right)\right]$$
$$\frac{-n}{(n+1)^2}\tilde{\sigma}_e^{n-1}\left[\frac{2n^2-n-1}{(n+1)^2}\tilde{\phi} - \ddot{\tilde{\phi}}\right] + \frac{6n}{(n+1)^2}\frac{d}{d\theta}\left[\tilde{\sigma}_e^{n-1}\dot{\tilde{\phi}}\right] = 0 \tag{D1}$$

for plane stress with $\tilde{\sigma}_e = (\tilde{\sigma}_r^2 + \tilde{\sigma}_\theta^2 - \tilde{\sigma}_r\tilde{\sigma}_\theta + 3\tilde{\sigma}_{r\theta}^2)^{1/2}$ and

$$\left[\frac{d^2}{d\theta^2} + \frac{n(n+2)}{(n+1)^2}\right]\left[\tilde{\sigma}_e^{n-1}\left(\frac{2n+1}{(n+1)^2}\tilde{\phi} + \ddot{\tilde{\phi}}\right)\right]$$
$$+ \frac{4n}{(n+1)^2}\frac{d}{d\theta}\left[\tilde{\sigma}_e^{n-1}\dot{\tilde{\phi}}\right] = 0 \tag{D2}$$

for plane strain and axisymmetric cases, with $\tilde{\sigma}_e = [3/4\,(\tilde{\sigma}_r - \tilde{\sigma}_\theta)^2 + 3\tilde{\sigma}_{r\theta}^2]^{1/2}$.
A superscripted dot $(\cdot)$ in Equations (D1) and (D2) indicates differentiation with respect to θ, and the stress functions $\tilde{\sigma}_r$, $\tilde{\sigma}_\theta$, and $\tilde{\sigma}_{r\theta}$ are given by

$$\tilde{\sigma}_r = \left[\frac{2n+1}{n+1}\tilde{\phi} + \ddot{\tilde{\phi}}\right]$$

$$\tilde{\sigma}_\theta = \left[\frac{n(2n+1)}{(n+1)^2}\tilde{\phi}\right]$$

$$\tilde{\sigma}_{r\theta} = \left[\frac{-n}{n+1}\dot{\tilde{\phi}}\right]$$

These equations are fourth order, nonlinear, homogeneous differential equations in $\tilde{\phi}$ in which the coefficients of $\tilde{\phi}$ and its derivatives are functions of the hardening parameter n only. The boundary conditions for these equations are $\tilde{\phi}(\pm \pi) = \dot{\tilde{\phi}}(\pm \pi) = 0$. Solutions for Mode I loading conditions, in addition, are required to be symmetric about the line $\theta = 0$ (x axis) of Figure 10.

The solution procedure to be outlined here has been provided by C.F. Shih and J.W. Hutchinson of Harvard University. Both Equations (D1) and (D2) may be written in the form

$$\tilde{\phi}^{\cdots\cdot} - f(\tilde{\phi}, \dot{\tilde{\phi}}, \ddot{\tilde{\phi}}, \dddot{\tilde{\phi}}) = 0 \qquad \text{(D3)}$$

For plane stress,

$$f = -\frac{c\,\ddot{\tilde{\phi}}}{2} - \left\{ \frac{n-1}{4}\beta\left[\dot{\beta}^2 + 4a\left(\tilde{\phi}\,\ddot{\tilde{\phi}} + \dot{\tilde{\phi}}^2\right) + 4b\left(\dot{\tilde{\phi}}\,\dddot{\tilde{\phi}} + \ddot{\tilde{\phi}}^2\right)\right] + \frac{(n-1)(n-3)}{4}\frac{\beta\dot{\alpha}^2}{\alpha} + (n-1)\dot{\alpha}\dot{\beta} + \frac{3n(n-1)}{(n+1)^2}\dot{\alpha}\dot{\tilde{\phi}} + \frac{\alpha}{n+1}\left[n\beta + \frac{n}{n+1}\gamma + \frac{6n}{n+1}\ddot{\tilde{\phi}}\right]\right\} \Big/ \left\{ 2\alpha + \frac{(n-1)}{2}\beta^2 \right\}$$

with

$$\alpha = \frac{\beta^2}{4} + a\,\tilde{\phi}^2 + b\,\dot{\tilde{\phi}}^2$$

$$\beta = c\,\tilde{\phi} + 2\,\ddot{\tilde{\phi}}$$

$$\gamma = d\,\tilde{\phi} - \ddot{\tilde{\phi}}$$

$$a = 3/4\, n^2\,(4n^2 + 4n + 1)/(n+1)^4$$

$$b = 3\, n^2/(n+1)^2$$

$$c = (2n^2 + 5n + 2)/(n+1)^2$$

$$d = (2n^2 - n - 1)/(n+1)^2$$

For plane strain and axisymmetric cases,

$$f = -\frac{(2n+1)}{(n+1)^2}\ddot{\tilde{\phi}} + \left[\alpha(\alpha\beta - b\ddot{\tilde{\phi}}) - \dot{\alpha}\left(e\frac{\dot{\alpha}\beta}{\alpha} + 2d\dot{\beta} + bd\dot{\tilde{\phi}}\right)\right.$$

$$\left. - d\beta\left(\frac{3}{2}\dot{\beta}^2 + 2c\ddot{\tilde{\phi}}^2 + 2c\dot{\tilde{\phi}}\dddot{\tilde{\phi}}\right)\right] / \left(\alpha + \frac{3}{2}d\beta^2\right)$$

with

$$\alpha = \frac{3}{4}\beta^2 + c\dot{\tilde{\phi}}^2$$

$$\beta = \ddot{\tilde{\phi}} + (2n+1)\tilde{\phi}/(n+1)^2$$

$$a = -n(n+2)/(n+1)^2$$

$$b = 4n/(n+1)^2$$

$$c = 3n^2/(n+1)^2$$

$$d = \frac{1}{2}(n-1)$$

$$e = (n-1)(n-3)/4$$

The function f is homogeneous of degree one in the variables $\tilde{\phi}$, $\dot{\tilde{\phi}}$, $\ddot{\tilde{\phi}}$, and $\dddot{\tilde{\phi}}$ in the sense that $f(\lambda\tilde{\phi}, \lambda\dot{\tilde{\phi}}, \lambda\ddot{\tilde{\phi}}, \lambda\dddot{\tilde{\phi}}) = \lambda f(\tilde{\phi}, \dot{\tilde{\phi}}, \ddot{\tilde{\phi}}, \dddot{\tilde{\phi}})$. Thus by the Euler theorem,[38] Equation (D3) may be written in the equivalent form

$$-\ddddot{\tilde{\phi}} + \partial f/\partial\tilde{\phi}\,\tilde{\phi} + \partial f/\partial\dot{\tilde{\phi}}\,\dot{\tilde{\phi}} + \partial f/\partial\ddot{\tilde{\phi}}\,\ddot{\tilde{\phi}} + \partial f/\partial\dddot{\tilde{\phi}}\,\dddot{\tilde{\phi}} = 0 \qquad \text{(D4)}$$

---

[38] Ince, E.L., "Ordinary Differential Equations," Dover, New York (1956).

Rather than solve the fourth order nonlinear differential equation, it is more convenient to employ a reduction of order[39] and solve instead two second order simultaneous nonlinear differential equations. When the variable $\tilde{\psi} = \ddot{\tilde{\phi}}$ is introduced, the following simultaneous equations result:

$$\tilde{\psi} - \ddot{\tilde{\phi}} = 0$$

$$-\ddot{\tilde{\psi}} + \frac{\partial f}{\partial \dot{\tilde{\psi}}}\dot{\tilde{\psi}} + \frac{\partial f}{\partial \tilde{\psi}}\tilde{\psi} + \frac{\partial f}{\partial \dot{\tilde{\phi}}}\dot{\tilde{\phi}} + \frac{\partial f}{\partial \tilde{\phi}}\tilde{\phi} = 0 \qquad \text{(D5)}$$

A quasi-linearization procedure is employed to solve Equations (D5) iteratively. Let $\tilde{\phi}_i(\theta)$ and $\tilde{\psi}_i(\theta)$ be the i *th* approximation to $\tilde{\phi}(\theta)$ and $\tilde{\psi}(\theta)$, respectively. Then the (i + 1) *th* approximation is obtained by employing the i *th* approximation in calculating the coefficients in Equations (D5) and solving the resulting linear differential equations. This is done through the use of a three-point central finite difference scheme, making the use of a computer mandatory.

The outlined procedure has been found to converge rapidly, usually within three iterations if an accurate initial choice (guess) is made for the stress function $\tilde{\phi}(\theta)$. Because of this, calculations outlined here have been carried out in a specialized manner. The elasticity solution for $\tilde{\phi}(\theta)$ is input as an initial guess and the iterative procedure is used to determine $\tilde{\phi}(\theta)$ for a relatively small value of the hardening coefficient n (typically, n = 1.5). The numerical solution obtained for that value of n is then used as the initial solution for the next higher value of n, say, n = 3, etc. This procedure has the advantage that it automatically (and economically) yields solutions for $\tilde{\phi}(\theta)$ for a sequence of values of the hardening coefficient n. In fact, C.F. Shih at Harvard University has tabulated values for $\tilde{\phi}(\theta)$ and its first three derivatives as well as corresponding stress, strain, and displacement components at two-degree intervals of θ for a sequence of values of n from 1.2 to 100. In addition, the parameters I of Equation (37) and B/r_0 of Equation (43) used in the finite element analysis are also given for each value of n. It is important to note that such calculations are dependent only on the material-hardening coefficient n, and once carried out, need never be repeated.

---

[39]Hildebrand, F.B., "Advanced Calculcus for Applications," Prentice-Hall, New York (1963).

REFERENCES

1. Sih, G.C., "Handbook of Stress Intensity Factors," Institute of Fracture and Solid Mechanics, Lehigh University (1973).

2. Tada, Hiroshi, "The Stress Analysis of Cracks Handbook," Del Research Corporation (1973).

3. Oglesby, J.J. and O. Lomacky, "An Evaluation of Finite Element Methods for the Computation of Elastic Stress Intensity Factors," NSRDC Report 3751 (Dec 1971).

4. Gifford, L.N., "Finite Element Analysis for Arbitrary Axisymmetric Structures," NSRDC Report 2641 (Mar 1968).

5. Sih, G.C. and P.C. Paris, "Symposium of Fracture Toughness Testing and Its Applications," Am. Soc. Mech. Eng. STP-381 (1965).

6. Wilson, W.K., "On Combined Mode Fracture Mechanics," Ph.D. Dissertation, University of Pittsburgh (1969).

7. Hilton, P.D. and J.W. Hutchinson, "Plastic Intensity Factors for Cracked Plates," Eng. Fract. Mech., Vol. 3 (1971).

8. Byskov, E., "The Calculation of Stress Intensity Factors Using the Finite Element Method with Cracked Elements," Int. J. Fract. Mech., Vol. 6, No. 2 (1970).

9. Tracey, D.M., "Finite Elements for Determination of Crack Tip Elastic Stress Intensity Factors," Eng. Fract. Mech., Vol. 3 (1971).

10. Hilton, P.D. and G.C. Sih, "Application of the Finite Element Method to the Calculation of Stress Intensity Factors," in "Mechanics of Fracture," Vol. 1, Noordhoff, Leydon, Netherlands (1973).

11. Wilson, W.K., "Finite Element Methods for Elastic Bodies Containing Cracks," in "Mechanics of Fracture," Vol. 1, Noordhoff, Leydon, Netherlands (1973).

12. Zienkiewicz, O.C., "The Finite Element Method in Engineering Science," McGraw-Hill Book Company, London (1971).

13. Hoff, N.J., "The Analysis of Structures," John Wiley and Sons, New York (1956).

14. Przemieniecki, J.S., "Theory of Matrix Structural Analysis," McGraw-Hill Book Company, New York (1968).

15. Bowie, O.L., "Rectangular Tensile Sheet with Symmetric Edge Cracks," Am. Soc. Mech. Eng., Paper 64-APM-3 (1964).

16. Brown, W.F. Jr. and J.E. Srawley, "Plane Strain Crack Toughness Testing of High Strength Metallic Materials," Am. Soc. Testing Mat. STP-410 (1967).

17. Pian, T.H.H., "Hybrid Models," International Symposium on Numerical and Computer Methods in Structural Mechanics, University of Illinois, Urbana (8–10 Sep 1971).

18. Bowie, O.L. and D.M. Neal, "Single Edge Crack in Rectangular Tensile Sheet," J. Appl. Mech., Vol. 32 (1965).

19. Bowie, O.L., "Solutions of Plane Crack Problems by Mapping Techniques," in "Mechanics of Fracture," Vol. 1, Noordhoff, Leydon, Netherlands (1973).

20. Benzley, S.E. and Z.E. Beisinger, "CHILES–A Finite Element Computer Program That Calculates the Intensities of Linear Elastic Singularities," Sandia Laboratories Report SLA-73-0894 (Sep 1973).

21. Hartranft, R.J. and G.C. Sih, "Alternating Method Applied to Edge and Surface Crack Problems," in "Mechanics of Fracture," Noordhoff Leydon, Denmark (1973).

22. Sih, G.C., "Introductory Chapter: A Special Theory of Crack Propagation," in "Mechanics of Fracture," Noordhoff, Leydon, Netherlands (1973).

23. Shih, C.F., "Small Scale Yielding Analysis of Mixed Mode Plane Strain Crack Problems," Harvard University Report DEAP S-1 (May 1973).

24. Hutchinson, J.W. and C.F. Shih, "Plastic Analysis of Mixed Plane Stress Crack Problems," Harvard University Report DEAP S-4 (Sep 1973).

25. Rice, J.R., "Mathematical Analysis in the Mechanics of Fracture," in "Fracture," Vol. 2, Academic Press (1968).

26. Rice, J.R., "A Path Independent Integral and the Approximate Analysis of Strain Concentrations of Notches and Cracks," Brown University Report ARPA 50-80, E39 (1967).

27. Rice, J.R. and G.F. Rosengren, "Plane Strain Deformation Near a Crack Tip in a Hardening Material," J. Mech. Physics and Solids, Vol. 16, No. 1 (1968).

28. Hutchinson, J.W., "Singular Behavior at the End of a Tensile Crack in a Hardening Material," J. Mech. Physics and Solids, Vol. 16, No. 1 (1968).

29. Hutchinson, J.W., "Plastic Stress and Strain Fields at a Crack Tip," J. Mech Physics and Solids, Vol. 16 (1968).

30. Eshelby, J.D., "Determination of the Elastic Field of an Ellipsoidal Inclusion, and Related Problems," Proc. Roy. Soc., London, Series A, Vol. 241 (1957).

31. Begley, J. and J.A. Landes, "The J-Integral as a Failure Criterion," Westinghouse Research Laboratories Report 71-1E7-FMPWR-P3 (1971).

32. Budiansky, B., "Extension of Michell's Theorem to Problems of Plasticity and Creep," Q. Appl. Math., Vol. 16 (1958).

33. Hilton, P.D., "Plastic Intensity Factors for Cracked Plates Subjected to Biaxial Loading," Int. J. Fract., Vol. 9, No. 2 (Jun 1973).

34. Rice, J.R. and M.A. Johnson, "The Role of Large Crack Tip Geometry Changes in Plane Strain Fracture," Brown University Report NYO-2394-38 (Sep 1969).

35. Wilson, W.K. and J.A. Begley, "Heavy Section Steel Technology Program Technical or Programmatic Manuscript No. 25–Variable Thickness Study of the Edge Cracked Bend Specimen," Westinghouse Electric Corporation Report WCAP-8237 (Nov 1973).

36. Benthem, J.P. and W.T. Koiter, "Asymptotic Approximations to Crack Problems," in "Mechanics of Fracture," Vol. 1, Noordhoff, Leydon, Netherlands (1973).

37. Chatterjee, S.N. and S.N. Prasad, "On Papkovich–Fadle Solutions of Crack Problems Relating to an Elastic Strip," Int. J. Eng Sci, Vol. II (1973).

38. Ince, E.L., "Ordinary Differential Equations," Dover, New York (1956).

39. Hildebrand, F.B., "Advanced Calculcus for Applications," Prentice-Hall, New York (1963).

INITIAL DISTRIBUTION

Copies	
1	DDR&E, Attn: Tech Lib
4	CNO 1 Plans, Prgms & Req Br (OP 311) 1 Tech Analy & Adv Gr (OP 098T) 1 Sub Program Br (OP 981G) 1 Tech Support Br (OP 916)
3	CHONR 1 Struc Mech Br (Code 439) 1 Undersea Prog (Code 466) 1 Res Coord (Code 104)
4	NAVMAT 1 MAT 033 1 MAT 033B 1 MAT 034B 1 MAT 03L4
7	NRL 1 W.F. Brown 1 W.S. Pellini 1 P.P. Puzak 1 J.M. Krafft 1 E.A. Lange 1 T.W. Crooker 1 H.L. Smith
1	US Naval Academy
1	PGSC, Monterey
1	USNROTC & NAVADMINU, MIT
1	NAVWARCOL
2	NADC 1 Code STD 1 Code ST-3
1	NELC
1	NUC
1	NWC
2	NSWC
1	NWL, Code EAD, R. Lindeman
1	NUSC

Copies	
15	NAVSEASYSCOM 1 SEA 03C (SHIPS 031) 1 SEA 033 (ORD 035) 1 SEA 035 (SHIPS 034) 1 SEA 035B (SHIPS 0342) 1 SEA 035B (SHIPS 03421) 1 SEA 035B (SHIPS 03422) 1 SEA 03511 (SHIPS 03423) 2 SEA 09G-32 (SHIPS 2052) 1 SEA 924 (SHIPS 425) 1 PMS 381 1 PMS 391 1 PMS 393 1 PMS 395 1 PMS 396
1	NAVAIR (320N)
1	NAVFAC (03211)
1	NISC (Code 10)
1	NAVSHIPYD PTSMH
1	NAVSHIPYD CHASN
1	NAVSHIPYD MARE
1	SUPSHIP, Newport News
1	SUPSHIP, Pascagoula
19	NAVSEC 1 SEC 6101 1 SEC 6101D 1 SEC 6101E 1 SEC 6110 1 SEC 6110D 1 SEC 6111 1 SEC 6113 1 SEC 6113B4 1 SEC 6114 1 SEC 6120 1 SEC 6120D 1 SEC 6122 1 SEC 6128 1 SEC 6128E 2 SEC 6129 1 SEC 6140 1 SEC 6144 1 SEC 6147C

Copies	
12	DDC
1	AMMRC, Warminster Code AMXMR-T, Dr. Burke
1	ASD/ENFSF, WPAFB, Attn: Mr. J.L. McFarland
1	AFFDL, WPAFB Dr. R.G. Forman
1	USCG CDR S. Loosmore
1	MARAD Mr. J. Nachtschein
1	NAS Comm. on Undersea Warfare
1	NASA, Goddard Space Flight Center Mr. P. Stern
3	NASA, Lewis Research Center 1 Dr. B. Gross 1 Mr. S.S. Manson 1 Dr. J.E. Srawley
2	Battelle Memorial Institute 1 W.E. Anderson 1 Dr. G.T. Hahn
3	Brown University 1 Prof. P.V. Marcal 1 Dr. D.M. Parks 1 Prof. J.R. Rice
2	Carnegie Melon Institute 1 Prof. J.L. Swedlow 1 T.A. Cruse
1	Catholic Univ of America Dr. S.R. Heller
1	Colorado State Univ Prof. F.W. Smith
1	Univ of Connecticut Prof A.J. McEvily
2	George Washington Univ 1 Prof. A.M. Freudenthal 1 Dr. H. Liebowitz
1	Georgia Institute of Tech Dr. J.M. Anderson
2	Harvard Univ 1 Prof. J.W. Hutchinson 1 Dr. C.F. Shih

Copies	
2	Univ of Illinois 1 Prof. A.H.S. Ang 1 Prof. W.H. Munse
14	Lehigh Univ 10 Prof. P. Hilton 1 Prof. G.R. Irwin 1 Prof. P.C. Paris 1 Prof. G.C. Sih 1 Prof. R.P. Wei
2	MIT 1 Dr. F.A. Mellinbock 1 Prof. Pin Tong
1	SWRI Dr. R. DeHart
1	Univ of Texas Dr. R.S. Dunham
2	VPI & SU 1 Prof. C.W. Smith 1 Prof. G.W. Swift
3	Univ of Washington 1 APL 1 Prof. A.S. Kobayashi 1 Dr. A.F. Emery
1	WHOI Mr. J. Mavor
1	General Dynamics Corp Electric Boat Div
1	Ingalls Shipbldg Corp
1	Newport News Shipbldg & Drydock Co
2	Sandia Laboratories 1 Dr. S.E. Benzley 1 M.L. Callabresi
2	Welding Research Council Mr. C.F. Larson, Sec.
3	Westinghouse Corp 1 Mr. S.A. Legge 1 Dr. W.K. Wilson 1 Dr. S.K. Chan

CENTER DISTRIBUTION

Copies	Code
1	00
1	17
1	172
10	172A
3	1721
25	1725
4	1727
1	173
1	173.2
1	173.4
1	173.5
1	174
1	1745
1	177
1	1844
1	28
1	2802
1	2814
1	282
5	2823
30	5614 - Reports Distribution
1	5641
1	5642 (A)
1	9401